NUREG/CR--4792-Vol.2

TI89 008910

PROBABILITY OF FAILURE IN BWR REACTOR COOLANT PIPING

Vol. 2: Pipe Failure Induced by Crack Growth and Failure of Intermediate Supports

Manuscript Completed: October 1987
Date Published: March 1989

Prepared by
T. Lo, S.E. Bumpus, D.J. Chinn, R.W. Mensing, G.S. Holman

Lawrence Livermore National Laboratory
7000 East Avenue
Livermore, CA 94550

Prepared for
Division of Engineering
Office of Nuclear Regulatory Research
U.S. Nuclear Regulatory Commission
Washington, D.C. 20555
NRC FIN No. A0133

Report NUREG/CR-4792, **Probability of Failure in BWR Reactor Coolant Piping**, is published in the following four volumes:

Vol. 1: Summary Report

Vol. 2: Pipe Failure Induced by Crack Growth and Failure of Intermediate Supports

Vol. 3: Probabilistic Treatment of Stress Corrosion Cracking in 304 and 316NG BWR Piping Weldments

Vol. 4: Guillotine Break Indirectly Induced by Earthquakes

This report is Volume 2 of the report series.

ABSTRACT

The U.S. Nuclear Regulatory Commission (NRC) contracted with the Lawrence Livermore National Laboratory (LLNL) to conduct a study to determine if the probability of occurrence of a double-ended guillotine break (DEGB) in the major coolant piping systems of nuclear power plants is large enough to warrant the current stringent design requirements of designing against the postulated effects of a DEGB. The study includes both the PWR (Pressurized Water Reactor) and the BWR (Boiling Water Reactor) plants in the United States. Earlier efforts concentrated on the reactor coolant loops of PWR plants, and the results indicated that the DEGB probability in these reactor coolant loops (RCLs) was very small.

Following the study of PWR plants, a study of BWR reactor coolant piping was performed. The Brunswick Steam Electric Plant at Southport, North Carolina was selected as the pilot plant for the BWR evaluation. The probability of pipe failure in three major coolant pipings was assessed: the recirculation loops, the primary steam lines, and the main feedwater lines. In the case of recirculation loops, both the existing and a proposed replacement system were studied. A probabilistic fracture mechanics approach was used in this study to estimate the crack growth and to assess the crack stability in the piping systems throughout the lifetime of the plant. The effects of the failure of intermediate pipe supports were also examined. The results of the assessment indicated that the probability of occurrence of DEGB due to crack growth and instability is small if the problem of intergranular stress corrosion cracking (IGSCC) is resolved by the use of the replacement system. The study of intermediate support failure yielded some guidelines for significant reduction of effort in assessing the effects of seismically induced failure of intermediate supports.

CONTENTS

FIGURES

TABLES

ACKNOWLEDGMENTS

This work was funded by the Mechanical/Structural Engineering Branch within the Office of Nuclear Regulatory Research of the U.S. Nuclear Regulatory Commission. Dr. J. O'Brien was the technical monitor of the work.

The authors express their appreciation to the personnel at the Carolina Power & Light (CP&L) Company for their cooperation in providing the design data. Thank is also extended to Dr. N. C. Tsai of NCT Engineering, Moraga, Calif., and to B. J. Benda of Structural Mechanics Associates, Inc., San Ramon, Calif., for their contribution to the support fragilities and the piping responses, respectively.

We also thank Dr. C. K. Chou of Lawrence Livermore National Laboratory (LLNL), Livermore, Calif., for his guidance, and Denece Bowden of LLNL for editorial assistance.

EXECUTIVE SUMMARY

The U.S. Nuclear Regulatory Commission (NRC) contracted with the Lawrence Livermore National Laboratory (LLNL), Livermore, Calif., to conduct a probabilistic assessment of the major coolant piping systems of all existing nuclear power plants in the United States. This assessment includes both the Pressurized Water Reactor (PWR) and the Boiling Water Reactor (BWR) plants. The goal was to determine if the probability of occurrence of double-ended guillotine breaks (DEGB) in these piping systems is small enough to safely eliminate the postulation of DEGB in the design requirement.

Earlier work addressed the reactor coolant loops (RCL) of PWR plants. The results indicated that the probability of having a DEGB in the RCLs of these plants is very low. Following the work on the PWR plants, LLNL started this pilot study of all BWR plants in the U.S. The Brunswick Steam Electric Plant located at Southport, North Carolina, was selected in this study as the pilot plant. Three major coolant systems were evaluated: the recirculation loops, the primary steam lines and the feedwater lines. In the case of the recirculation loops, both the existing and the proposed replacement systems were examined.

This volume of the report documents studies related to pipe failure induced by crack growth, and failure of intermediate pipe supports. The effects of intergranular stress corrosion cracking (IGSCC) were not considered in the studies described above. IGSCC was found to be a problem in many recirculation loops of BWR plants including Brunswick. Work on the effects of IGSCC on the existing Brunswick recirculation loops is addressed in another volume of this report. The study of pipe failure due to indirect sources other than the failure of intermediate supports is documented in yet another volume of this report.

The probabilistic fracture mechanics approach used in previous PWR plant studies was again used in this study. Two types of analyses were performed: a best-estimate analysis and an uncertainty analysis. The former considers only the best-estimate models of relevant parameters and their associated randomness; the latter takes into account the uncertainty of the models. In these analyses, the supports were assumed to maintain their function during an earthquake.

The results indicate that the lifetime system leak and DEGB probabilities for the Brunswick major coolant piping systems are low and fall within narrow ranges. The best-estimate lifetime leak probabilities vary from .24E-5 to 3.8E-5 over 40 years. The best-estimate DEGB probabilities are over four orders of magnitude lower than the leak probabilities and vary from .40E-10 to 1.5E-10 over the lifetime of the plant.

Seven parameters which have large modeling uncertainty are considered in the uncertainty analysis. These parameters are crack depth, crack aspect ratio, crack existence probability, non-detection probability, thermal expansion stresses, seismic stresses, and the shape of seismic hazard curves. We used the Latin Hypercube sampling technique in the uncertainty analysis and obtained the results in the form of empirical cumulative distributions of the system failure probability. The modeling uncertainty distribution of the leak and DEGB probabilities are very wide for all piping systems considered. The probability range for leak between the 10th and 90th percentiles for the replacement recirculation loops, the primary steam lines, and the feedwater lines are 6.2E+2, 1.7E+3, and 1.7E+3, respectively, on the logarithmic scale; note that each "probability range" presented in this manner is the ratio of the respective 90th-percentile leak probability to the 10th-percentile value. The corresponding ranges for DEGB probabilities are 1.7E+4, 2.7E+4, and 1.1E+5, respectively. These wide (i.e. several order-of-magnitude) ranges are consistent with our previous studies of the PWR plants.

Because of the complexity of the problem involving the failure of intermediate supports, we performed a demonstrative assessment of the replacement recirculation loops. The goal was to gain insight in the hope that a simple approach could be found. In this demonstrative study, a few simplifying assumptions were made. The simplified study uses the system DEGB probabilities of the no-support-failure case described in the previous paragraphs and calculates the failure probabilities for fifteen with-support-failure cases in which one or more supports fail. The overall system failure probability is the sum of all the cases including both the cases with and without support failure.

The results of the support failure analysis indicate that the extrapolation or truncation of the seismic hazard curve has a significant effect on the overall system failure probability. The overall system failure probability is dominated by the no-support-failure case if the truncation is approximately two times safe shutdown earthquake (SSE) or less. The with-support-failure cases start to dominate when the truncation is more than two times SSE.

The seismic hazard curves have large modeling uncertainties not only because of the lack of seismicity data for any earthquakes above the SSE but also because of the limit on the acceleration level the soil can transmit. Therefore, the relative contribution to failure between the no-support-failure case and the cases involving support failure is highly uncertain. In this assessment, the maximum overall system failure probability of the replacement recirculation system was found to be 4.3E-6 per plant lifetime at the seismic hazard truncation level of 5SSE and can be considered as the upper bound value.

The most important result of this demonstrative study is that guidelines are now available to reduce greatly the amount of work in studying the effects of the failure of intermediate supports. In

general, for a piping system, only a couple of with-support-failure cases and a few weld joints for each case need be considered.

Another modeling uncertainty studied in assessing the effects of support failure is that associated with estimating support fragilities. Overall system failure probabilities associated with fragilities at 10% and 90% on the uncertainty distribution were calculated for the replacement recirculation system. The effects of the extrapolation or truncation of the seismic hazard curve are similar to the best-estimate case described earlier. The upper bound of overall system failure probability of the 90% case is 1.7E-4 per lifetime of the plant at the seismic hazard truncation level of 5SSE.

1. INTRODUCTION

1.1 Objective

In nuclear power plants, postulation of double-ended guillotine breaks (DEGB) in major piping systems has resulted in severe design loading conditions. These loading conditions caused difficulties and excessive costs in areas of design, construction, maintenance with unnecessary radiation exposure of maintenance personnel. Many believe that DEGB is an extremely unlikely event, and that considering DEGB in piping design may be unnecessary.

The Nuclear Regulatory Commission (NRC) contracted with the Lawrence Livermore National Laboratory (LLNL) to conduct a probabilistic assessment of major coolant pipings of all existing nuclear power plants in the U.S., both for pressurized water reactor (PWR) and boiling water reactor (BWR) plants. The goal was to determine if the probability of occurrence of DEGB is small enough to safely eliminate the postulation of DEGB in the design requirement.

Earlier work was focused on the reactor coolant loop (RCL) piping of PWR plants. The results indicated that the probability of having a DEGB in the RCLs of these plants are indeed very small. As a result, design requirements associated with DEGB are no longer required by the NRC for the RCL systems.

Following the work on the PWR plants, LLNL started a study of BWR reactor coolant piping. Unit 2 of the Brunswick Steam Electric Plant located at Southport, North Carolina, was selected in this study as the BWR pilot plant. A probabilistic evaluation was made of its recirculation loops, primary steam lines, and feedwater lines.

This volume of the report documents the work related to the pipe failure induced by crack growth, overstress in the pipes, and failure of intermediate pipe supports.

1.2 Scope of Work

In the probabilistic assessment of each piping system, we perform two separate evaluations: (1) DEGB due to direct crack growth of flaws in the pipe weld joints or a simple overstressing in the piping system, and (2) DEGB indirectly induced by sources other than crack growth, such as the failure of pipes or component supports. This volume presents the direct part of the probabilistic assessment of the Brunswick Plant and includes part of the DEGB results from indirect sources. That is, this study also assessed the effects of the failure of intermediate pipe supports such as the hangers and the snubbers. Volume 4 of this report (Ref. 8.5) addresses the DEGB due to other indirect sources besides the intermediate supports. The effects of intergranular stress corrosion cracking (IGSCC) on the existing

Brunswick recirculation loops was addressed in Volumes 1 and 3 of this report.

Stress corrosion cracking was found to be a problem in many recirculation loops of the BWR plants including Brunswick. However, in the study documented in this volume, the effects of IGSCC were not considered. The results documented in this volume provided a basic piece of information in assessing the improvements that can be realized if the IGSCC problem can be resolved and eliminated.

A probabilistic fracture mechanics approach was again used in this pilot study to estimate crack growth and to assess the crack stability during the lifetime of the plant. In addition to DEGB assessment, the probability of leak was also estimated.

Two types of variability, or uncertainty, in many important parameters are considered. One, called random uncertainty in this study, represents the inherent physical randomness; the other, called modeling uncertainty, is associated with the lack of knowledge or detailed information about the parameters to describe them precisely. We used a Monte Carlo simulation to calculate the leak or DEGB probability at a weld joint, considering the randomness of the parameters. We used a Latin Hypercube sample design to generate a set of runs to describe modeling uncertainty.

2. MAJOR COOLANT PIPING SYSTEMS OF THE BRUNSWICK PLANT

In this study, we focus on three major piping systems of the Brunswick Plant: the recirculation loops, the primary steam (or main steam) lines, and the feedwater lines.

2.1 Recirculation Loops

Two recirculation piping systems at the Brunswick Plant are studied in this report: an existing system and a proposed replacement system. The existing system is made of Type 304 stainless steel, which was found to be susceptible to intergranular stress corrosion cracking (IGSCC) in many BWR plants. It was the intention of the replacement system to solve this problem by using the less IGSCC-susceptible Type 316 stainless steel (ASME SA-358 Class 1 nuclear grade).

2.1.1 Existing Recirculation System

The existing recirculation piping system of the Brunswick Plant comprises two loops linked together at the header by a pair of equalizer valves. Fig. 2.1 shows the plan and elevation views of the recirculation system. These two loops (Loops A and B) are the mirror image of each other on two sides of the reactor pressure vessel except that a shutdown supply line of the residual heat removal (RHR) system is connected to the suction line of Loop B. The 24-inch shutdown return branches of the RHR system are connected to the discharge lines just below the header.

For each loop, the coolant flows out of the reactor vessel via a 28-inch diameter suction pipe and flows into a 28-inch discharge line due to the action of a recirculation pump between these two pipes. A suction valve is located on one side of the pump and a discharge valve on the other. A 22-inch header downstream from the 28-inch discharge line distributes the coolant to five 12-inch risers, which return the coolant to the reactor vessel. The header and the risers are part of the discharge piping. However, for convenience, we will call only the 28-inch piping downstream from the recirculation pump as the discharge line in this study. A 4-inch diameter bypass line with a bypass valve is connected to the discharge line on either side of the discharge valve. There are 51 circumferential welds in the piping. Table 2.1 shows the dimensions, the material types, and the number of welds for each pipe section. Only the Loop B elevation is shown in this figure. The pipe material is SA-240 Type 304 stainless steel except the bypass lines, which are SA-376 Type 304 stainless steel. The suspension system of recirculation Loop B shown in Fig. 2.2 includes four variable spring hangers for the pipes and three constant support hangers for the pump. The loop has ten snubbers designated as SSB1 to SSB6, two SSB9s, and two SSB12s. The two SSB9s are located on the suction line just below the tee which connects to the shutdown supply line of RHR system. SSB12 snubbers support the discharge piping under the branch tee to the shutdown return line. The recirculation pump is supported by SSB1 through SSB3. The pump motor, which is on top of the pump, is

supported by SSB4 through SSB6. Loop A has the same snubber arrangement except that one SSA10 replaces the two SSB9s of Loop B and is at a much lower elevation.

2.1.2 Recirculation Loop Replacement System

The replacement system of the recirculation loops closely resembles the existing system. Loop A corresponds to the existing Loop B, and Loop B corresponds to the existing Loop A. The replacement piping system is made of Type 316 stainless steel (SA-358 Class 1, nuclear grade). It is structurally simpler than the existing system and has fewer weld joints. It has no bypass lines. It also has no equalizer valves and, therefore, the two loops are structurally independent of each other. Figure 2.2 shows the plan and elevation views of the system. The dimensions, material types, and the weld information are presented in Table 2.2.

2.2 Main Steam Lines

The main steam or primary steam piping system consists of four 24-inch diameter carbon steel pipes designated as Lines A, B, C, and D. Lines A and B are on one side of the reactor pressure vessel while Lines C and D are on the other side as shown in Fig. 2.3. These two groups are nearly the mirror images of each other about a vertical plane through the center of the reactor vessel. Line A corresponds to Line D and Line C corresponds to Line B. The material type is A106 Grade B. Each primary steam line originates from the reactor vessel upper cylindrical shell. Lines A and D have two safety-relief valves each, while Lines B and C have four. These safety-relief valves are provided with discharge piping to a pressure suppression chamber called the torus.

Downstream from the steam line header for the safety-relief valves, each of the primary steam lines has an isolation valve before passing through the drywell wall via a penetration assembly, which consists of head fittings, guard pipe and bellow to protect the integrity of the containment. In this study, we evaluate welds of the primary steam line inside the drywell and the welds before the first isolation valve outside the drywell. Therefore, no description of the primary steam lines beyond the drywell is given here. The pipe dimensions, material type and the weld numbers are presented in Table 2.3.

2.3 Feedwater Lines

The general arrangement of the feedwater system of the Brunswick Plant is shown in Fig. 2.4. It consists of two branches designated Loops A and B. These two branches are the mirror images of each other about a vertical plane passing through the axis of the reactor pressure vessel. There is no structural connection between these two branches. Each branch has an 18-inch diameter feedwater line, which penetrates the drywell wall. It has an isolation valve on either sides of the

drywell wall and a penetration assembly to maintain containment integrity. The 18-inch line splits out into two 12-inch lines which connect to the upper cylindrical shell of the reactor vessel. The relevant information about the system is presented in Table 2.3 along with the information about the primary steam lines.

Table 2-1. Pipe properties of the existing recirculation loops.

	Suction	Discharge	Header	Riser	Bypass
Nominal size (in)	28	28	22	12	4
Outside diam (in)	28.169	28.519	22.003	12.706	4.500
Wall thickness (in)	1.151	1.326	1.038	0.631	0.337
Material type	SA-240 Type 304 SS	SA-240 Type 304 SS	SA-240 Type 304 SS	SA-240 Type 304 SS	SA-376 Type 304 SS
Welds (per loop)	10	6	5	20	10

Table 2-2. Pipe properties of the replacement recirculation loops.

	Suction	Discharge	Header	Riser	Bypass
Nominal size (in)	28	28	22	12	n/a
Outside diam (in)	28.000	28.000	22.000	12.750	n/a
Wall thickness (in)	1.209	1.390	1.750	0.688	n/a
Material type	SA-358 Type 316 SS	SA-358 Type 316 SS	SA-358 Type 316 SS	SA-358 Type 316 SS	n/a
Welds (per loop)	11	5	2	12	n/a

Table 2-3. Pipe properties of the primary steam lines and the main feedwater lines.

	Main Steam*	Feedwater	
Nominal size (in)	24	18	12
Outside diam (in)	24.000	18.000	12.750
Wall thickness (in)	1.218	1.375	0.843
Material type	SA-106 Type B Seamless	SA-333 Grade 6	SA-333 Grade 6
Welds (per line)	16	13	16

* Branch "A"

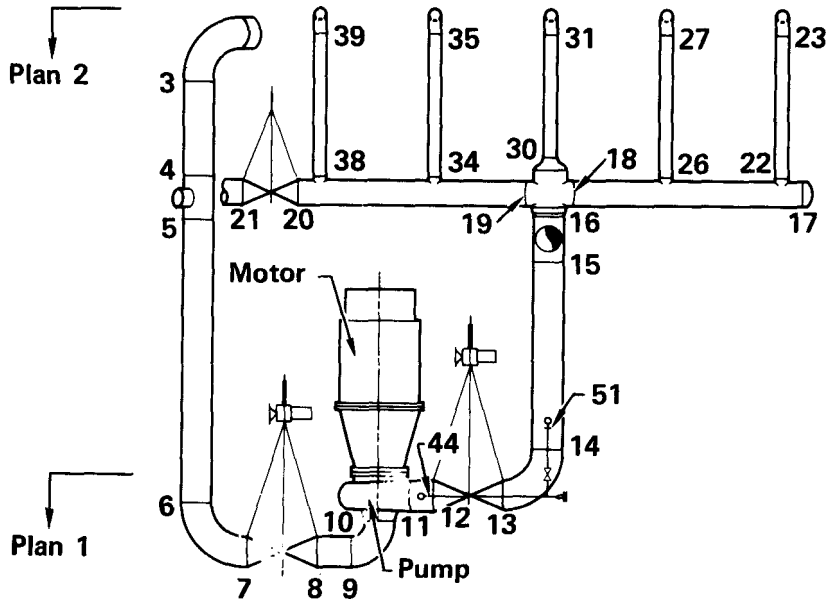

Elevation
Loop 'B'

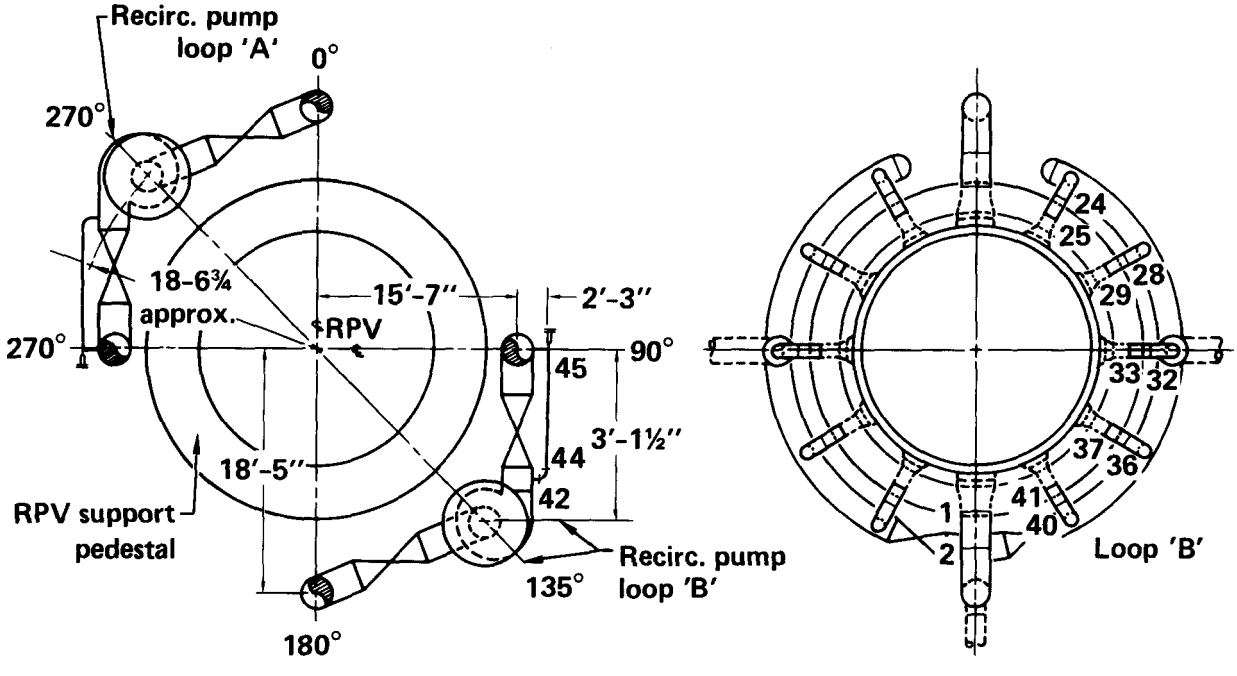

Plan 1

Plan 2

Figure 2.1. Existing Brunswick recirculation loops.

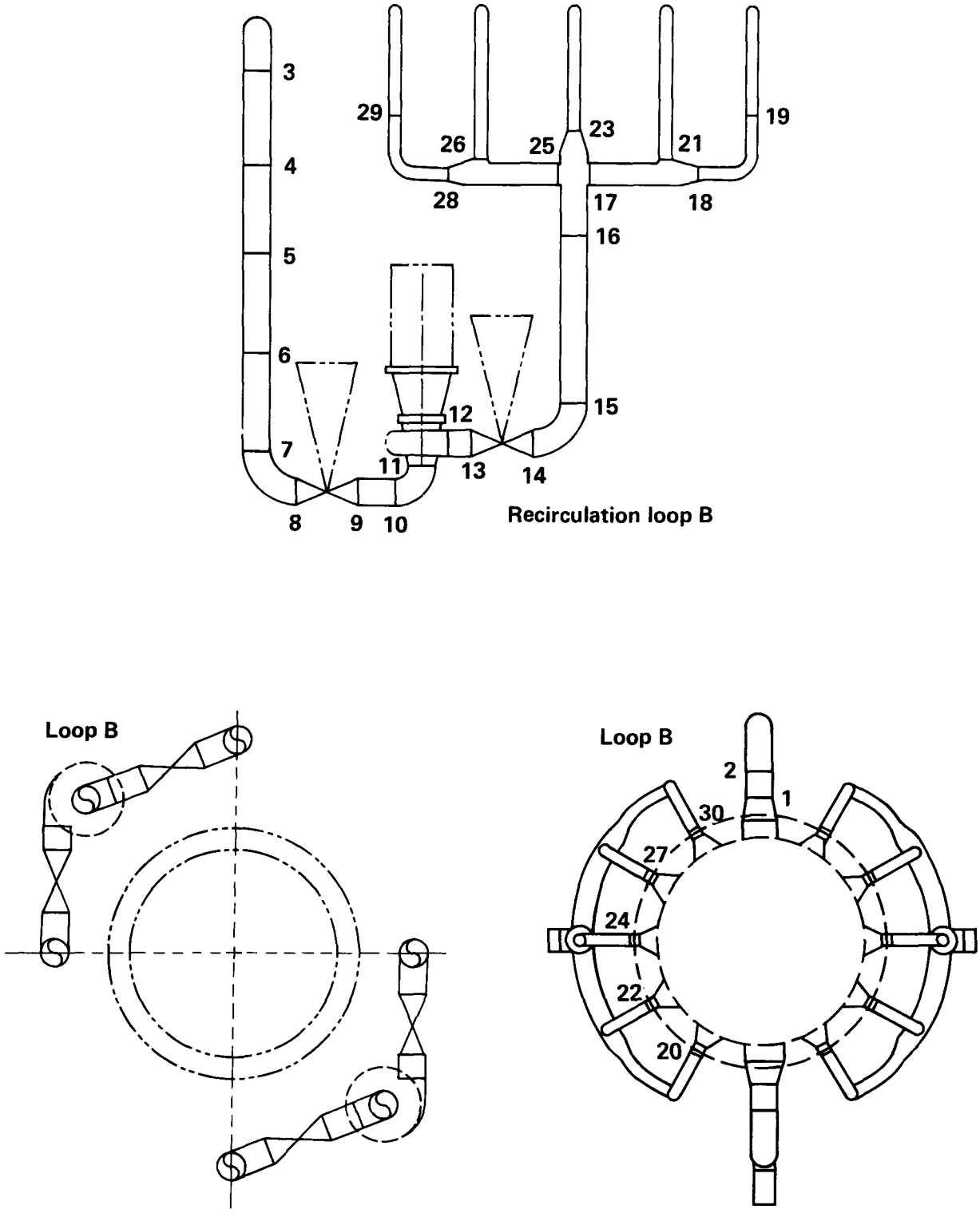

Figure 2.2. Proposed replacement system of the Brunswick recirculation loops.

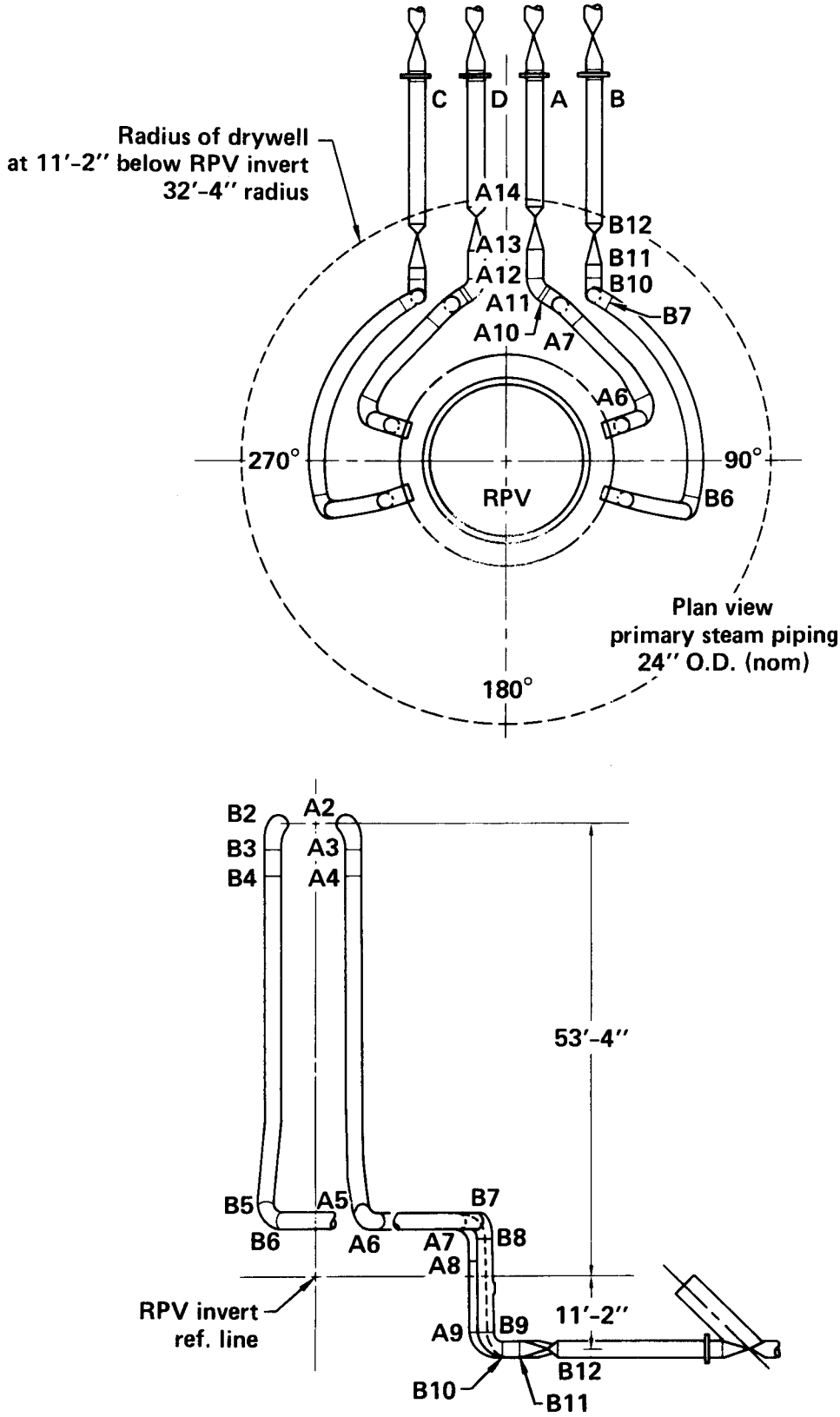

Figure 2.3. Brunswick main steam lines.

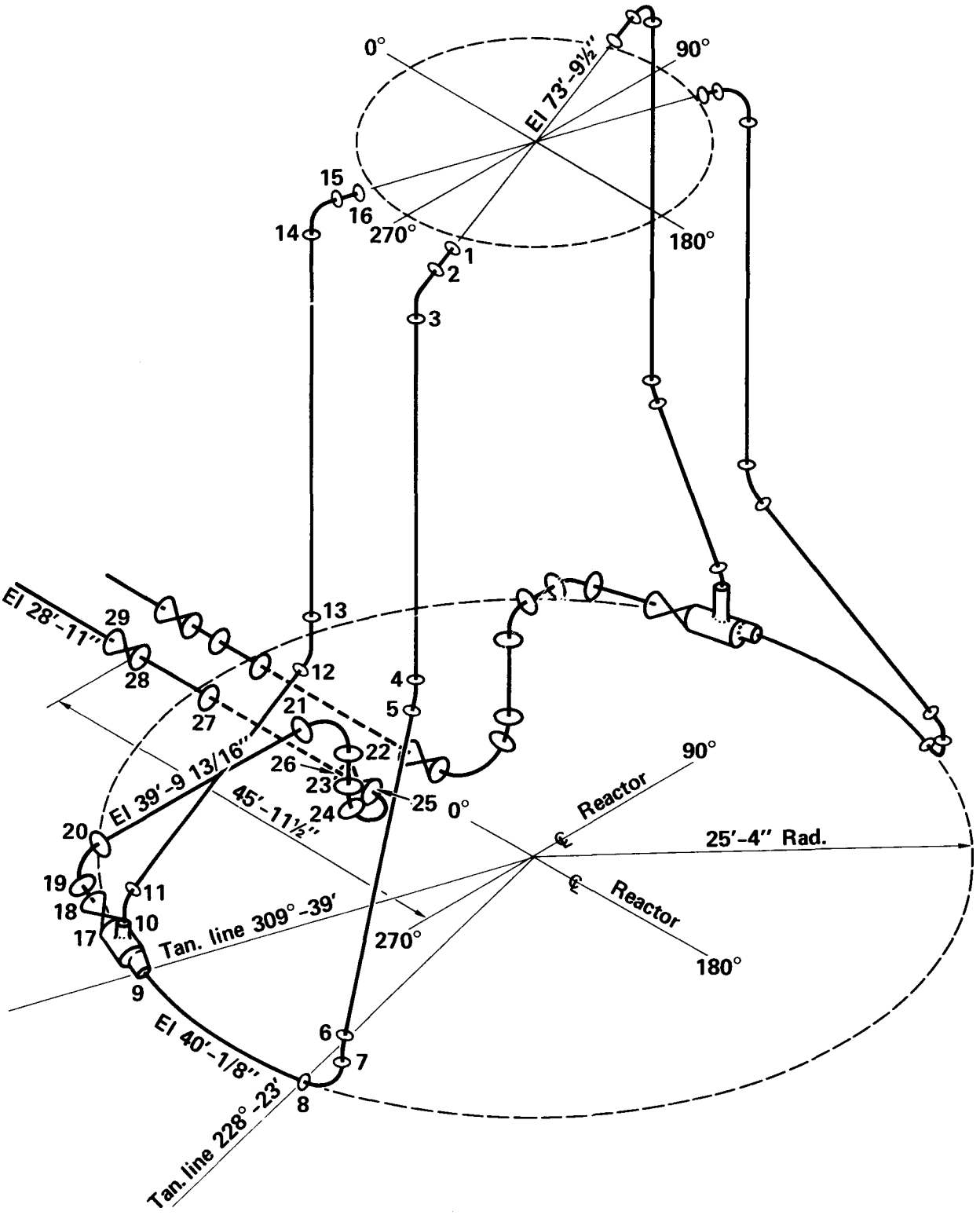

Figure 2.4. Brunswick main feedwater lines.

3. METHOD OF ANALYSIS

The effects of a seismic event on pipe failure probability were assessed in our two earlier studies: the direct and the indirect pipe failure analyses. In the direct pipe failure analysis, the effect of support failure is not addressed. Likewise, the indirect pipe failure analysis did not include the effect of existing cracks in the weld joints. A comprehensive probabilistic pipe failure analysis should merge the methodologies of the indirect analysis and the direct analysis. However, in practice, this merger is not always possible due to the constraints of time and resources. Besides, the margin of improvement in results might not be worth the additional effort. In this study, a great portion of the results is still based on our earlier approach of separating direct and indirect pipe failure analyses. However, a demonstrative combined analysis using the replacement recirculation loop system is performed and documented in Section 7. The results of this combined analysis will provide some valuable insight about the improvements and the amount of work involved.

The following paragraphs describe briefly the direct pipe failure analysis methodology. The indirect DEGB analysis is included in another volume of this report (Ref. 8.5) and will not be discussed here. The direct pipe failure analysis can be divided into two parts. The first involves the calculation of conditional leak or DEGB probabilities as functions of time at individual weld joints given the plant conditions such as the operating transients and the seismic events of specific intensities. The second part, "system failure" probability analysis, involves the estimation of a leak or a DEGB probability for the entire piping system, taking into consideration all of the associated weld joints.

3.1 Failure Probabilities of Individual Weld Joints

Figure 3.1 shows a flow chart of the first part of the probabilistic reliability assessment of a piping system. This analysis process slightly modifies our earlier work on the reactor coolant loops of PWR plants (Refs. 4.12, 4.14 and 4.16). In previous analyses, the failure is assumed to be due entirely to the growth of pre-existing cracks. The failure due to overstress was not addressed. The earlier approach is acceptable if the piping stresses are low compared to the ultimate strength of the pipe material. This situation is usually the case during normal operation of the plant. However, during an earthquake, the seismic stress depends on the earthquake intensity and can be very high if an earthquake of high intensity occurs. The most critical situation is that a support having a low fragility level would fail and, as a result, induce high seismic stress in the piping system.

In our previous study of RCLs of PWR plants, the pipes are supported by the in-line components (i.e., reactor pressure vessel, steam generators, and reactor coolant pumps); thus, there are no intermediate supports. We conservatively assumed in the indirect DEGB analysis that

the pipe failure probability is equal to unity given that the component support fails. We also observed in the direct DEGB assessment that the probability of seismically induced failure is usually many orders of magnitude lower than the effect of other events. We believe that there would be no significant increase in the probability of seismically induced failure even if the probability of overstress were taken into consideration. However, in this study, the failure due to overstress is considered even though the effect of the overstress might not be a significant factor. Considering the overstress in the piping system is essential in a combined direct and indirect analysis. This consideration will be demonstrated in Section 7 when the effects of intermediate support failure are examined.

The distance between weld joints is not great, and the stresses in these joints are a fairly good representation of the stress situation of the entire piping system. Besides, we assumed that flaws or cracks exist only at weld joints. Thus, it is more convenient to monitor the stresses at these limited locations rather than the entire piping system in calculating the pipe failure probabilities for the no-crack cases as well as the with-crack cases.

If cracks exist, the size of the cracks can increase either due to growth or due to instability under the existing loads in the system. Failure in one of the following two modes can occur as the crack size increases in both radial and circumferential directions:

1. The crack becomes through-wall and results in a leak.

2. The crack grows to a complete circumferential crack first before it goes through the wall. This results in a double-ended guillotine break (DEGB).

We used fracture mechanics theory to study the crack growth and the crack tip instability. This assessment is the complicated probabilistic fracture mechanics approach developed over the years at LLNL under the sponsorship of the U.S. NRC.

If no crack exists in a weld joint, the pipe would fail only if the combined stress exceeds the material's ultimate strength. This exceedance can easily be assessed by monitoring the stress level at individual weld joints, which were considered to be representative of the whole piping system as stated earlier. Failure probability can easily be calculated through the pipe stress and the probability distribution of the estimated ultimate strength of the material. The probability calculation for the no-crack case is straight forward and no detailed description is needed.

The probabilistic fracture mechanics methodology for individual weld joints was documented in detail in our previous reports (Refs. 4.12, 4.14, and 4.16). However, for completeness in this report, a brief review of the methodology is presented. Readers familiar with this methodology are urged to go directly to the next chapter.

For each weld joint of the piping system, a Monte Carlo simulation is used to calculate the conditional leak or DEGB probability at any specific time of the plant life. The weld joint was subjected to a stress history associated with plant events, such as the normal heatup or cooldown, the anticipated transients, and the occurrence of potential earthquakes.

The simulation starts with the random selection of sample crack sizes from a sampling space (Appendix A, Ref. 6.16) and the calculation of conditional probabilities associated with these crack sizes. Fracture mechanics theory is then applied to calculate the growth of these cracks and to determine if pipe fracture, i.e., either leak or DEGB, will occur as the cracks grow during the lifetime of the plant. Various parameters related to crack and leak detections, such as pre-service inspection, hydrostatic proof test, in-service inspections, and leak detection, are simulated. This simulation process is depicted in Fig. 3.2.

Fatigue crack growth takes into account the cyclic stress history of various thermal transients and postulated seismic events. The applied failure criteria involve either the critical net-section stress approach or the tearing modulus instability approach. The selected approach depends upon its applicability to the material characteristics and the geometric conditions of the pipe. The stress states of the plant vary as the various loading events occur throughout the plant life. Therefore, we monitor or calculate the state of the cracks, considering the effects of these loading events as time progresses. The time of occurrence of these loading events can be either deterministic or stochastic. In this study, we treat the seismic events as stochastic and assume that they are described by a Poisson process in calculating the system failure probability. Other plant transients are considered uniformly spaced through the life of the plant.

The occurrence interval of most of the significant plant events, such as the heatup and cooldown, are more or less uniform in nature. Other events are either insignificant, or a suitable event occurrence interval other than uniform can be found. The pre-service inspection was performed before the plant went into operation and was evaluated as such. In-service inspections were neglected in this study because inspection programs vary greatly from plant to plant, and they cannot be modeled with reasonable confidence. Not considering in-service inspection is conservative and consistent with our previous assessment of PWR plants.

Significant plant transients affecting the recirculation loops are discussed in Section 5. We believe that the pressure and temperature conditions for the primary steam lines and the feedwater lines are not significantly different from those of the recirculation loops during transients. Therefore, the same transient conditions were also used for these piping systems.

We assessed the effect of an earthquake of specific intensity on the conditional failure probability at each weld joint at specific times during the plant life. First, we determined the probability of failure with no seismic events. Then we imposed earthquakes of specified intensity, usually expressed in terms of peak ground accelerations, on normal operating conditions. The increase in the failure probability after the earthquake was added constitutes the contribution of the seismic event to the failure probability. This process was repeated for a wide range of earthquake intensities.

The above calculation procedure yields the conditional leak or DEGB probabilities (conditioned on the existence of a crack and on the occurrence of an earthquake of given intensity) as a function of time for a specific weld joint. This analytical process is repeated for all the welds in the piping system of interest.

3.2 Failure Probability of a Piping System

The results of the Monte Carlo simulation described in the previous section are the conditional failure probabilities of individual weld joints. These probabilities are conditional on the existence of a crack at the weld and the occurrence, at any specific time, of an earthquake with a specific peak ground acceleration. Earthquake intensities expressed as peak ground accelerations can range from zero to several times the safe shutdown earthquake value. Four scenarios ("events") are considered in calculating the system failure probability.

Event 1: One or more earthquakes occur during plant life; failure occurs simultaneously with the first earthquake (i.e. the earthquake causes failure).

Event 2: One or more earthquakes occur during plant life; failure occurs prior to the first earthquake (i.e. the earthquake does not cause failure).

Event 3: A failure occurs without any earthquake occurring during plant life.

Event 4: One or more earthquakes occur during plant life; failure occurs after the first earthquake.

Any of the above scenarios can imply system failure. Figure 3.3 graphically describes these four scenarios in terms of (a) the number of earthquakes occurring during the life of the plant and (b) the time of pipe failure relative to the time of the first earthquake.

We did not consider the probability of Scenario 4, because the plant would be shut down after an earthquake for complete inspection and repairs, and the plant condition would be altered by then. The technical details of the probability of these scenarios are in Vol. 7 of Ref. 4.12 and Appendix B of Ref. 4.16.

3.3 Uncertainty of Parameters

Two types of variability, or uncertainty, associated with each of the parameters are considered in this study. One type, random uncertainty, represents the inherent physical variation or randomness of the parameters. Modeling uncertainty, the other type, accounts for the lack of complete knowledge or detailed information about the probabilistic characteristics (distribution) of the parameters to describe them precisely. A detailed discussion of these two types of uncertainties can be found in Ref. 4.16 and will not be repeated here.

A deterministic value can often be used to represent a parameter if the variation is negligible; otherwise, a distribution is required. We used distributions to describe both the inherent randomness and the modeling uncertainty of many parameters. Since the random uncertainties of input parameters contribute to the value of the probability of pipe fracture, they are part of the pipe fracture analysis and are included in the calculation process shown in Fig. 3.2. Modeling uncertainties are treated in a different manner as presented in Section 6.2.

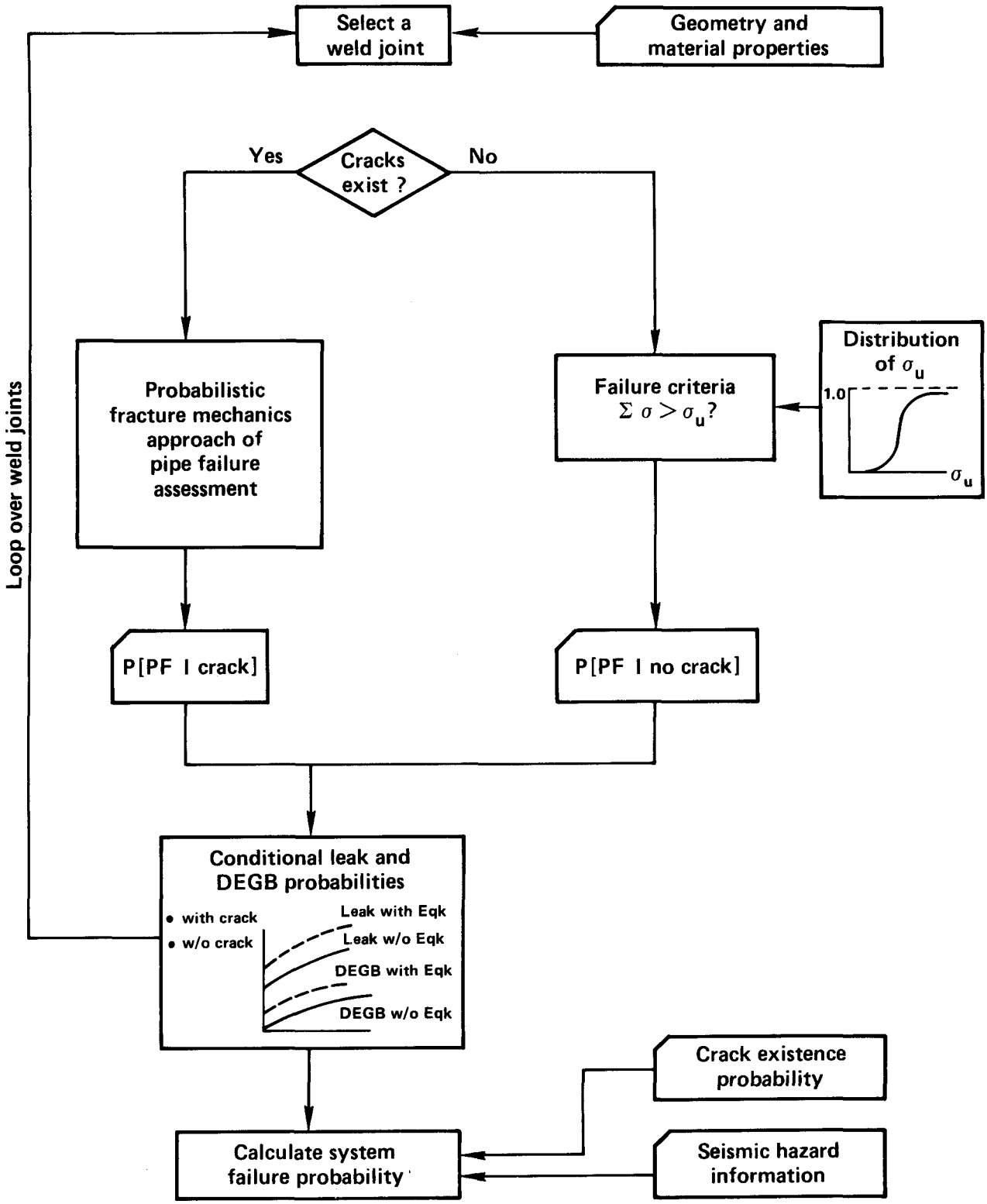

Figure 3.1. Flow chart for the probabilistic assessment of piping integrity.

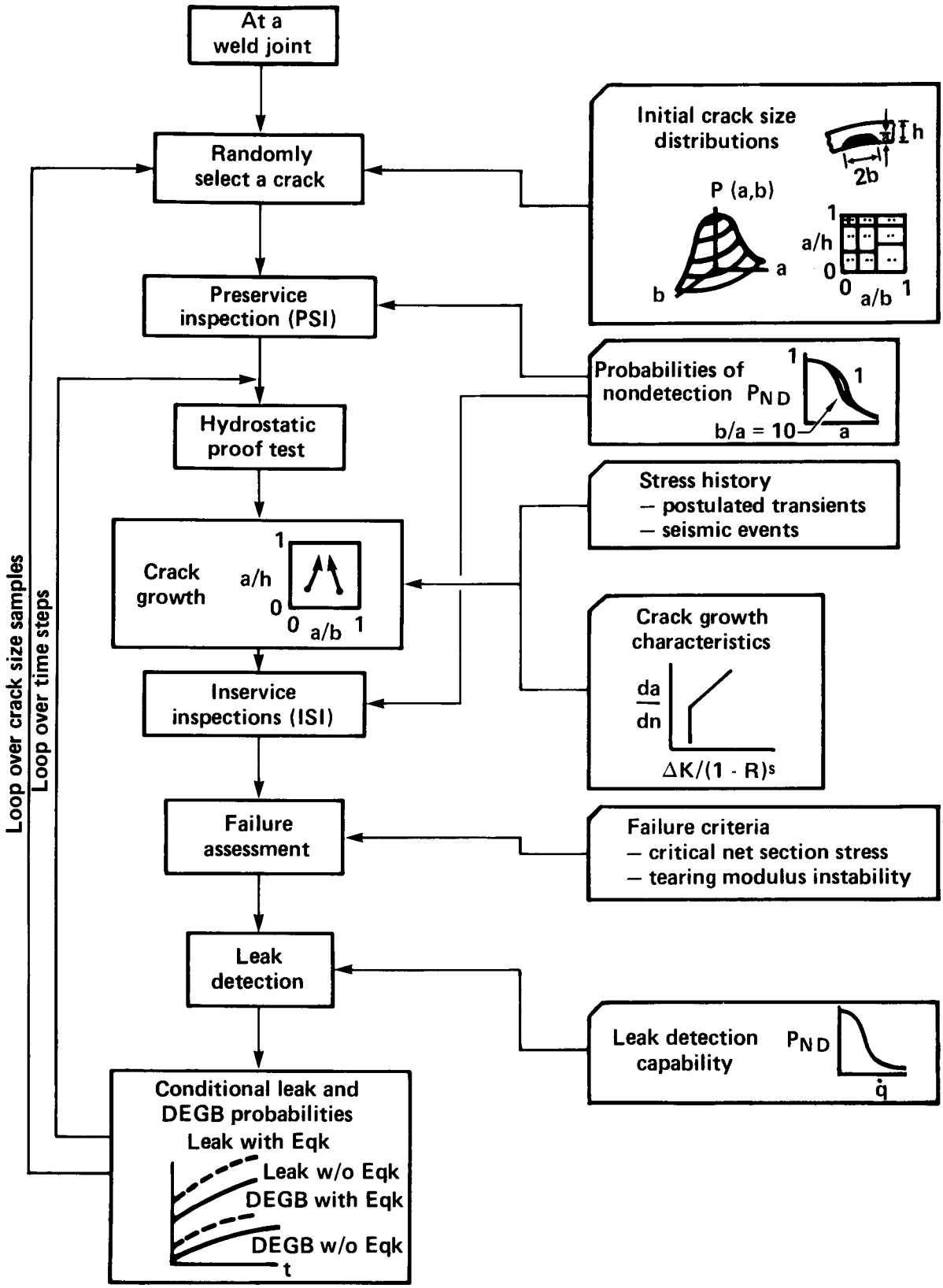

Figure 3.2. Methodology for using probabilistic fracture mechanics to assess pipe failure.

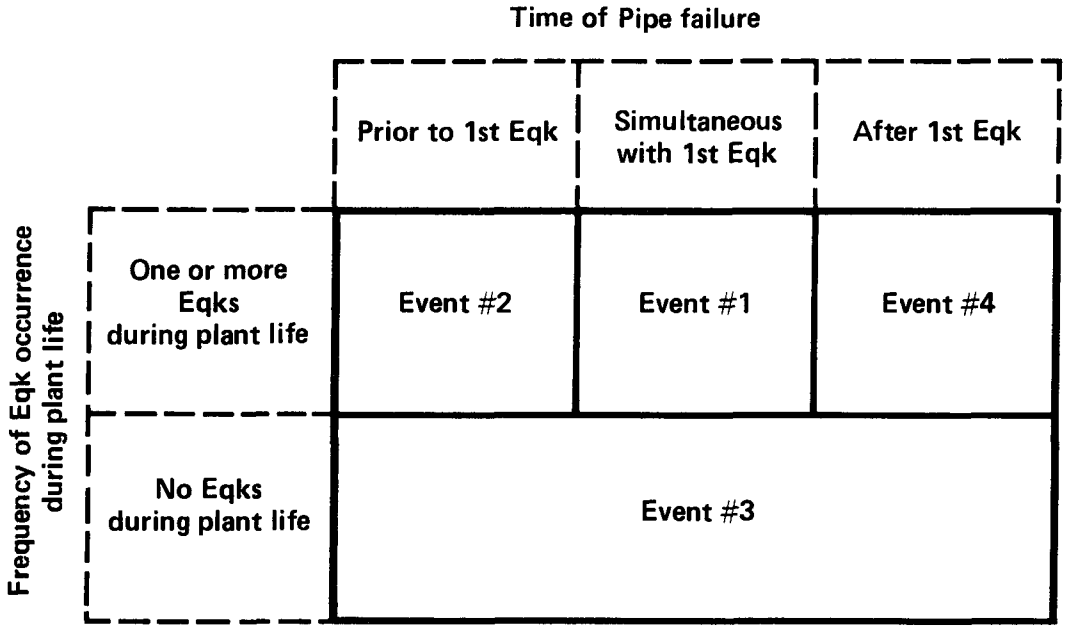

Figure 3.3. The Venn diagram of system failure.

4. INPUT INFORMATION AND SIMULATION MODELS

The following list is the input information needed for the probabilistic fracture mechanics assessment of piping integrity.

- material properties
- initial crack size distributions
- inspection detection probability
- loading conditions and loads
- crack growth characteristics
- failure criteria
- leak detection capability
- crack existence probability
- seismic hazard information

Table 4.1 presents a brief summary of this information and related simulation models. The following discussion describes this information in detail, except for loading conditions and loads which are discussed in Section 5.

4.1 Material Properties

SA-240 Type 304 stainless steel was used in the existing Brunswick recirculation loop piping. A replacement recirculation piping system using SA-358 Type 316 stainless steel aimed at IGSCC effects has been proposed by the Carolina Power & Light (CP&L) Company. A design analysis was carried out by the General Electric Company. SA-106 Type B and SA-333 Grade 6 carbon steels were used for the primary steam lines and the feedwater lines, respectively. Table 4.2 presents the yield strength, ultimate strength, and the flow stress of these materials between 400 ^{o}F and 600 ^{o}F, which is the approximate range of the operating temperature. These material properties were based on the statistical data presented in Refs. 4.1, 4.2 and 4.3 assuming a normal distribution. The mean values are close to the values given in Ref. 4.4. The flow stress is the average of the yield stress and the ultimate stress.

The stress-strain relationship and the fracture properties are two essential material properties in the assessment of crack stability using the tearing modulus approach (Section 4.5).

4.1.1 The Stress-Strain Relationship

To account for the non-linear behavior of materials in assessing crack stability problems, the following uniaxial stress-strain relationship is frequently used:

$$\frac{\epsilon}{\epsilon_0} = \frac{\sigma}{\sigma_0} + \alpha\left(\frac{\sigma}{\sigma_0}\right)^n \qquad (4\text{-}1)$$

This stress-strain relationship is sometimes referred to as the Ramberg-Osgood material model. The first term on the right represents the linear-elastic portion of material property, and the second term is associated with the fully plastic condition, where

σ_0 = a reference stress (usually the yield stress),

α = a material constant, and

n = the strain hardening exponent of the material
(σ_0 is related to ϵ_0 by $\epsilon_0 = \sigma_0 / \epsilon$.)

Figure 4.1 presents the stress-strain relationships of SA-106B carbon steel and Type 304 Stainless steel. The SA-106B curve was fitted in Ref. 4.5 to the Ramberg-Osgood model based on the information provided in Ref. 4.6. This curve was used also for the pipe material of the feedwater lines, which is SA-333 carbon steel. The stress-strain curve for Type 304 stainless steel is adopted from Ref. 4.7.

4.1.2 Fracture Properties

The other material property used to assess the crack instability problem is the J-resistance curve (or "J-R" curve). The J-R curve represents the material's resistance to crack extension, and it is a plot of the J-integral, J, versus the crack extension, da. J-R curves can be obtained from tests and are available in the literature for some material as described in Ref. 4.8. The corresponding J-T curve can be calculated once the J-R curve becomes available.

The variable T is another important parameter for assessing crack stability and is called the tearing modulus. The tearing modulus is the slope of the J-R curve, or dJ/da, normalized by a multiplication factor σ / ϵ_0^2 to render it dimensionless.

The J-T curves for Type 304 stainless steel and SA-106 Type B carbon steel were derived from the J-R curves documented in Refs. 4.8 and 4.9, respectively. These curves were for a temperature of 550 ^{o}F and were derived from the lowest J-R curve for conservatism. These J-T curves are presented in Figs. 4.2 and 4.3.

4.2 Initial Crack Size Distributions

In this study, we considered only circumferential cracks at the weld joints. Two-dimensional cracks of semi-elliptical shape on the interior pipe surface (as shown in Fig. 4.4) are assumed. We used two parameters to represent this crack shape. The first parameter is the crack depth a; the other is the crack aspect ratio β, which is defined as the ratio of the half crack length b to the crack depth (or b/a).

The randomness of these two shape parameters was modeled, and the modeling uncertainties associated with them were quantified.

4.2.1 Initial Crack Depth Distribution

Several distributions intended to model the inherent randomness of crack depth were proposed in various studies (Fig. 4.5). Here, we used the Marshall distribution (Ref. 4.10), which is considered very conservative. However, we modified it slightly to eliminate the physical impossibility of having a crack depth greater than the pipe thickness h. The modified Marshall distribution has the following marginal density function:

$$P(a) = \frac{e^{-a/\mu}}{\mu(1-e^{-h/\mu})} \qquad (4\text{-}2)$$

where:

$$0 \leq a \leq h$$

$$\mu = 0.246 \text{ in}$$

The modified Marshall distribution is considered in this study to be the best-estimate model of the crack depth distribution (Vol. 2 of Ref. 4.11). To account for the modeling uncertainty associated with using the Marshall distribution, we adopted a triangular distribution on the parameter $1/\mu$, considering $\mu = 0.246$ inches of the Marshall distribution as the median or the 50th percentile. As the upper bound, we used Eq. (4-2) with $1/\mu = 3$ to envelop the distributions proposed by several investigators. The value of $1/\mu$ for the lower bound crack depth distribution is selected as 5.0. The lower bound was conservative and discounted the distributions suggested by Wilson and by Becher and Hansen as indicated in Vol. 5 of Ref. 4.12. Figure 4.5 also shows the upper and lower bound curves.

4.2.2 Initial Crack Aspect Ratio Distribution

A truncated lognormal distribution with the probability density function shown as a solid line in Fig. 4.6a was used to model the randomness of the aspect ratio β (Vol. 5 of Ref. 4.12). The distribution with $\rho = 0.01$ was considered the best estimate model (Vol. 2 of Ref. 4.11). Here, ρ is defined as the percentage of cracks with β greater than 5 and is equal to the shaded area under the density function in Fig. 4.6a. To account for modeling uncertainty, the characteristic β_m was assumed to have a lognormal distribution with a median (or 50th percentile value) equal to the value of β_m corresponding to $\rho = 0.01$. The upper uncertainty limit on β_m was selected to correspond to $\rho = 0.1$. Figure 4.6b shows the complementary cumulative

marginal distributions of the crack aspect ratio corresponding to various uncertainty bounds of the modeling uncertainty.

4.3 Inspection Detection Probability

Ultrasonic examination is the most frequently used method of non-destructive inspection in nuclear power plant pipes. The probability of non-detection P_{ND} has been quantified in many studies (Refs. 4.12 and 4.13). Based on the available data, P_{ND} is adequately characterized by the following relationship:

$$P_{ND} = 1/2(1-\epsilon)\ \mathrm{ERFC}(\nu \ln[A/A']) + \epsilon \qquad (4\text{-}3)$$

where:

$A = \pi/4\ aD_B \quad (2b < D_B)$
$= \pi/2\ ab \quad (2b > D_B)$

D_B = ultrasonic beam diameter

$A' = \pi/4\ a'D_B$

$\nu = 1.33$ for carbon steel
$= 1.60$ for stainless steel

and ERFC is the complementary error function. A value of 0.005 is used for ϵ to represent the lower bound value of P_{ND}. A beam diameter of one inch was used. There is large modeling uncertainty in the ultrasonics detection. This modeling uncertainty was represented by a lognormally distributed parameter a' in this study as follows.

For wrought steel,

Median value of a' = 0.25
Logarithmic standard deviation $\beta = 1.25$.

For cast steel,

Median value of a' = 1.25
Logarithmic standard deviation $\beta = 1.25$.

In the existing recirculation loop piping, all Type 304 stainless steel piping is wrought except the bypass line, which is cast. For the replacement recirculation loops, the risers are cast Type 316 stainless steel and the rest of the piping is wrought. All primary steam and feedwater lines are wrought carbon steel. The effects on the non-detection probability due to these two different median values of a'

for wrought and cast steels are represented by the following ratio, which is plotted in Fig. 4.7 as a function of the crack depth a.

$$\text{Ratio} = P_{ND}(a'=1.25) \,/\, P_{ND}(a'=0.25) \qquad (4\text{-}4)$$

The ratio can be as high as two orders of magnitude in the non-detection probability.

4.4 Crack Growth Characteristics

The subcritical fatigue crack growth is an important phenomenon that leads to pipe failure under low-level cyclic stress conditions. The fatigue crack growth rate (da/dn) for both the stainless steel and the carbon and low-alloy ferritic steel can be characterized by the Paris model in terms of two important parameters: the cyclic stress intensity factor ΔK and the load ratio R.

4.4.1 Crack Growth Model of Stainless Steel

The fatigue crack growth model used in this report for the stainless steel is the same as that of Refs. 4.11 and 4.12. It follows the Paris model and can be represented by the following equation.

$$\frac{da}{dn} = C\,[K']^m \qquad (4\text{-}5)$$

where:

da/dn = fatigue crack growth rate (in/cycle)

K' = effective stress intensity factor
= $K/\sqrt{(1-R)}$

ΔK = cyclic stress intensity factor
= $K_{max} - K_{min}$ (ksi-√in)

R = load ratio = K_{min}/K_{max}

m = an empirical constant; m = 4 for stainless steel

C = a lognormally distributed empirical constant; for stainless steel, median = 9.14E-12, standard deviation = 2.2E-11, C = 0 for $K' < 4.6$ (ksi-√in).

This fatigue crack growth model along with the test data is shown in Fig. 4.8. This crack growth model was used previously in the evaluation of reactor coolant loops in Westinghouse plants.

4.4.2 Crack Growth of Ferritic Steel

The fatigue crack growth model used for the primary steam and the feedwater lines is a modified version of the reference fatigue crack growth model for carbon and low-alloy ferritic steel contained in Appendix A of Section XI of the ASME code. This modified growth model is represented in the following form (Ref. 4.14):

$$\frac{da}{dn} = Q\,[C\,\Delta K^{m}] \qquad (4\text{-}6)$$

where the expression inside the brackets represents the ASME Code reference fatigue crack growth model (Fig. 4.9) and is dependent on the value of the load ratio R. The multiplication factor Q is a log-normally distributed random variable. Values for the logarithmic mean and standard deviation of Q are listed in Table 4.3 for different values of R and ΔK.

This fatigue crack growth model was developed from the same data base as the ASME reference model. However, the ASME model was based on a 95% global confidence limit for the mean of the data and was intended to be conservative for design purposes (Ref. 4.15). The growth model used here and represented by Eq. (4-6) is the best-estimate model of the data with randomness characterized by Q. The ASME model is conservative by an approximate factor of 1.5 as compared to the median of Eq. (4-6). In this analysis, we used a threshold value of 2.58 ksi-$\sqrt{in}$ for K (Ref. 4.4), below which the crack growth rate is considered to be negligible. This crack growth model was used previously in the assessment of the reactor coolant loops of Combustion Engineering plants (Ref. 4.16).

4.5 Failure Criteria

Two criteria are available to assess the stability of crack growth in structures that are stressed beyond the region of applicability of linear-elastic fracture mechanics. One criterion is the critical net-section stress approach, and the other is the tearing modulus stability approach. These two failure criteria are discussed in the following subsections. A comparison of these two approaches in terms of their effects on the estimation of pipe failure probability is presented in Ref. 4.17.

4.5.1 Critical Net-Section Stress Approach

In the critical net section stress approach, a crack is considered to be unstable if the stress in the remaining ligament of pipe cross-section exceeds a specific uniform tensile stress, which is usually the flow stress, σ_f, i.e.

$$p_A > \sigma_f (A - A_c) \quad (4\text{-}7)$$

where p_A is the applied axial load on the cross-sectional area, A, of an uncracked pipe, and A_c is the area of the crack. The net-section stress approach is a simple and convenient method (Ref. 4.18). It is based on the experimental results of a center-cracked stainless steel panel in tension. The net-section stress approach, however, is applicable only to very ductile materials such as stainless steel.

The critical net section stress criterion described in Eq. (4-7) is for pipes under axial tension only. We developed another form for the net section stress approach considering both axial force and bending moment. A detailed description is presented in Appendix A. This new form also considers the true elliptical area of the crack geometry. The following paragraph briefly describes this new approach.

In this varied form of the net section stress approach, instability still occurs when the absolute stress in the remaining ligament exceeds the flow stress.

$$\sigma > \sigma_f \quad (4\text{-}8)$$

However, with a bending moment also considered in the loading, the stress on the section will go through the classical complete stress reversal found in plastic load limit analysis, with the exception that the maximum stress is not the yield stress but the flow stress.

The actual check is completed in two parts. The first part considers only the axial force given by Eq. (4-7) to determine if the pipe has become unstable, and therefore, has failed. If the pipe is not unstable, the axial force is used to obtain a stress reversal location at the instability limit. This calculation begins with the equation

$$p = \sigma_f (A_1 - A_2) \quad (4\text{-}9)$$

where:

p = the axial load

σ_f = the flow stress

A_1 = the area above the stress reversal point

A_2 = the area below the stress reversal point

These areas are further related by

$$A_1 + A_2 = A_{net} = A - A_c \tag{4-10}$$

A limiting moment can next be found based on the calculated stress reversal point and the remaining ligament geometry. This calculation converges in one iteration and accounts for crack closure in compression and for the integrations which cannot be obtained in closed form. The second part of the check then compares the actual applied moment to the calculated limiting moment.

$$M_{app} > M_{limit} \tag{4-11}$$

Two cases are checked because, for the applied axial load, two stress reversal points can generally be found depending on the direction of the limit moment.

4.5.2 Tearing Modulus Stability Approach

Unlike the critical net-section approach, the approach using the J-integral and the tearing modulus can be used to assess stability in both the radial and circumferential direction. Crack extension occurs when the J-integral at the crack front reaches the corresponding value of the material's J-resistance curve; i.e., when

$$J = J_{mat} \tag{4-12}$$

The above equilibrium condition does not imply instability. However, under this condition, crack instability is ensured when the applied tearing modulus exceeds the corresponding value of the J-resistance curve. That is when

$$T > T_{mat} \tag{4-13}$$

The tearing modulus T is the slope of the J versus crack extension curve multiplied by E/σ_0^2 to render it dimensionless; i.e.,

$$T = \frac{E}{\sigma_0^2} \left(\frac{\partial J}{\partial a}\right)_{\Delta T} \tag{4-14}$$

The subscript in Eq. (4-14) represents a partial derivative with ΔT fixed. The ΔT is the total displacement of the system including the cracked body and is defined as

$$\Delta T = \Delta + C_M P \tag{4-15}$$

where:

C_M = the compliance of the structure connected in series with the cracked body

P = the external load, and

Δ = the load point displacement of the cracked body.

Here Δ is equal to the sum of Δ_c, the load point displacement due to the crack, and Δ_{nc}, the displacement of the body without the crack in place. Using Eq. (4-15), the tearing modulus of Eq. (4-14) can be rewritten as

$$T = \frac{E}{\sigma_0^2} \left\{ \left(\frac{\partial J}{\partial a}\right)_p - \left(\frac{\partial J}{\partial p}\right)_a \left(\frac{\partial \Delta}{\partial a}\right)_p \left[C_M + \left(\frac{\partial \Delta}{\partial p}\right)_a\right]^{-1} \right\} \tag{4-16}$$

Instability in the radial direction results in a leak. However, instability in both radial and circumferential directions must exist for a DEGB to occur. The technical basis of the tearing modulus approach is sound. Unfortunately, calculating J and T is a complicated task and usually requires a finite element procedure. Obviously the finite element method is not practical within a Monte Carlo simulation where many crack samples are monitored for growth and stability. Tabulated solutions or solutions in functional form for J and T for various crack sizes and many loading conditions are needed for economy.

The J and T solutions for two-dimensional cracks shown as Case A in Fig. 4.10 are non-existent. Therefore, the stability assessment in the radial direction is based on tabulated results (Refs. 4.19 and 4.20) for part-through complete circumferential cracks (Case B). In the circumferential direction, the stability assessment is based on solutions (Ref. 4.21) for through-wall part-circumferential cracks (Case C). The following assumptions were made in order to use these results:

1. The J-integral and the tearing modulus in the radial direction of a two-dimensional crack with crack depth a and aspect ratio β are equal to the corresponding values of a part-through complete circumferential crack of the same depth a.

2. The J-integral and the tearing modulus in the circumferential direction of a two-dimensional crack with crack depth a and aspect ratio β are equal to the corresponding value of a through-wall part-circumferential crack with crack length equal to $2a\beta$.

These two assumptions are believed to be conservative because the J-integral solution for any two-dimensional crack is bounded by these two extreme conditions. Note also that these existing solutions are for straight-run pipes under uniaxial tension. This condition implies that conservative assumptions are needed to handle cases were bending moments exist.

4.6 Leak Detection Capability

In this study, a leak is considered to be detected once a crack results in 3 or more gpm of coolant leakage. Once the leak is detected, the crack is considered to be fixed, and we assume that neither further crack growth nor failure will occur. The calculation then continues for the next crack in the Monte Carlo simulation process. The method of calculating crack opening and coolant flow is documented in Ref. 4.12.

4.7 Crack Existence Probability

We calculated the crack existence probability based on the assumption that the cracks in weld joints occur as events of a Poisson process (Vol. 7 of Ref. 4.12). The existence probability of exactly n cracks can be represented as follows:

$$P_n = (v\ \lambda_v)^n\ e^{-(v\ \lambda_v)}/\ n! \qquad (4\text{-}17)$$

where v is the weld volume of a weld joint, and λ_v is the rate of cracks per unit volume. A value of 1.0E-4 per cubic inch is a reasonable estimate for λ_v. Since the probability of two or more cracks existing in a weld is small compared to the existence probability of one crack (P_1) for typical reactor coolant loop weld joints, we considered only singular cracks in this study. Due to the large uncertainty of this parameter, we assume that the modeling uncertainty of the crack existence probability can be is described by a lognormal distribution and that the median value is 1.0E-4 per cubic inch and the 90th percentile of the modeling uncertainty is 5.0E-4.

4.8 Seismic Hazard Information

There are three areas of interest in addressing the problem of seismic hazard. One area is the probability of earthquakes of specific magnitude or intensity at the plant site. This probability is usually represented by hazard curves. Another area is associated with the occurrence of a specific number of earthquakes during a given observation period. The third area is the characterization of the free-

field ground motion of an earthquake, which is usually characterized as the time history or response spectrum with a specific peak ground acceleration (PGA). The first two areas are discussed here; the third is included in Section 5.

4.8.1 Seismic Hazard Curves

To assess the seismic effect, seismic hazard curves are used to model the frequency of occurrence of earthquakes of different intensity. Randomness of earthquake magnitude is typically modeled by plots of annual frequency of exceedance vs. peak ground acceleration. Since we usually know very little about the frequency of earthquakes (especially high intensity earthquakes) of different magnitudes at the site of interest. Quantification of modeling uncertainty is essential. Modeling uncertainty is generally represented by hazard curves with the various subjective probabilities corresponding to different percentiles of the distribution. The best-estimate seismic hazard curve is the median, or 50th percentile, hazard curve.

Generic and site-specific seismic hazard curves were used in our previous studies (Refs. 4.14 and 4.16). Based on existing site-specific hazard curves from six plants located east of the Rocky Mountains, generic seismic hazard curves for eastern United States (Fig. 4.11) were developed and used in those studies for plants located east of the Rocky Mountains that did not have site-specific seismic hazard curves. We used these generic seismic hazard curves for the Brunswick Plant for the same reason.

4.8.2 Probability of Earthquake Occurrence

Earthquakes are usually assumed to occur as events of a stationary Poisson process. The probability of exactly n earthquakes occurring during a time interval of length t years is given by

$$P_n = (\lambda_0 t)^n \, e^{-\lambda_0 t} / n! \qquad (4\text{-}18)$$

where λ_0 is the expected frequency of earthquakes per year and n = 0, 1, 2, ... Based on Eq. (4-18), it can be proven (see Ref. 4.12, Vol. 7) that the time to the first earthquake is an exponential random variable having a probability density function equal to $\lambda_0 \exp(-\lambda_0 t)$, $t > 0$.

4.9 Other Input

The hydrostatic proof tests were assumed to be performed during plant shut down when no load except dead weight exists in the piping. The in-service inspection is neglected in this study because such inspection programs vary greatly from plant to plant; they cannot be modeled with reasonable confidence. We get conservative results by not taking into account the effect of in-service inspection.

REFERENCES

4.1 G.V. Smith, "An Evaluation of the Yield, Tensile, Creep, and Rupture Strengths of Wrought 304, 316, 321, and 347 Stainless Steels at Elevated Temperatures," ASTM Data Series DS 5S2, American Society for Testing and Materials, 1969.

4.2 W.F. Simmons and J.A. Van Echo, "The Elevated-Temperature Properties of Stainless Steels," ASTM Data Series DS5-S1, American Society for Testing and Materials, 1965.

4.3 W.F. Simmons and H.C. Cross, "Elevated-Temperature Properties of Carbon Steels," ASTM Special Tech. Publ. No. 180, American Society for Testing and Materials, 1955.

4.4 M.E. Mayfield, T.P. Forte, E.C. Rodabaugh, B.N. Leis, and R.J. Eiber, **Cold Leg Integrity Evaluation**, Battelle Columbus Laboratories, Columbus, OH, prepared for the U.S. Nuclear Regulatory Commission, NUREG/CR-1319 (February 1980).

4.5 D.O. Harris, **J-Integral and Tearing Modulus Expressions for Circumferential Cracks in Pipes**, Failure Analysis Associates, Palo Alto, CA, FME-R-4/PA07442, prepared for the Lawrence Livermore National Laboratory (December 1983).

4.6 D. Weinstein, M.T. Wang. J.D. Heald, and A.E. Pickett, "Carbon Steel in the BWR: Evaluation of Piping Steels in High Temperature Water Environment," Corrosion Advisory Committee Workshop: Stress Corrosion and Corrosion Fatigue of Carbon and Low Alloy Steels, hosted by the Electric Power Research Institute, Palo Alto, California, May 1979.

4.7 M.D. German, W.R. Andrews, V. Kumar, C.F. Shih, H.G. deLorenzi, and D.F. Mowbray, **Elastic-Plastic Fracture Analysis Steel Pipes**, General Electric Company, Schenectady, NY, prepared for Electric Power Research Institute, Palo Alto, CA, EPRI NP-2608-LD, Sept. 1982.

4.8 K.H. Cotter, H. Chang, and A. Zahoor, **Application of Tearing Modulus Stability Concepts to Nuclear Piping**, Fracture Proof Design Corporation, prepared for BWR Owners'Group and Electric Power Research Institute, February, 1982.

4.9 M.F. Kanninen, G.M. Wilkowski, J. Pan, J. Ahmad, C.W. Marschall, E. R. Gilbert, C. H. Popelar, and D. Broek, **The Development of a Plan for the Assessment of Degraded Nuclear Piping by Experimentation and Tearing Instability Fracture Mechanics Analysis**, Battelle Columbus Laboratories, prepared for the U.S. Nuclear Regulatory Commission, NUREG/CR-3142, June 1983.

4.10 W. Marshall, **An Assessment of the Integrity of PWR Pressure Vessels**, report by a study group chaired by Marshall, HM Stationery Office, London, Oct. 1976.

4.11 **Probability of Pipe Failure in the Reactor Coolant Loop Piping of Westinghouse Plants**, Lawrence Livermore National Laboratory, Report UCID-19988, NUREG/CR-3660, Vols. 1-3 (1984).

4.12 **Probability of Pipe Fracture in the Primary Coolant Loop of a PWR Plant**, Lawrence Livermore National Laboratory, Report UCID-18967, NUREG/CR-2189, Vols. 1-9 (September 1981).

4.13 D.O. Harris, **The Influence of Crack Growth Kinetics and Inspection on the Integrity of Sensitized BWR Piping Welds**, Science Applications, Inc. Palo Alto, CA, prepared for Electric Power Research Institute, Palo Alto, CA, EPRI NP-1163, Sept. 1979.

4.14 H.H. Woo, **The Impact of In-service Inspection on the Reliability of Nuclear Piping**, Lawrence Livermore National Laboratory, Report UCRL-19725 (December 1983).

4.15 W.H. Benford, "Technical Basis for Revised Reference Crack Growth Rate Curves for Pressure Boundary Steels in LWR Environment," Journal of Pressure Vessel Technology, 102, (1980).

4.16 T. Lo, R.W. Mensing, H.H. Woo, and G.S. Holman, **Probabilitiy of Pipe Failure in the Reactor Coolant Loops of Combustion Engineering PWR Plants; Volume 2: Pipe Failure Induced by Crack Growth**, Lawrence Livermore National Laboratory, Report UCRL-53500, NUREG/CR-3663 (January 1984).

4.17 T. Lo, "Failure Criteria Used in a Probabilistic Fracture Mechanics Code," Lawrence Livermore National Laboratory, UCRL-91242, presented at the 8th International Conference on Structural Mechanics in Reactor Technology, Brussels, Belgium, August 19-23, 1985.

4.18 E. Smith, "Application of The Net-Section Stress Approach to Pipe Failure," International Journal of Pressure Vessel & Piping, 10, (1982).

4.19 C.F. Shih, M.D. German, and V. Kumar, "An Engineering Approach for Examining Crack Growth and Stability in Flawed Structures," International Journal of Pressure Vessel & Piping, 9, (1981).

4.20 V. Kumar, M.D. German, and C.F. Shih, **An Engineering Approach for Elastic-Plastic Fracture Analysis**, General Electric Company, Schenectady, NY, prepared for Electric Power Research Institute, Palo Alto, CA, EPRI NP-1931, July 1981.

4.21 V. Kumar, M.D. German, W.W. Wilkening, W.R. Andrews, H.G. deLorenzi, and D.F. Mowbray, **Advances in Elastic-Plastic Fracture Analysis**, General Electric Company, Schenectady, NY, prepared for the Electric Power Research Institute, Palo Alto, CA, NP-3607, August, 1984.

Table 4.1. Input information and simulation models for the probabilistic fracture mechanics approach.

Piping material		Type 316 or 304 Stainless Steel	SA-106 Type B SA-333 Grade 6 Ferritic Steel
Initial crack size distribution	Depth, a (*,+)	Random -- modified Marshall dist. (Fig. 4.5) Modeling -- triangular distribution (Fig. 4.5)	
	Aspect ratio, β (*,+)	Random -- truncated lognormal (Fig. 4.6a) Modeling -- lognormal (Fig. 4.6b)	
Probability of non-detection (+)		$P_{ND} = 1/2\ (1-\epsilon)\ ERFC\ (\nu \ln A/A') + \epsilon$ $= 1.33;\ \epsilon = 0.005$ $A' = 0.785a'D$ (D = ultrasonic beam diameter) $a' = 0.25$ (Wrought steel) $\nu = 1.25$ (Cast steel) $A = 0.785aD$ (2b < D) $= 1.571ab$ (2b > D)	
Dead weight, pressure, thermal expansion+, seismic (*,+)		Random -- lognormal Modeling -- lognormal	Random -- lognormal Modeling -- lognormal
Crack growth model (*)		Fig. 4.8	Fig. 4.9 & Table 4.3
Failure criteria		Critical net section stress	Tearing modular instability
Minimum detectable leak rate		3 gpm	3 gpm
Crack existence probability (*,+)		Poisson distribution with rate parameter equal to 1.0E-4 per cubic inch of weld volume	
Seismic occurrence probability		Poisson distribution	Poisson distribution
Seismic hazard curves (*,+)		Generic (Fig. 4.11)	Generic (Fig. 4.11)

* Distribution was used in representing random uncertainty
\+ Modeling uncertainty was considered

Table 4.2. Yield strength, ultimate strength, and flow stress of pipe material at elevated temperature (400-600 oF).

Distribution	Yield Strength (ksi)		Ultimate Strength (ksi)		Flow Stress (ksi)	
	Mean	Std Dev	Mean	Std Dev	Mean	Std Dev
Type 304 Stainless Steel	23.5	4.0	63.0	4.4	43.0	4.2
Type 316 Stainless Steel	21.6	3.7	68.1	4.8	44.9	4.3
A106 Grade B, A333 Grade 6 Carbon Steel	30.0	4.7	70.0	7.6	50.0	6.2

Table 4.3. Constants associated with the random variable Q in the fatigue crack growth model for carbon and low-alloy steels.

Ranges for R and K*	Mean of ln Q	Standard Deviation of ln Q
$R \leq 0.25$		
$\Delta K < 19$	-0.408	0.542
$\Delta K \geq 19$	-0.408	0.542
$R \geq 0.65$		
$\Delta K < 12$	-0.367	0.817
$\Delta K \geq 12$	-0.367	0.817
$0.65 > R > 0.25$		
$\Delta K < 12 + 7W$	$-0.367W - 0.408W'$	$0.817 + 0.542W'$
$\Delta K \geq 12 + 7W$	$-0.367W - 0.408W'$	$0.817 + 0.542W'$

where: $W = (R - 0.25)/0.4$
$W' = 1 - W$

* ranges for R and ΔK correspond to ASME reference fatigue crack growth curves for carbon and low-alloy ferritic steels (see Fig. 4.9).

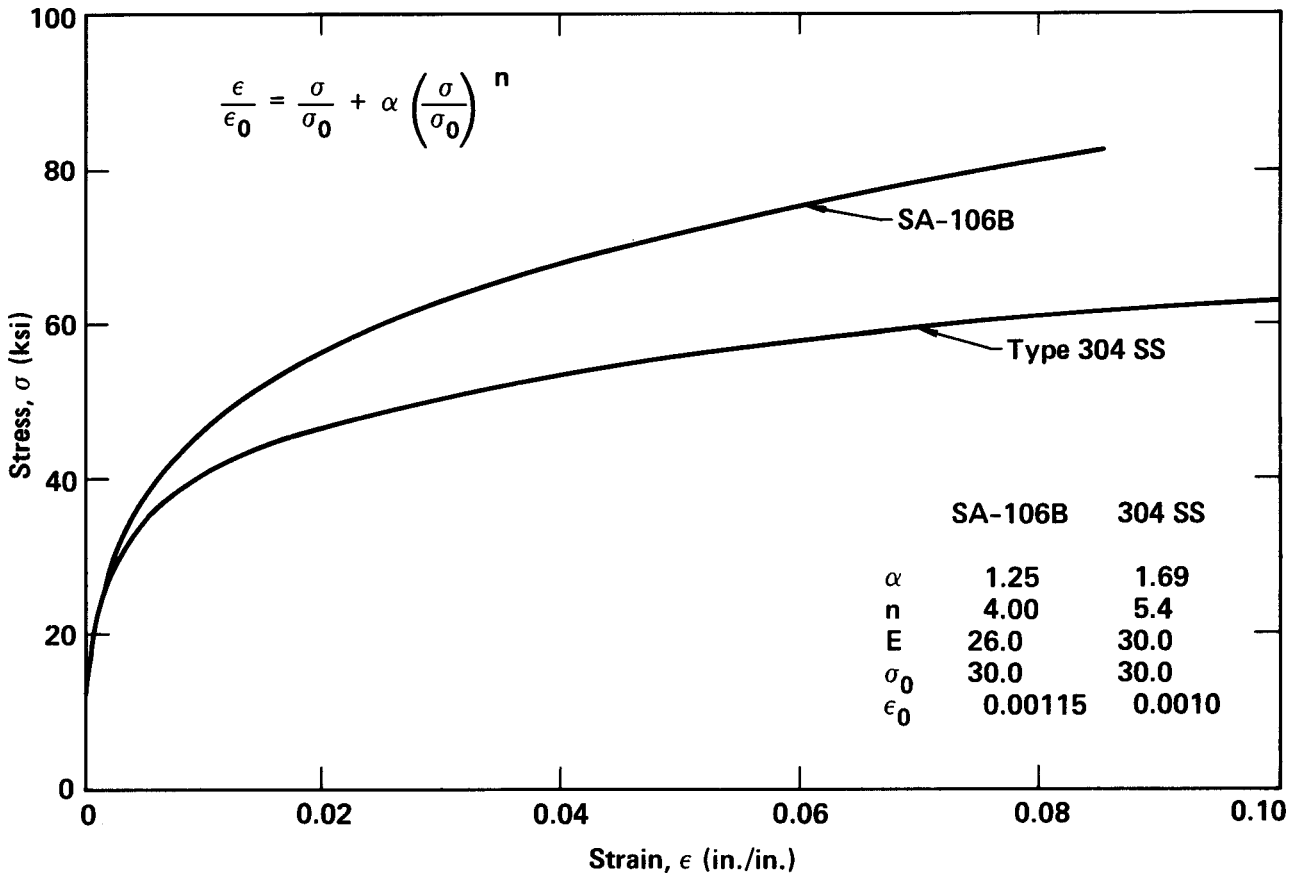

Figure 4.1. Stress-strain relationships of Type 304 stainless steel and SA-106B carbon steel.

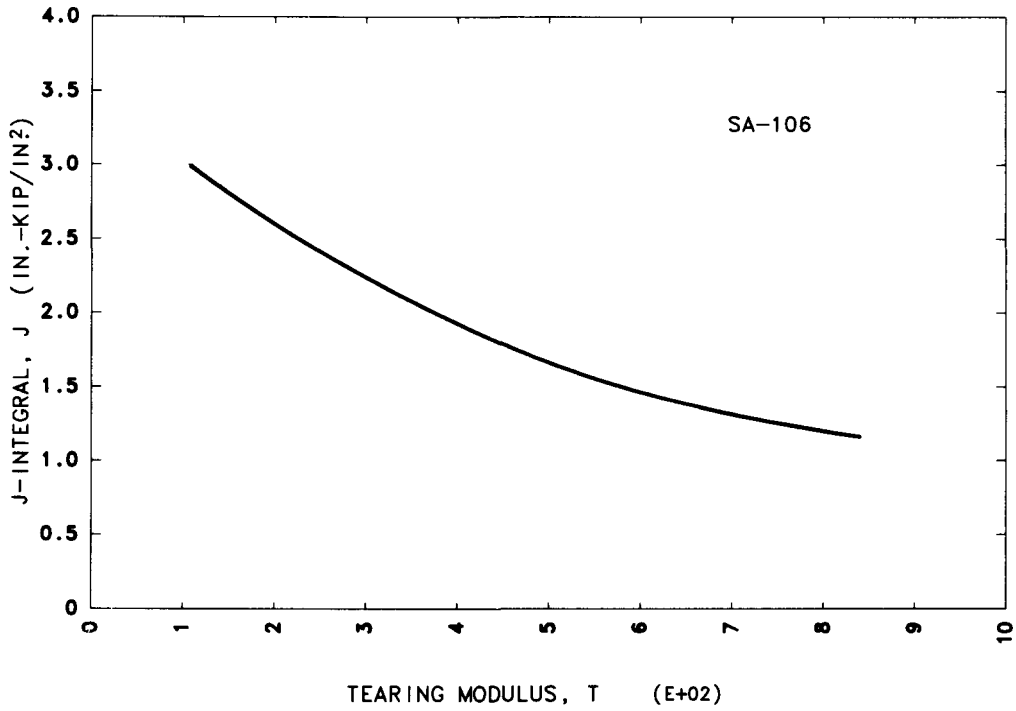

Figure 4.2. Stability diagram of SA-106B carbon steel.

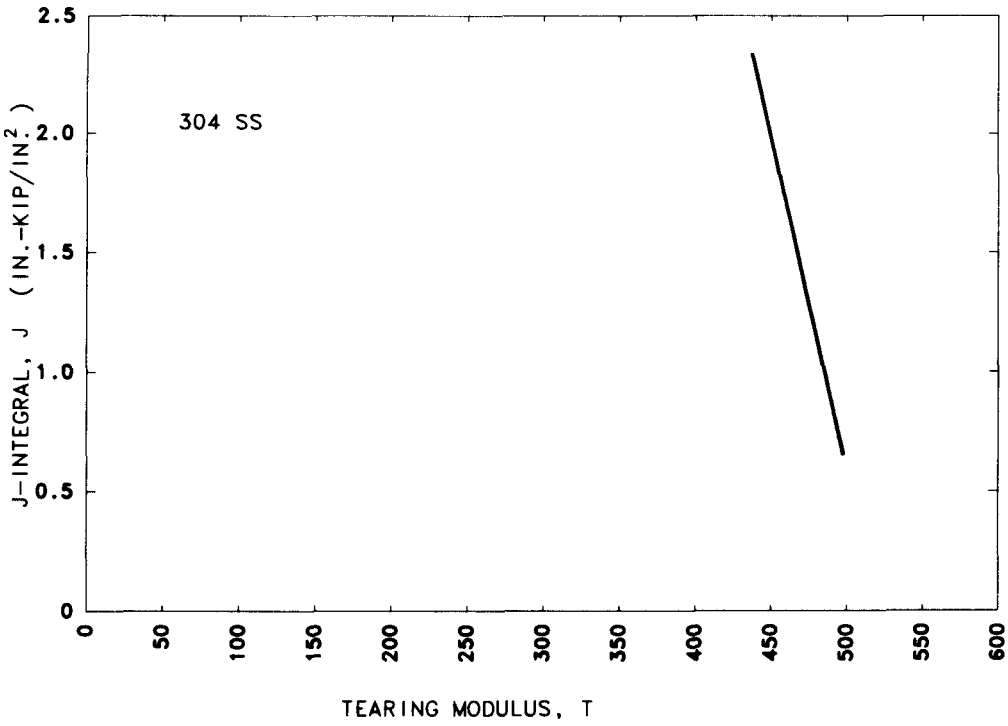

Figure 4.3. Stability diagram of Type 304 stainless steel.

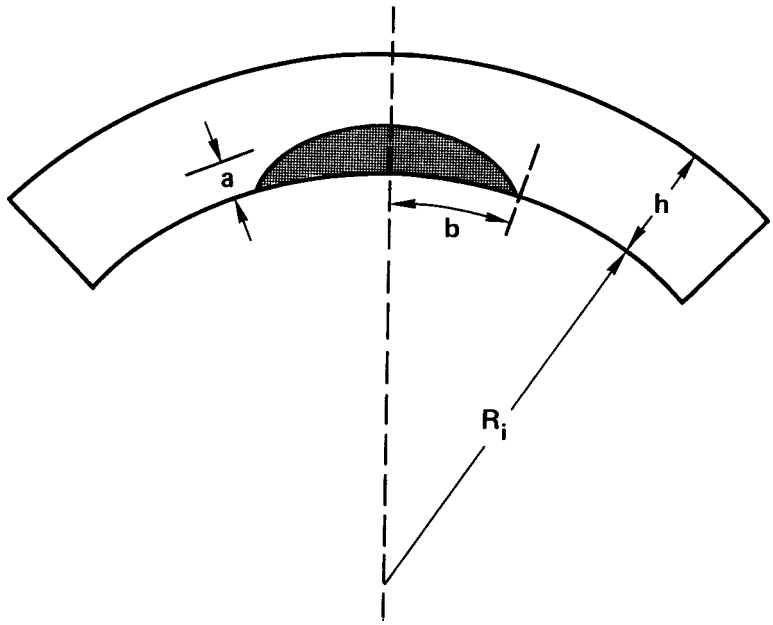

Figure 4.4. Geometry of a semi-elliptical inner surface crack.

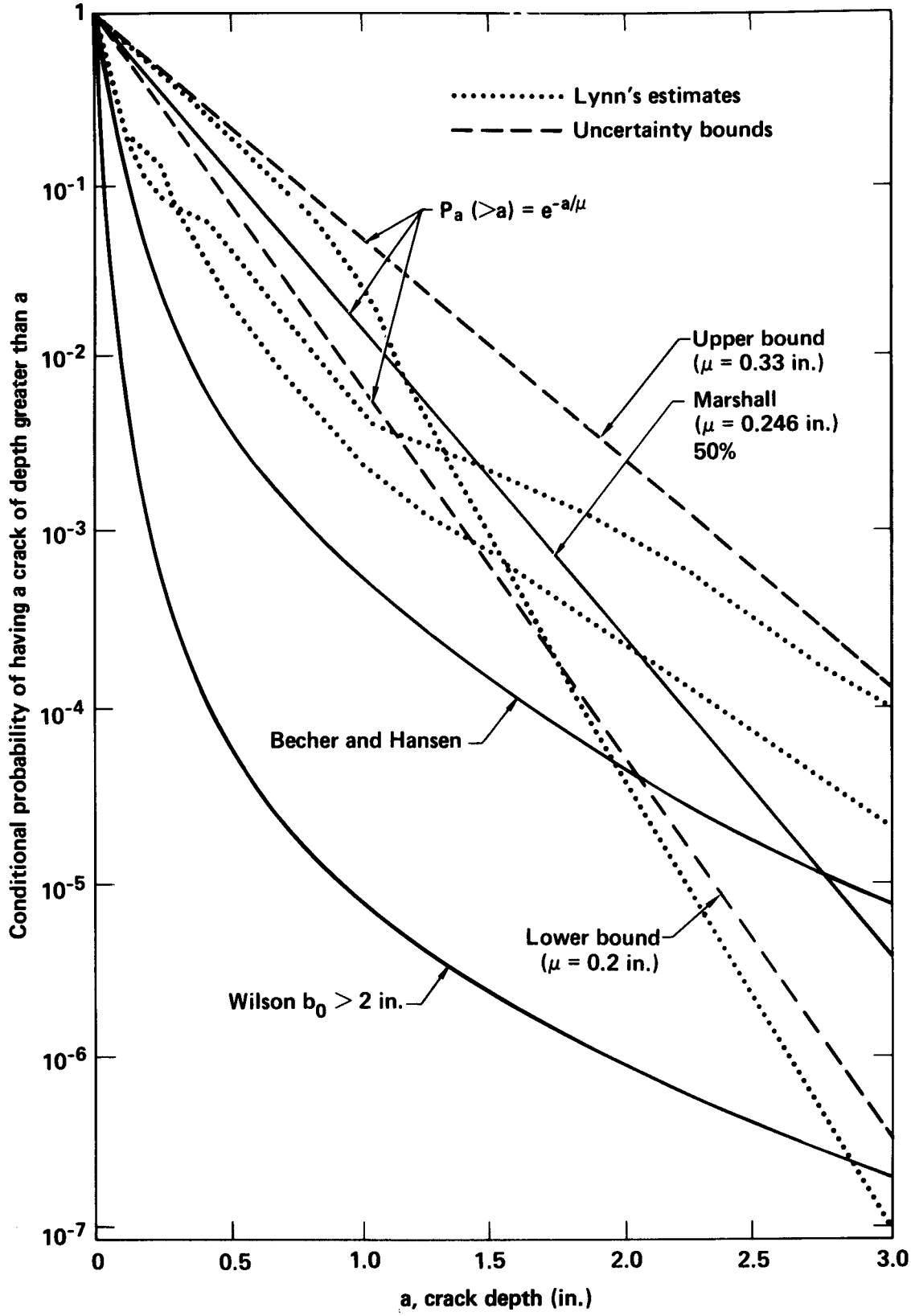

Figure 4.5. Various complementary cumulative marginal crack depth distributions.

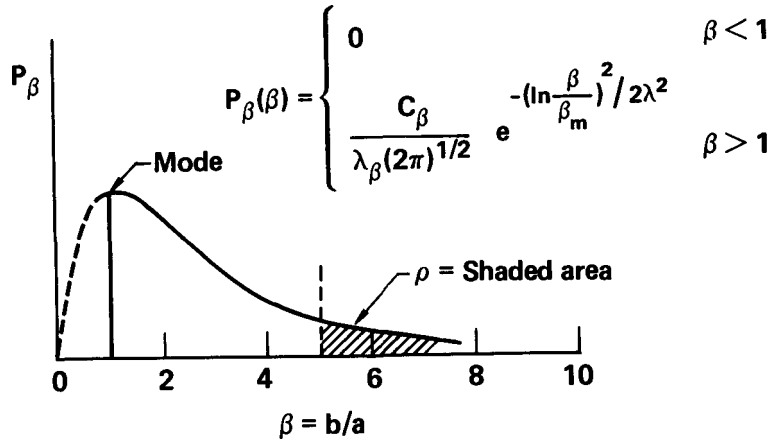

Figure 4.6a. Truncated lognormal distribution for the crack aspect ratio.

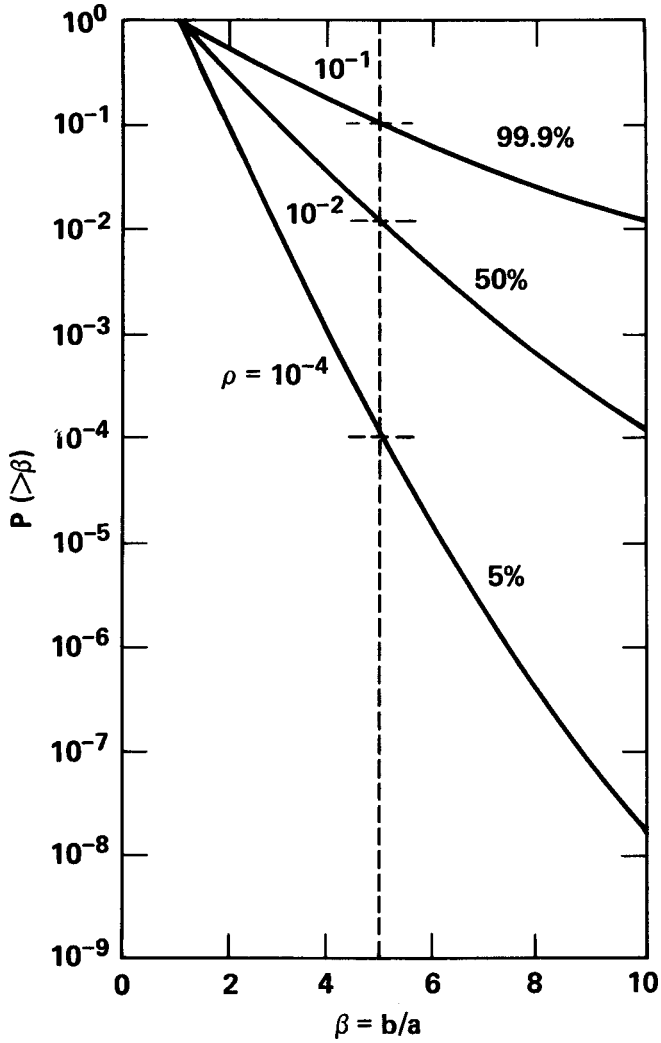

Figure 4.6b. Various complementary cumulative marginal distributions for the crack aspect ratio.

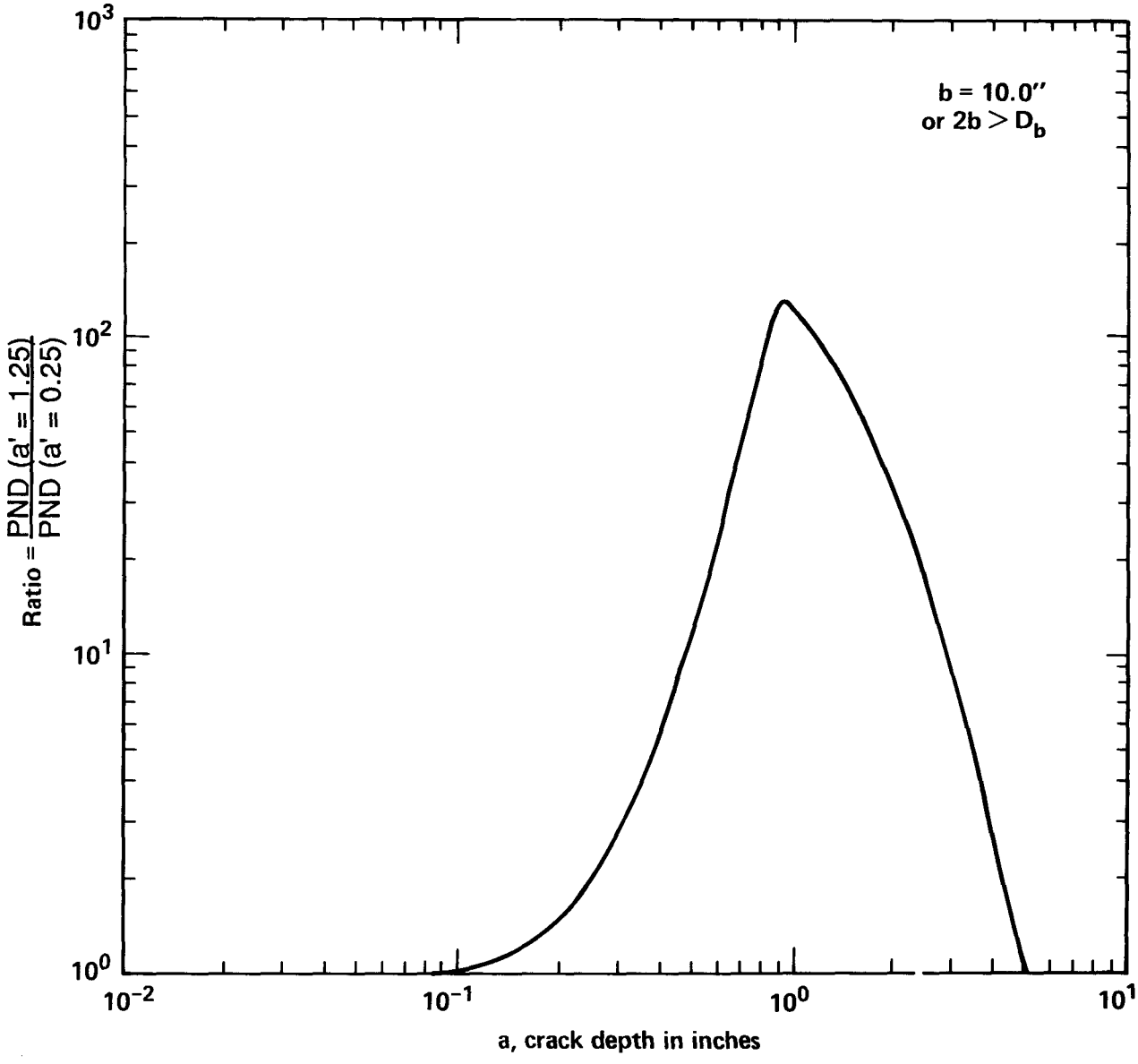

Figure 4.7. The ratio of the wrought steel and cast steel non-detection probability models.

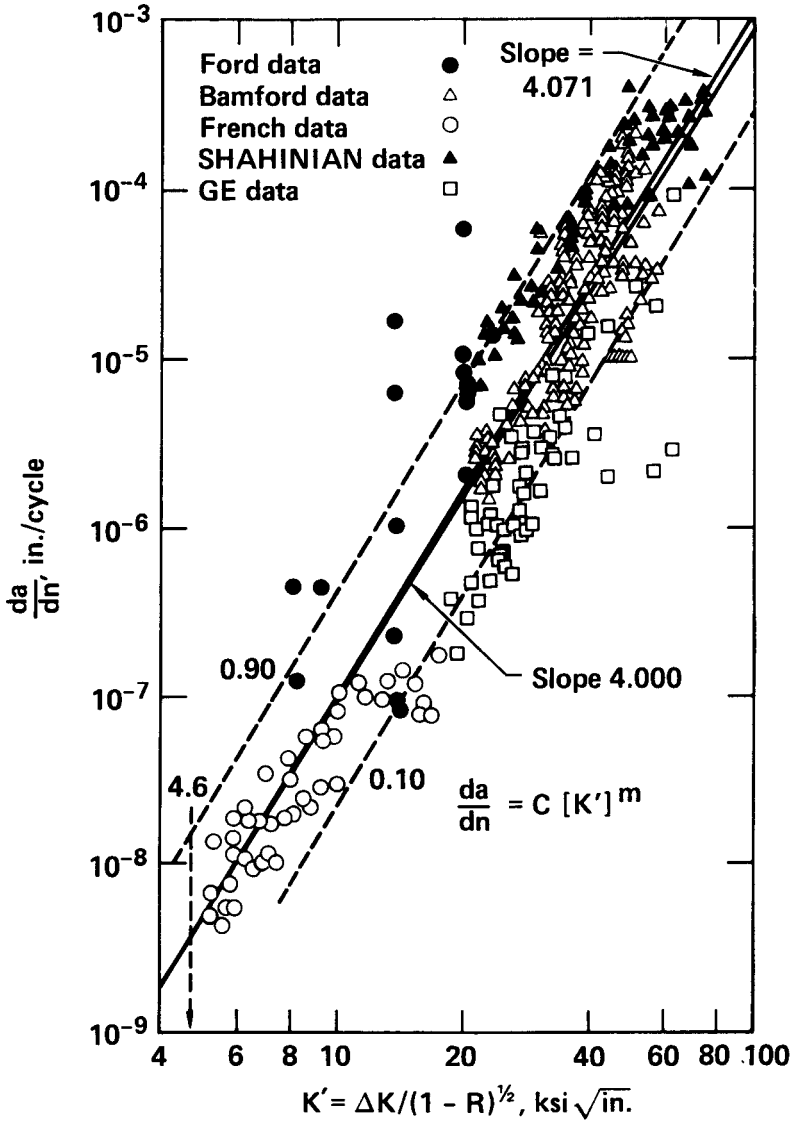

Figure 4.8. Fatigue crack growth rate data and the least-square fit model.

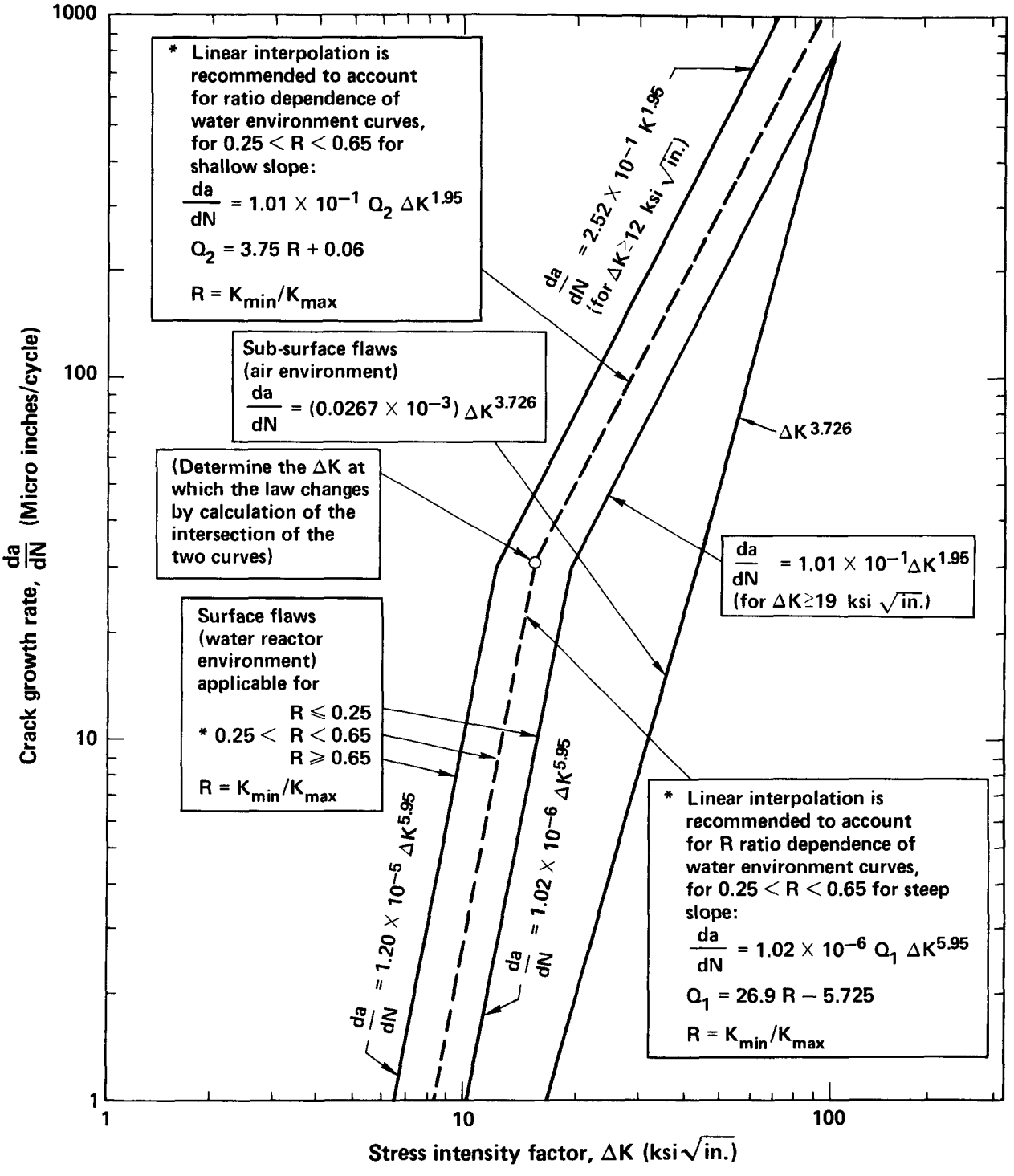

Figure 4.9. ASME reference fatigue crack growth curves for carbon and low-alloy ferritic steels.

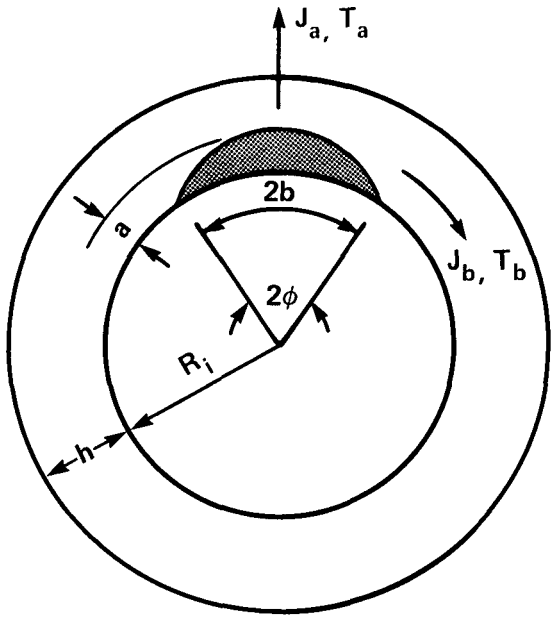

(a)

Assumptions

1. $J_a = J'_a$
   $T_a = T'_a$

2. $J_b = J'_b$
   $T_b = T'_b$

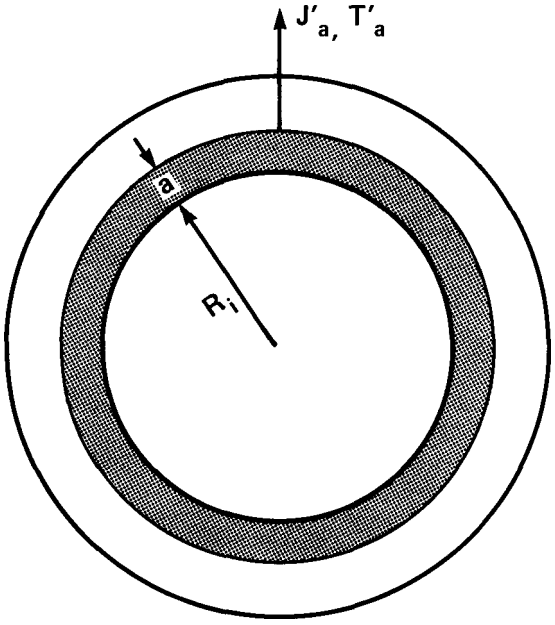

(b)

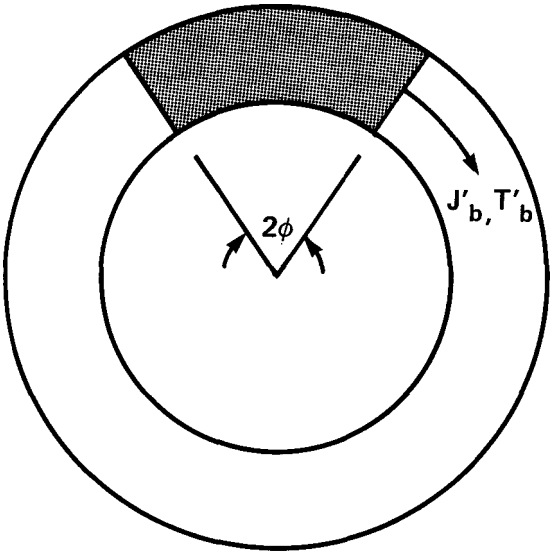

(c)

Figure 4.10 Postulated geometries for (a) two-dimensional cracks, (b) part-through complete circumferential cracks, and (c) through-wall part-circumferential crakcs.

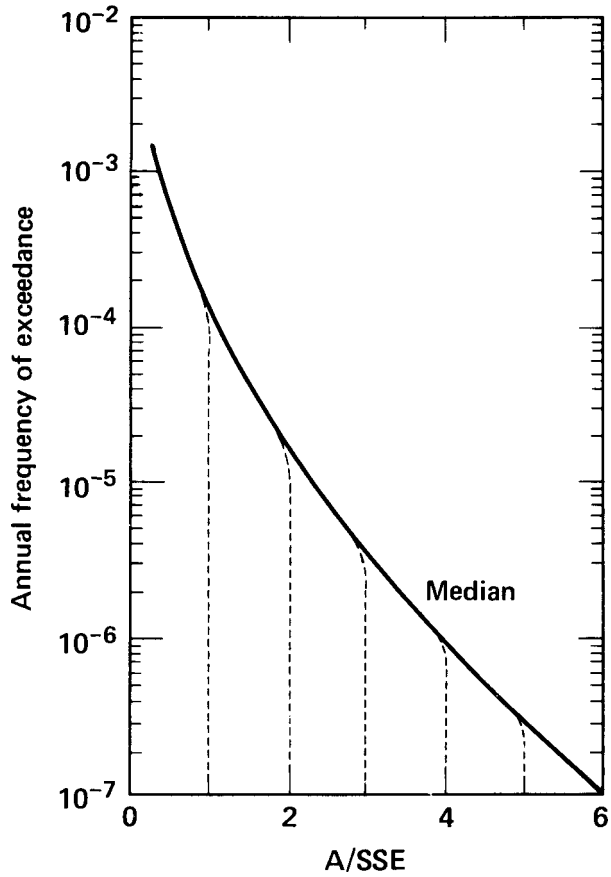

Figure 4.11. Generic seismic hazard curves for sites east of the Rocky Mountains. The dashed lines represent truncations at the indicated maximum PGA levels.

5. LOADING CONDITIONS AND THE LOADS

5.1 Loading Conditions

The loads of interest in this study are (1) dead weight, (2) the pressure and thermal expansion loads due to various loading conditions such as the normal and the postulated plant transients or conditions, and (3) the seismic events. These three load parameters are important to crack growth and pipe failure. Table 5.1 presents the maximum pressure and temperature variations for the recirculation loops due to the postulated plant transients or plant conditions along with the number of the expected lifetime occurrences of these transients. These transient conditions were used for design purpose, and the actual plant condition will most likely be less severe. Therefore, we believe that using Table 5.1 as the expected plant transients or conditions in this piping reliability assessment is conservative and sufficient for our purpose. The transient conditions for the primary steam and the feedwater lines are not expected to vary significantly from those of the recirculation loops. We therefore used the same set of transient conditions for the evaluation of the primary steam lines and the feedwater lines.

According to Table 5.1, the startup and the shutdown transients are the most severe transients or plant conditions in terms of the variations of maximum temperature and pressure, and the number of cycles in the lifetime of the plant. Other transients have low values in at least one of the three parameters important to crack growth and pipe failure. In this study, we considered the startup and the shutdown transients only. However, the number of cycles of these events is increased by one-third to 160 cycles to cover the effects of other plant transients or events for conservatism. The one-third factor is judgmental, and no justification is given here.

5.2 Description of Loads

The loading conditions considered in this study are dead weight, pressure and thermal loads due to normal plant operation and various postulated transients, and seismic loads. There are two types of thermal loads. One is the uniform stress through the pipe wall thickness due to the thermal expansion along the pipe axis; the other is the stress caused by the thermal gradient across the thickness of the pipe. We refer to the later as the radial gradient thermal stress or simply gradient thermal stress. In previous studies (Refs. 4.12, 4.14, and 4.16), we found that the radial gradient thermal stress was not significant and was neglected. Since the thicknesses of the pipes of interest in the Brunswick Plant are much thinner than those of the RCLs in the PWR plants, the radial gradient thermal stress was not expected to be a significant factor and was therefore again neglected. Therefore, our evaluation considered only the uniform thermal expansion stresses.

Carolina Power & Light (CP&L) Company provided all the loads except some of the seismic loads. The dead weight and the pressure loads were used without any modification since they were calculated using straight forward calculation methods or finite element analyses and were believed to contain a limited amount of conservatism.

Throughout this study, we considered only the normal stresses since they are oriented in the direction to most influence crack growth and instability for circumferential cracks. For crack growth calculations, we calculated the maximum principal stress resulting from the axial force, and the bending and torsional moments for each loading condition. We assumed that the calculated principal stress was normal to the pipe cross-section. The maximum normal stresses thus calculated at the extreme fiber of the pipe were further assumed to act over the entire cross-section of the pipe. Thus, we ignored the stress variations along the circumference which result from bending.

For the failure assessment, axial force and bending moment are used as described in Section 4.6. In both the crack growth and the failure assessments, we used the worst combination of signs of the moments due to different loads.

5.2.1 Dead Weight and Pressure Loads

Dead weight is generally not a dominating load compared with other loads in the piping system design. The pressure load was calculated as $pR_i^2/2R_m h$, where p is the internal coolant pressure, h is the thickness of the pipe, and R_i and R_m are the inside radius and the mean radius. We neglected the variability of the dead load and the pressure load.

5.2.2 Uniform Thermal Expansion Loads

We believe that the thermal stresses calculated by design engineers are usually conservative, and that uncertainty exists in these calculated stresses and is mainly due to the difference in assumptions and calculation methods used by different engineers. We therefore made two assumptions (Refs. 4.14 and 4.16) regarding uniform thermal expansion stress:

1. The variation in the calculated thermal expansion stress can be described by a lognormal distribution with a median equal to 80% of the design value.

2. There is only a 10% probability that the true thermal stress exceeds the design.

The median, or the 50th percentile of the modeling uncertainty, is considered our best-estimate model of the thermal stress. No random uncertainty is considered in this case.

5.2.3 Seismic Loads

The calculation of seismic loads, or stresses, is much more complicated than that of other loads. It involves a chain of methodologies: the characterization of free-field ground motion, soil-structure interaction, structural response, and subsystem response. Large random and modeling uncertainties exist in each link of the seismic methodology chain. Due to the complexity of the analyses and the associate large uncertainties, design engineers make conservative assumptions along each step of the methodology chain. It is important to estimate the realistic seismic responses and to quantify their uncertainty. The CP&L seismic results are for two levels of earthquake intensities: the operating basis earthquake (OBE) and the safe shutdown earthquake (SSE). In this study, we consider a wide spectrum of earthquake intensities varying from as low as a quarter of the OBE to as high as five times the SSE and, therefore, we need to estimate the seismic responses of this whole seismic range accordingly.

Our method of estimating the realistic seismic responses for a wide range of seismic intensities uses structural response factors. The basic idea of this method is to estimate both the conservatism that the engineers incorporated in their design calculation processes and the uncertainties associated with the calculated values. In this method, we estimated the structural response factors, or the median response factors, and the associated statistical distribution parameters representing both the random and modeling uncertainties. The best-estimate structural response is the ratio of the calculated response to the median response factor. The median response factors represent the conservatism of the methodologies that the design engineers used in calculating seismic responses. This method has been used frequently in the seismic risk assessment of nuclear power facilities.

The seismic responses were calculated in a long chain of methodologies. The calculation starts with the characterization of free-field ground motion and followed in sequence by the soil-structure interaction, the structural responses, and the piping and component responses. Because of the large conservatism that engineers incorporated in their design calculations, it is not unusual that the best-estimate response values can be a factor of five, or sometimes even be one order of magnitude, lower than the calculated values for a given earthquake intensity. The following section gives a brief overview of this estimation method.

5.2.3.1 Seismic Response Estimation Methodology

The median seismic response factor F_R of a piping system or a component relates the <u>actual</u> capacity of that piping system or component to resist seismic loads as compared to its <u>design</u> capacity. In short, the seismic response factor is a measure of the margin of conservatism inherent in the design process. The seismic response factor is the product of a structural response factor F_{RS} and a subsystem response factor F_{RP}, i.e.

$$F_R = F_{RS} * F_{RP} \quad (5\text{-}1)$$

The seismic response factor and the structural response factor are themselves each a product of a series of response factors representing various important parameters in the seismic methodology chain. The following subsections explain the structural response and subsystem response factors.

5.2.3.2 Structural Response Factors

Several important parameters are included in estimating the structural response factor. These parameters are associated with the design ground motion spectrum, the synthetic time history, the soil-structure interaction, the structural damping, and the modeling technique of the structure. Thus the structural response factor, F_{RS}, is the product of factors representing the effects of these parameters:

$$F_{RS} = F_G * F_{SA} * F_{SSI} * F_D * F_{MODEL} \quad (5\text{-}2)$$

Each of these factors is discussed below.

F_G The Ground Motion Factor accounts for the variability in the design ground motion versus the best-estimate ground motion for the Brunswick site.

F_{SA} The Spectral Shape Factor represents the margin of conservatism of the synthetic time history over the design ground spectrum.

F_{SSI} The Soil-Structure Interaction Factor accounts for the effect of the variability in the soil-structure interaction analysis technique on the calculated floor response spectrum.

F_D The Structural Damping Factor accounts for how variability of structural damping affects the structural response.

F_{MODEL} The Structural Modeling Factor accounts for the effects of the structural modeling technique on the structural responses.

Under contract to LLNL, NCT Engineering made a detailed evaluation of all these parameters and estimated the statistical value of these factors for Unit 2 of the Brunswick plant (Ref. 5.1). Table 5.2 summarizes the results. Two assumed best-estimate structural damping values are considered. Case (a) has 7% and 10% of critical structural damping for horizontal and vertical responses, respectively, and is more conservative than Case (b) of 10% and 15%. In this study, we used the more conservative set of dampings given in Case (a).

5.2.3.3 Subsystem Response Factor

As with the structural response factor, the subsystem response factor is a product of a set of factors representing the effects of many important parameters. These factors are the spectral shape factor, F_{SA}, the piping damping factor, F_D, the piping modeling factor, F_{MODEL}, and the analysis methodology factor, F_{METHOD}. The formulation is as follows:

$$F_{RP} = F_{SA} * F_D * F_{MODEL} * F_{METHOD} \quad (5\text{-}3)$$

The definitions of several of these factors are similar to those of the structural response factors except that they are for the subsystem responses.

F_{SA} The Spectral Shape Factor represents the effects of design vs actual floor response spectrum on piping response.

F_D The Piping Damping Factor is the ratio of calculated subsystem response in design using a specific damping value to that of the best-estimate for different damping values corresponding to the seismic intensity of interest. This factor is obtained by estimating the structural responses due to different damping levels and the damping value used in the design calculation.

F_{MODEL} The Modeling Factor accounts for the effect of the variability in the piping modeling technique on the subsystem response.

F_{METHOD} The Methodology Factor accounts for the margin of the response spectrum method of analysis over the time history analysis.

Table 5.3 lists the response factors associated with the the seismic analysis of the subsystems. The detailed discussion on the derivation of these factors is also in Ref. 5.1. Note that two sets of F_D values were given in Table 5.3. One set was estimated by NCT Engineering based on their best judgment. The other set was calculated by LLNL based on an analysis using the SIMQKE computer code (Ref. 5.2). These two sets of damping response factors are very close to each other and confirmed their accuracy.

In the analysis using the SIMQKE code, a horizontal artificial time-history matching a floor response spectrum with 0.5% damping (i.e. the design damping used for Brunswick) was obtained first. This floor response spectrum was the floor spectrum at the bottom of the sacrificial shield wall and was used in the design of the equipment inside the Brunswick drywell. With this time history, floor response spectra corresponding to 2%, 3%, 4%, and 5% damping values can be calculated with the SIMQKE code. To estimate the damping response factors for a given subsystem damping, it is only necessary to find the ratios of spectral values at 0.5% damping and at the damping of interest for the

dominate frequency of the piping system under consideration. In this study, the recirculation loop was used in deriving these damping response factors.

5.2.3.4 Seismic Response Factors for the Brunswick Plant

In the case of the recirculation loops, the primary steam lines, and the feedwater lines of the Brunswick Plant, we used the values tabulated in Tables 5.2 and 5.3 even though some of the response factors were derived based on just one of the recirculation loops. This approximation is reasonable because these three piping systems of interest are all located inside the reactor drywell cavity and their pipe sizes are compatible. This approximation greatly reduced the amount of work without significant loss of accuracy. Following the procedure described in the previous sections, a seismic response factor can be calculated for a piping system and an earthquake intensity level of interest. Of course, proper structural and subsystem damping values corresponding to this earthquake level will have to be assumed in this calculation. To estimate other levels of earthquake intensity levels, it is necessary to estimate proper damping values and to calculate an earthquake level factor. This factor is needed to scale from the base earthquake level used in the design calculation to the earthquake level of interest. For example, in the Brunswick plant, the OBE corresponding to 0.08 g peak ground acceleration was the base earthquake level used in design. The structural damping and the piping damping used was 7% and 0.5%, respectively. To estimate an earthquake level of five times SSE, the earthquake level factor will be one-tenth or 0.10. The structural and piping damping values were estimated to be 7% and 5%, respectively.

We believe that the structural damping will not increase significantly as the earthquake level goes up. We conservatively assumed that the structural damping values are the same for all earthquake levels under consideration. That is, 7% for horizontal motion and 10% for vertical. For the piping systems, we assumed that the dampings are 0.5%, 2%, 3%, 4%, and 5% for the OBE, SSE, 3SSE, 4SSE and 5SSE. These damping values are conservative compared to the values recommended by the ASME code Case Number N-411, which was adopted by the NRC in its regulatory review process.

Table 5.4 shows the calculation of the seismic response factors for different levels of earthquake intensity.

REFERENCES

5.1 N. C. Tsai and W. L. Wong, **Snubber Capacity and Seismic Response Factors for the Recirculation Loops at Brunswick Unit 2**, NCT Engineering, Lafayette, CA, prepared for the Lawrence Livermore National Laboratory (September 1985).

5.2 D. Gasparini and E. H. Vanmarcke, **Simulated Earthquake Motions Compatible with Prescribed Response Spectra**, Massachusetts Institute of Technology, prepared for the National Science Foundation, Report PB-252-896 (January 1976).

Table 5.1. Transient conditions for the recirculation loops.

Transients	Lifetime Cycles	Max. Temp. Variation (^{o}F)	Max. Pres. Variation (psig)
1. Startup	120	452	1050
2. Turbine roll & increase to rated power	120	24	0
3. Loss of feedwater heater	10	32	0
4. Partial feedwater heater bypass	70	10	0
5. All scrams	40 140	128 152	885 810
6. Shutdown	120	452	1050
7. Single relief or safety valve blowdown	8	452	1050
8. Loss of feedwater pumps isolation valves closed	10	246	940
9. Design hydrostatic test	130	0	1250

Table 5.2. Response factors associated with the structural response, F_{RS}.

$$F_{RS} = F_G * F_{SA} * F_{SSI} * F_D * F_{MODEL}$$

		Median Response Factor	Logarithmic Std Dev (Uncertainty)	Logarithmic Std Dev (Random)
F_G		1.00	0.10	0.15
F_{SA}		1.10	0.08	0.06
F_{SSI}		1.10	0.15	0.05
F_D [1]	(a)	1.46	0.14	0.10
	(b)	1.59	0.14	0.10
F_{MODEL}		1.00	0.10	0.00
F_{RS} [2]	(a)	1.77	0.26	0.20
	(b)	1.92	0.26	0.20

Notes:

1. Two cases of assumed best-estimate structural damping values:

   (a) Horizontal = 7% Vertical = 10%
   (b) Horizontal = 10% Vertical = 15%

2. RMS sum of individual parameters may not sum to indicated value due to round-off

Table 5.3. Response factors associated with the subsystem response, F_{RP}.

$$F_{RP} = F_{SA} * F_D * F_{MODEL} * F_{METHOD}$$

			Median Response Factor	Logarithmic Std Dev (Uncertainty)	Logarithmic Std Dev (Random)
F_{SA}			0.84	0.05	0.10
F_D	(a)	2%	1.30 (1.37)	0.10	0.05
	(b)	3%	1.46 (1.48)	0.10	0.05
	(c)	4%	1.58 (1.57)	0.10	0.05
	(d)	5%	1.68 (1.66)	0.10	0.05
F_{MODEL}			1.00	0.10	0.00
F_{METHOD}			1.08	0.10	0.17
F_{RS}	(a)	2%	1.18 (1.24)	0.18	0.20
	(b)	3%	1.33 (1.34)	0.18	0.20
	(c)	4%	1.43 (1.42)	0.18	0.20
	(d)	5%	1.52 (1.51)	0.18	0.20

Note:

Two cases of assumed best-estimate pipe damping values. The median response factors in parentheses were developed by NCT Engineering. The others without parentheses were estimated by LLNL using the SIMQKE computer code.

Table 5.4. Seismic response factors.

Response Factor	OBE	SSE	3 SSE	5 SSE
Earthquake level factor	1	1/2	1/6	1/10
Structural response factor, F_{RS}	1.77	1.77	1.77	1.77
Structural damping factor, F_D	1.30	1.46	1.58	1.68
Piping response factor, F_{RP} = $F_{SA} * F_{MODEL} * F_{METHOD}$	0.91	0.91	0.91	0.91
Seismic Response Factor, F_R	2.09	1.18	0.42	0.27

Std Dev (Uncertainty) = $[(.26)^2 + (.10)^2 + (.10)^2 + (.10)^2]^{1/2} = .32$

Std Dev (Random) = $[(.20)^2 + (.05)^2 + (.0)^2 + (.17)^2]^{1/2} = .28$

6. RESULTS OF THE ANALYSIS

6.1 General Discussion

As described in Section 3.3, the uncertainty in this study was divided into two categories: the random uncertainty and the modeling uncertainty. The random uncertainty is associated with the inherent physical variation of the parameters. The modeling uncertainty is due to the lack of knowledge or detailed information about the probabilistic characteristic of the random parameters. The inherent randomness of all parameters is usually described either by constants or by distributions and was considered in the Monte Carlo simulation process depicted in Fig. 3.2. The modeling uncertainties were sampled using a Latin Hypercube design. A description of the Latin Hypercube sampling design is given in Section 6.2. Seven parameters with large modeling uncertainties were identified and considered. These parameters with large modeling uncertainties are crack depth, crack aspect ratio, thermal expansion stresses, seismic stresses, seismic hazard curves, crack existence probability, and the probability of non-detection.

The models for those parameters whose modeling uncertainties were neglected are considered the best-estimate models. For parameters for which modeling uncertainties were considered, the best-estimate models are the models corresponding to the median, or 50th percentile values, in their modeling uncertainty distributions. We performed two types of analyses: a best-estimate analysis and an uncertainty analysis. The former produce a single point estimate of the probability of DEGB (or leak) based on the best estimate of the distribution of all random parameters. The latter takes into account modeling uncertainty in addition to the randomness of the parameters, hence produce an uncertainty distribution for the estimate of the probability of DEGB (or leak).

In this probabilistic piping reliability analysis, we considered Loop B of the existing and the proposed replacement recirculation systems, Branch A of the primary steam system, and the feedwater line located in the third and fourth quadrants of the reactor cavity as shown in Fig. 2.4. The selection is arbitrary since each branch closely resembles any other branch (or branches in the case of primary steam system) of the same system. The results are representative of their respective systems.

6.2 Best-Estimate Analysis

The best-estimate analysis uses the best-estimate models that include random uncertainty in calculating system leak or DEGB probability in accordance with the analytical procedure using the Monte Carlo simulation as presented in the flow chart in Fig. 3.2. The best-estimate analysis creates a single point estimate of the failure probability for each piping system of interest. The results for the Brunswick major coolant piping systems are shown in Table 6.1 for leak probabilities and in Table 6.2 for DEGB probabilities. The leak or DEGB probabili-

ties are presented as the probability values over the lifetime of the plant, which is assumed to be 40 years.

The probability values associated with the three events that constitute the overall system failure probability are presented in columns 1, 2, and 3 of Tables 6.1 and 6.2. The sum of Events 2 and 3 (column 4) represents the probability of failure induced by causes other than earthquake. The total failure probability, which is the sum of Events 1, 2, and 3, is presented as the last column (column 5) in these tables. As described in Ref. 4.16, the individual probability values of Event 2 and Event 3 are affected by the subjective threshold peak ground acceleration value, which defines the earthquake below which ground motion is neglected. However, the sum of Events 2 and 3, which represents the failure probability induced by causes other than earthquake, are not very sensitive to the variation of this threshold peak ground acceleration if the threshold value is not too small.

While best-estimate models were used for many parameters, some other parameters were based on conservative assumptions. Therefore, this best-estimate analysis actually yields conservative results. The effects of IGSCC were not considered in the existing recirculation loops even though they were made of the IGSCC susceptible Type 304 stainless steel. Neglecting IGSCC effects on the other systems is reasonable since the materials used are not susceptible to IGSCC effects.

The best-estimate lifetime system leak and DEGB probabilities for the Brunswick major coolant piping systems are rather low and fall within narrow ranges. The total lifetime leak probabilities vary from .24E-5 to 3.8E-5. The DEGB probabilities are at least four orders of magnitude lower than the leak probabilities. They vary from .40E-10 to 1.5E-10 over the lifetime of the plant.

The seismically induced DEGB probabilities (Event 1) for the existing and the replacement recirculation loops are higher than the probabilities due to other causes. This situation differs from our previous observation of the RCL systems of the PWR plants and the results of the rest of this study. In previous studies (Refs. 4.12, 4.14, 4.16, and 6.1), the seismically induced failure, either leak or DEGB, was lower than the failure due to other causes except for the Diablo Canyon and the San Onofre 2 & 3, which are located in areas of high seismicity on the West coast. Even for San Onofre 2 & 3, the seismically induced failure probability was only slightly higher than failure due to other causes. Therefore, the dominant failure event, or scenario, can vary from system to system and from plant to plant depending on the stress values caused by various loading conditions.

The stresses in a piping system are dependent not only on the loading conditions but also on the geometry of the system. Table 6.3 and Table 6.4 show the leak and DEGB probabilities of dominant weld joints within various piping sections of the systems. The results are

presented in terms of the failure probability due to earthquake (Event 1) and the failure probability due to other causes (Event 2 plus Event 3). One general observation is that the failure probability increases as the pipe size decreases. This observation is consistent with our previous observation that the pipe thickness and the ratio of circumference to thickness are generally small for smaller pipe sizes, and, as a result, the failure probability goes down as the pipe size goes up.

The recirculation loop piping consists of pipes of various sizes. In both the existing and the replacement systems, the failure is dominated by the smallest piping section. In the case of the bypass line in the existing recirculation loops, the seismically induced DEGB probability is about 30 times higher than that due to other causes.

6.3 Uncertainty Analysis

As described in Section 6.1, the best-estimate analysis yields a point estimate of both leak and DEGB probabilities for each plant of interest using the parametric values or curves corresponding to the median of the distribution of the modeling uncertainty. That is to say, the values of the calculated leak or DEGB probabilities are not known with certainty. Therefore, a range of values or a distribution for the leak and DEGB probabilities considering the whole range of modeling uncertainty is important in addition to the point estimate produced in the best-estimate analysis. This range provides uncertainty bounds on leak and DEGB probabilities. This type of analysis is called an uncertainty analysis. Seven parameters which have large modeling uncertainty are considered in this analysis. These parameters are crack depth, crack aspect ratio, thermal expansion stresses, seismic stresses, shape of seismic hazard curves, crack existence probability, and the probability of non-detection.

Another parameter with large uncertainty is the extrapolation or truncation of the seismic hazard curve. There is a question about how far a seismic curve should be extrapolated or truncated. This question arises because no seismicity data is available at very high levels (above one SSE) of earthquake intensity and because there is a limit to how high an acceleration g-level the soil can transmit. The extrapolation or truncation of the seismic hazard curve has insignificant effect on the system failure probability of the Brunswick recirculation loops if no support failure is assumed; however, the extrapolation has a very large effect if support failure is considered. Since this section addresses system failure probability for the case of no support failure, uncertainty in extrapolation of seismic hazard curves is not included. This extrapolation uncertainty is addressed in Section 7 along with the effect of support failure.

We used the Latin Hypercube sampling technique to develop a set of samples that could be used to estimate the distribution of leak or DEGB probability due to modeling uncertainty. The basic procedure for the uncertainty analysis using the Latin Hypercube (LHC) sampling technique

was described in detail in Refs. 4.16 and 6.2. A brief description follows.

1. For each parameter, divide the distribution due to modeling uncertainty into n equiprobable intervals.

2. Select a random value within each interval. A total of n values spread over the distribution for each parameter is obtained. Repeat this process for all m parameters for which modeling uncertainty is to be considered.

3. Randomly combine a value without replacement from each distribution to form a set. A total of n sets of m values is obtained. Each set includes a value for each of the m parameters. The n sets represent an LHC sample.

4. Calculate P[LEAK] and P[DEGB] following the procedure presented in Section 3.1 and in Fig. 3.1 for each of the combinations. A total of n values is obtained.

5. Construct a distribution of leak or DEGB probability from these n values for each plant.

The resultant distribution shows the effect of modeling uncertainty in the estimation process. Figure 6.1 is a schematic diagram of the uncertainty analysis using the Latin Hypercube sampling technique. We did the uncertainty analysis for three systems of interest in the Brunswick Plant, using a sample size of 20 in each case. The existing recirculation system was not considered because the failure probability of the existing system is dominated by the IGSCC effects. The purpose of performing probabilistic analysis for this existing system is to provide information to evaluate the net effect of IGSCC through a comparison with the results presented in Volume 1 of this report series.

Tables 6.5, 6.6, and 6.7 are the leak probability results of the uncertainty analysis. The DEGB probabilities are presented in Tables 6.8, 6.9, and 6.10. Figures 6.2 and 6.3 show typical system leak and DEGB probabilities. The results are presented in the same format as Tables 1 and 2. For each of the 20 cases of LHC samples, the probability values for various failure events and combination of events are presented. These 20 cases are sorted in descending order of the total system failure probability. The data are presented as empirical cumulative distribution functions. Empirical cumulative distribution of the total system failure probabilities are further plotted in Figs. 6.2 and 6.3. These figures show the effect of modeling uncertainty in a probabilistic fracture mechanics analysis of the Brunswick major coolant systems.

The modeling uncertainty distribution of the leak and DEGB probabilities are rather wide for all three systems considered. Based on the empirical cumulative distributions, the probabilities corresponding to the 10th, 50th, and 90th percentile are estimated and presented

in Tables 6.11 and 6.12. The probability range for leak between the 10th and 90th percentiles for the replacement recirculation loops, the primary steam lines, and the feedwater lines are 6.2E+2, 1.7E+3, and 1.7E+3, respectively, on the logarithmic scale; note that each "probability range" presented in this manner is the ratio of the respective 90th-percentile leak probability to the 10th-percentile value. The corresponding ranges for DEGB probabilities are 1.7E+4, 2.7E+4, and 1.1E+5, respectively. These wide (i.e. several order-of-magnitude) ranges are consistent with our previous studies of the PWR plants.

The best-estimate failure system probabilities are also presented in Tables 6.11 and 6.12. Note that the best-estimate failure probabilities are not necessarily close to to the medians of the uncertainty distributions. While some are rather close, there is a factor of 2.8 for the leak on the feedwater line, and a factor of 8.8 for the DEGB on the replacement recirculation loop.

Another observation is that the failure probabilities are small even at the 90th percentile level of the modeling uncertainty distribution. The highest levels are 1.2E-3 and 5.0E-8 for the leak and the DEGB, respectively. Both of these probabilities are for the feedwater line.

REFERENCES

6.1 D.J. Chinn, G.S. Holman, T. Lo, and R.W. Mensing, **Probability of Pipe Failure in the Reactor Coolant Loops of Westinghouse PWR Plants, Volume 4: Pipe Failure Induced by Crack Growth in West Coast Plants**, Lawrence Livermore National Laboratory, Report UCID-19988, NUREG/CR-3660, Vol. 4 (March 1985).

6.2 W.J. O'Connell, T.Y. Chuang, R.W. Mensing, P. D. Smith, and J. J. Johnson, **Ranking of Sources of Uncertainty in the SSMRP Seismic Methodology Chain**, Lawrence Livermore National Laboratory, Report UCRL-53027, NUREG/CR-2092 (June 1981).

Table 6.1. Best-estimate leak probabilities of major coolant piping systems.

Piping System	Leak Probability*				
	Event 1	Event 2	Event 3	Event 2+3	Event 1+2+3
Recirculation Loop B (Existing)	.453-07	.332-06	.678-05	.711-05	.715-05
Recirculation Loop B (Replacement)	.331-06	.179-05	.358-04	.376-04	.380-04
Primary Steam Line A	.870-08	.145-06	.223-05	.238-05	.239-05
Feedwater line (in 3rd & 4th quadrant of the reactor cavity)	.238-07	.333-06	.507-05	.540-05	.543-05

* see Section 3.2 for event definitions.

Table 6.2. Best-estimate DEGB probabilities of major coolant piping systems.

Piping System	DEGB Probability*				
	Event 1	Event 2	Event 3	Event 2+3	Event 1+2+3
Recirculation Loop B (Existing)	.144E-09	.256E-12	.958E-11	.984E-11	.154E-09
Recirculation Loop B (Replacement)	.805E-11	.584E-13	.219E-11	.225E-11	.103E-10
Primary Steam Line A	.454E-12	.408E-11	.652E-10	.693E-10	.698E-10
Feedwater line (in 3rd & 4th quadrant of the reactor cavity)	.411E-11	.884E-12	.353E-10	.362E-10	.403E-10

* see Section 3.2 for event definitions.

Table 6.3. Lifetime leak probabilities of dominant welds within each section of the piping systems.

Piping System		Leak Probability			
		Due to Earthquake		Due to Other Causes	
Recirculation Loop B (Existing)	Bypass	#42	.19E-07	#51	.14E-05
	Riser	#30	.38E-08	#26	.42E-06
	Header	#19	.15E-09	#19	.53E-07
	Discharge	#16	.10E-09	#15	.33E-07
	Suction	#4	.12E-09	#4	.35E-07
Recirculation Loop B (Replacement)	Riser	#23	.69E-07	#18	.38E-05
	Header	#17	.02E-09	#17	.85E-08
	Discharge	#12	.10E-09	#12	.19E-07
	Suction	#1	.06E-09	#10	.23E-07
Primary Steam Line A		#5	.16E-08	#2	.21E-06
Feedwater line (in 3rd & 4th quadrant of the reactor cavity)	12-in line	#16	.55E-08	#2	.83E-06
	18-in line	#27	.12E-08	#26	.82E-07

Note: "#" designates dominant weld number

Table 6.4. Lifetime DEGB probabilities of dominant welds within each section of the piping systems.

Piping System		DEGB Probability			
		Due to Earthquake		Due to Other Causes	
Recirculation Loop B (Existing)	Bypass	#42	.14E-09	#45	.50E-11
	Riser	#30	.94E-12	#30	.25E-12
	Header	#19	.47E-15	#19	.67E-14
	Discharge	#16	.13E-15	#11	.85E-15
	Suction	#4	.14E-16	#1	.23E-36
Recirculation Loop B (Replacement)	Riser	#24	.27E-11	#18	.18E-11
	Header	#17	.46E-15	#17	.23E-14
	Discharge	#12	.28E-15	#14	.57E-15
	Suction	#1	.22E-17	#1	.26E-37
Primary Steam Line A		#5	.76E-13	#2	.97E-11
Feedwater line (in 3rd & 4th quadrant of the reactor cavity)	12-in line	#16	.99E-12	#16	.85E-11
	18-in line	#27	.64E-12	#27	.14E-11

Note: "#" designates dominant weld number

Table 6.5. Leak probabilities of twenty Latin Hypercube samples for the Brunswick recirculation loop B.

CASE	EVENT 1	EVENT 2	EVENT 3	EVENT 2+3	EVENT 1+2+3
2	.1047E-05	.1942E-04	.1342E-02	.1361E-02	.1362E-02
6	.1719E-05	.1468E-04	.3817E-03	.3964E-03	.3981E-03
9	.2977E-05	.1826E-04	.3395E-03	.3578E-03	.3607E-03
11	.1328E-05	.1604E-04	.2589E-03	.2749E-03	.2763E-03
16	.6087E-05	.1509E-04	.1133E-03	.1284E-03	.1345E-03
18	.1864E-05	.1357E-04	.6543E-04	.7900E-04	.8086E-04
17	.2059E-05	.7505E-05	.5826E-04	.6577E-04	.6782E-04
10	.4721E-06	.3106E-05	.5276E-04	.5587E-04	.5634E-04
15	.1173E-05	.4468E-05	.4132E-04	.4579E-04	.4696E-04
19	.8604E-06	.8772E-05	.3403E-04	.4280E-04	.4366E-04
3	.3224E-06	.9390E-06	.3659E-04	.3753E-04	.3785E-04
13	.9256E-06	.2541E-05	.3007E-04	.3261E-04	.3354E-04
20	.8516E-06	.2537E-05	.1676E-04	.1930E-04	.2015E-04
8	.1385E-06	.6807E-06	.1314E-04	.1382E-04	.1396E-04
14	.1647E-06	.1031E-05	.1067E-04	.1170E-04	.1187E-04
4	.6102E-07	.2177E-06	.7660E-05	.7878E-05	.7939E-05
5	.1943E-07	.1990E-06	.6658E-05	.6857E-05	.6876E-05
7	.1343E-08	.2619E-07	.6998E-06	.7260E-06	.7273E-06
12	.8462E-08	.3932E-07	.5761E-06	.6154E-06	.6239E-06
1	.3065E-09	.6462E-08	.5093E-06	.5158E-06	.5161E-06

Table 6.6. Leak probabilities of twenty Latin Hypercube samples for the Brunswick primary steam line A.

CASE	EVENT 1	EVENT 2	EVENT 3	EVENT 2+3	EVENT 1+2+3
3	.3642E-05	.5528E-04	.2068E-02	.2123E-02	.2127E-02
19	.2110E-04	.1216E-03	.4395E-03	.5611E-03	.5822E-03
12	.6888E-06	.9387E-05	.1003E-03	.1097E-03	.1104E-03
11	.4431E-06	.6040E-05	.6923E-04	.7527E-04	.7571E-04
20	.1625E-05	.2489E-04	.4319E-04	.6808E-04	.6971E-04
14	.5456E-06	.6426E-05	.4953E-04	.5596E-04	.5650E-04
4	.9013E-07	.1160E-05	.3072E-04	.3188E-04	.3197E-04
9	.5394E-07	.6594E-06	.9077E-05	.9736E-05	.9790E-05
1	.3103E-08	.5721E-07	.8365E-05	.8422E-05	.8425E-05
16	.4575E-07	.5930E-06	.3624E-05	.4217E-05	.4263E-05
7	.1370E-07	.1680E-06	.3004E-05	.3172E-05	.3186E-05
18	.2632E-07	.3855E-06	.2095E-05	.2481E-05	.2507E-05
8	.4222E-08	.1088E-06	.1936E-05	.2045E-05	.2049E-05
10	.4324E-08	.1190E-06	.1354E-05	.1473E-05	.1477E-05
13	.1532E-07	.1195E-06	.1179E-05	.1299E-05	.1314E-05
2	.7487E-09	.1429E-07	.7656E-06	.7799E-06	.7806E-06
6	.1788E-08	.2462E-07	.5395E-06	.5641E-06	.5659E-06
15	.2428E-08	.4886E-07	.3524E-06	.4013E-06	.4037E-06
5	.1667E-08	.1324E-07	.3025E-06	.3157E-06	.3174E-06
17	.2290E-08	.3753E-07	.2055E-06	.2430E-06	.2453E-06

Table 6.7. Leak probabilities of twenty Latin Hypercube samples for one of the Brunswick feedwater lines.

CASE	EVENT 1	EVENT 2	EVENT 3	EVENT 2+3	EVENT 1+2+3
17	.1408E-04	.2555E-03	.1183E-02	.1439E-02	.1453E-02
14	.8927E-05	.1432E-03	.1058E-02	.1201E-02	.1210E-02
5	.2540E-06	.1911E-04	.4572E-03	.4763E-03	.4766E-03
1	.1958E-06	.2630E-05	.3126E-03	.3152E-03	.3154E-03
9	.2690E-06	.3888E-05	.5712E-04	.6101E-04	.6128E-04
2	.1174E-06	.9662E-06	.4255E-04	.4352E-04	.4363E-04
8	.7428E-07	.2211E-05	.3355E-04	.3576E-04	.3584E-04
7	.1045E-06	.1644E-05	.2937E-04	.3101E-04	.3112E-04
16	.1483E-06	.4301E-05	.2634E-04	.3064E-04	.3079E-04
11	.4429E-07	.2224E-05	.2737E-04	.2959E-04	.2964E-04
6	.4999E-07	.4726E-06	.1090E-04	.1137E-04	.1142E-04
12	.4122E-07	.6832E-06	.7244E-05	.7927E-05	.7968E-05
4	.1417E-08	.2693E-06	.7382E-05	.7651E-05	.7653E-05
13	.1441E-07	.7484E-06	.5976E-05	.6724E-05	.6739E-05
19	.2188E-07	.6783E-06	.2150E-05	.2828E-05	.2850E-05
18	.6459E-08	.2237E-06	.9586E-06	.1182E-05	.1189E-05
15	.1055E-07	.1380E-06	.1011E-05	.1149E-05	.1160E-05
3	.1588E-08	.2457E-07	.9362E-06	.9608E-06	.9624E-06
10	.5553E-09	.4292E-07	.5709E-06	.6138E-06	.6144E-06
20	.5205E-07	.2213E-06	.3322E-06	.5535E-06	.6056E-06

Table 6.8. DEGB probabilities of twenty Latin Hypercube samples for the Brunswick recirculation loop B.

CASE	EVENT 1	EVENT 2	EVENT 3	EVENT 2+3	EVENT 1+2+3
16	.1565E-08	.1611E-33	.9036E-33	.1065E-32	.1565E-08
3	.9886E-09	.3577E-34	.1027E-32	.1063E-32	.9886E-09
17	.7360E-09	.6437E-11	.3765E-10	.4409E-10	.7801E-09
19	.2603E-09	.4418E-10	.1533E-09	.1975E-09	.4578E-09
9	.7772E-10	.4804E-11	.8133E-10	.8613E-10	.1639E-09
15	.7171E-10	.5309E-12	.8801E-11	.9332E-11	.8104E-10
13	.5349E-10	.1091E-33	.9626E-33	.1072E-32	.5349E-10
10	.1465E-10	.5296E-12	.6701E-11	.7231E-11	.2188E-10
6	.9936E-11	.5096E-34	.1007E-32	.1058E-32	.9936E-11
4	.5463E-11	.7974E-13	.3052E-11	.3132E-11	.8595E-11
7	.3749E-12	.1434E-12	.5687E-11	.5830E-11	.6205E-11
14	.1917E-11	.9712E-14	.7635E-13	.8606E-13	.2003E-11
18	.1282E-11	.6681E-15	.2453E-14	.3121E-14	.1285E-11
8	.1055E-11	.7763E-14	.1138E-12	.1216E-12	.1177E-11
12	.1066E-11	.8857E-34	.9861E-33	.1075E-32	.1066E-11
11	.3678E-12	.1734E-15	.2141E-14	.2314E-14	.3701E-12
1	.1846E-13	.1592E-14	.1149E-12	.1165E-12	.1350E-12
2	.2345E-14	.1672E-14	.9431E-13	.9598E-13	.9833E-13
20	.5118E-13	.1094E-17	.6197E-17	.7291E-17	.5119E-13
5	.3436E-22	.3985E-34	.1034E-32	.1074E-32	.3436E-22

Table 6.9. DEGB probabilities of twenty Latin Hypercube samples for the Brunswick primary steam line A.

CASE	EVENT 1	EVENT 2	EVENT 3	EVENT 2+3	EVENT 1+2+3
19	.2434E-07	.5922E-08	.4157E-07	.4749E-07	.7183E-07
4	.1109E-09	.9458E-10	.5825E-08	.5920E-08	.6030E-08
11	.1693E-09	.7304E-10	.2185E-08	.2258E-08	.2427E-08
12	.3291E-10	.4093E-10	.6606E-09	.7015E-09	.7344E-09
14	.1112E-10	.1811E-10	.1810E-09	.1991E-09	.2102E-09
9	.3352E-11	.6265E-11	.1220E-09	.1283E-09	.1316E-09
6	.3809E-12	.8175E-12	.2445E-10	.2527E-10	.2565E-10
15	.7346E-12	.1411E-11	.1631E-10	.1772E-10	.1846E-10
10	.4903E-12	.6031E-12	.1502E-10	.1562E-10	.1611E-10
8	.2735E-12	.3788E-12	.1479E-10	.1517E-10	.1544E-10
17	.1807E-12	.9199E-12	.6456E-11	.7376E-11	.7557E-11
13	.2303E-12	.4728E-12	.5283E-11	.5756E-11	.5986E-11
20	.8058E-12	.5922E-12	.2165E-11	.2757E-11	.3563E-11
3	.6923E-13	.3509E-13	.2860E-11	.2895E-11	.2964E-11
7	.8512E-13	.3841E-13	.1247E-11	.1285E-11	.1371E-11
5	.4119E-13	.2395E-13	.8306E-12	.8546E-12	.8957E-12
2	.1635E-14	.8282E-14	.5377E-12	.5460E-12	.5476E-12
16	.1985E-12	.1275E-14	.1992E-13	.2120E-13	.2197E-12
18	.2805E-13	.1586E-13	.1683E-12	.1842E-12	.2122E-12
1	.1024E-17	.7227E-18	.1654E-15	.1661E-15	.1671E-15

Table 6.10. DEGB probabilities of twenty Latin Hypercube samples for one of the Brunswick feedwater lines.

CASE	EVENT 1	EVENT 2	EVENT 3	EVENT 2+3	EVENT 1+2+3
14	.3973E-07	.3422E-08	.1018E-06	.1052E-06	.1450E-06
17	.2854E-07	.1895E-08	.3247E-07	.3437E-07	.6291E-07
1	.2320E-10	.3389E-11	.1297E-08	.1300E-08	.1324E-08
2	.7979E-10	.8155E-11	.9284E-09	.9366E-09	.1016E-08
6	.4058E-10	.7659E-11	.5093E-09	.5170E-09	.5575E-09
8	.1780E-10	.6241E-11	.2908E-09	.2970E-09	.3148E-09
19	.4997E-10	.7710E-11	.8789E-10	.9560E-10	.1456E-09
12	.1225E-10	.2614E-11	.8503E-10	.8764E-10	.9989E-10
11	.5502E-11	.1593E-11	.7171E-10	.7330E-10	.7881E-10
4	.8652E-12	.5867E-12	.5610E-10	.5669E-10	.5755E-10
20	.5489E-10	.1135E-13	.1195E-12	.1309E-12	.5502E-10
9	.4955E-11	.9593E-12	.3889E-10	.3985E-10	.4480E-10
16	.6990E-11	.7416E-12	.1496E-10	.1570E-10	.2269E-10
5	.2560E-12	.1791E-12	.1245E-10	.1263E-10	.1289E-10
18	.2909E-11	.7235E-12	.9191E-11	.9915E-11	.1282E-10
15	.2256E-11	.4007E-13	.1108E-11	.1148E-11	.3404E-11
7	.6008E-12	.5886E-15	.8164E-13	.8223E-13	.6830E-12
13	.6008E-12	.5886E-15	.8164E-13	.8223E-13	.6830E-12
10	.2169E-13	.8674E-14	.3678E-12	.3765E-12	.3982E-12
3	.1793E-13	.2428E-14	.2098E-12	.2122E-12	.2302E-12

Table 6.11. Leak probabilities at the 10th, 50th, and 90th percentiles of the uncertainty distribution.

Piping System	Leak Probability			
	10%	50%	90%	Best Estimate
Recirculation Loop B (Replacement)	6.4E-07	4.0E-05	4.0E-04	3.8E-05
Primary Steam Line A	3.2E-07	3.7E-06	5.4E-04	2.4E-06
Feedwater line (in 3rd & 4th quadrant of the reactor cavity)	7.0E-07	1.9E-05	1.2E-03	5.4E-05

Table 6.12. DEGB probabilities at the 10th, 50th, and 90th percentiles of the uncertainty distribution.

Piping System	DEGB Probability			
	10%	50%	90%	Best Estimate
Recirculation Loop B (Replacement)	6.0E-14	8.0E-12	1.0E-09	7.0E-11
Primary Steam Line A	2.0E-13	1.2E-11	5.5E-09	1.0E-11
Feedwater line (in 3rd & 4th quadrant of the reactor cavity)	4.5E-13	6.0E-11	5.0E-08	4.0E-11

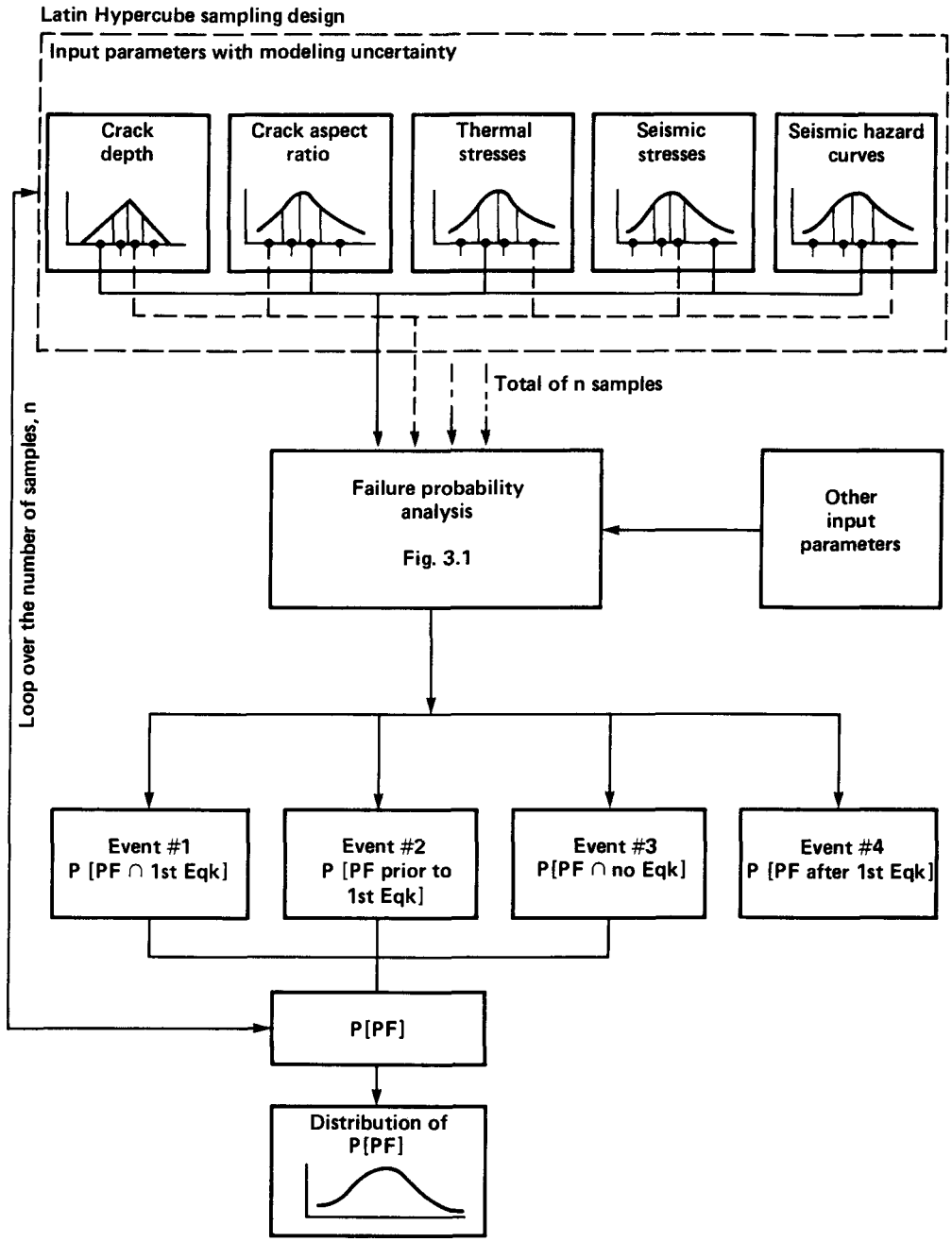

Figure 6.1. Schematic diagram of the uncertainty analysis using the Latin Hypercube sampling design.

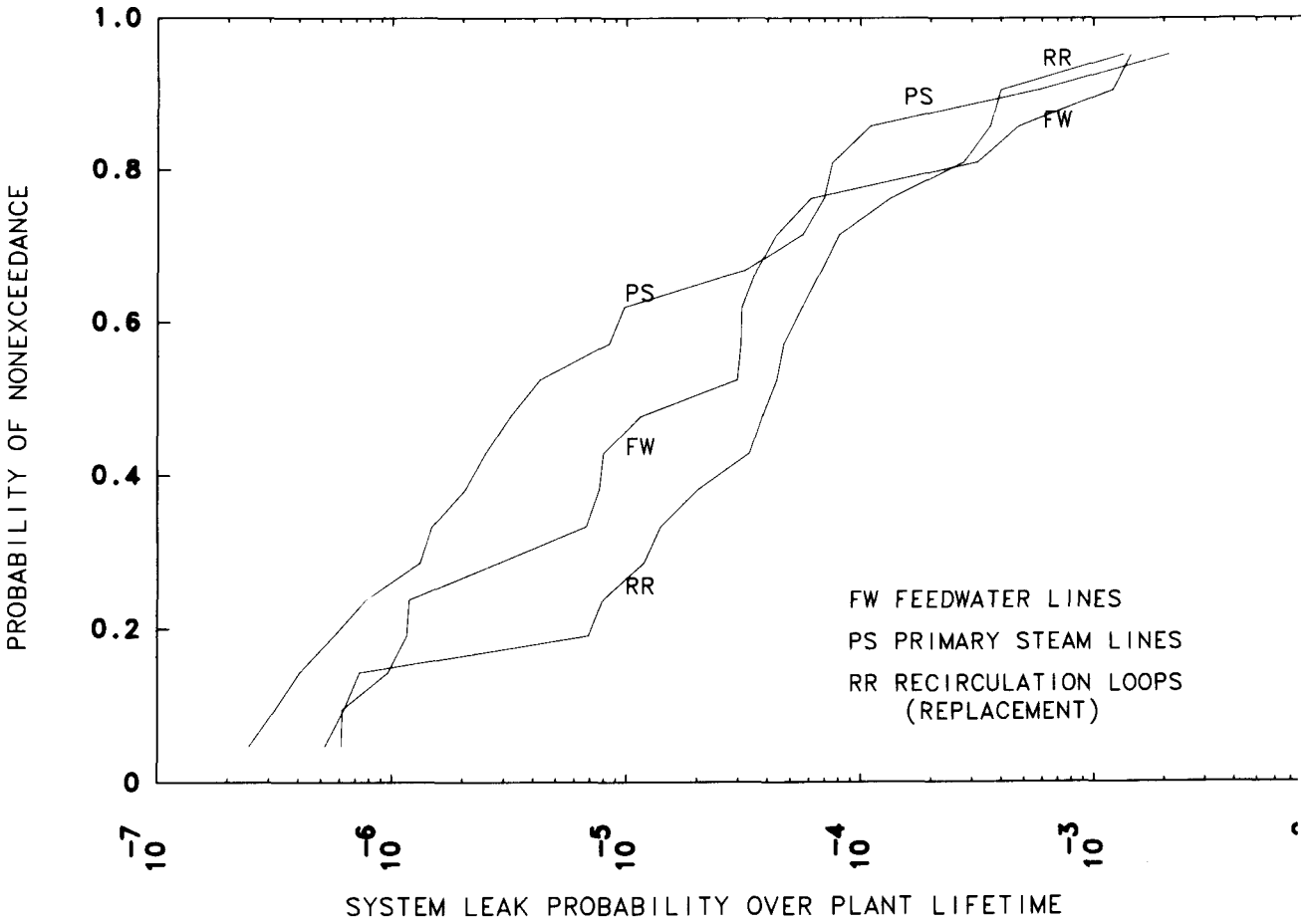

Figure 6.2. Empirical cumulative distribution function for the leak probability of the Brunswick major coolant systems.

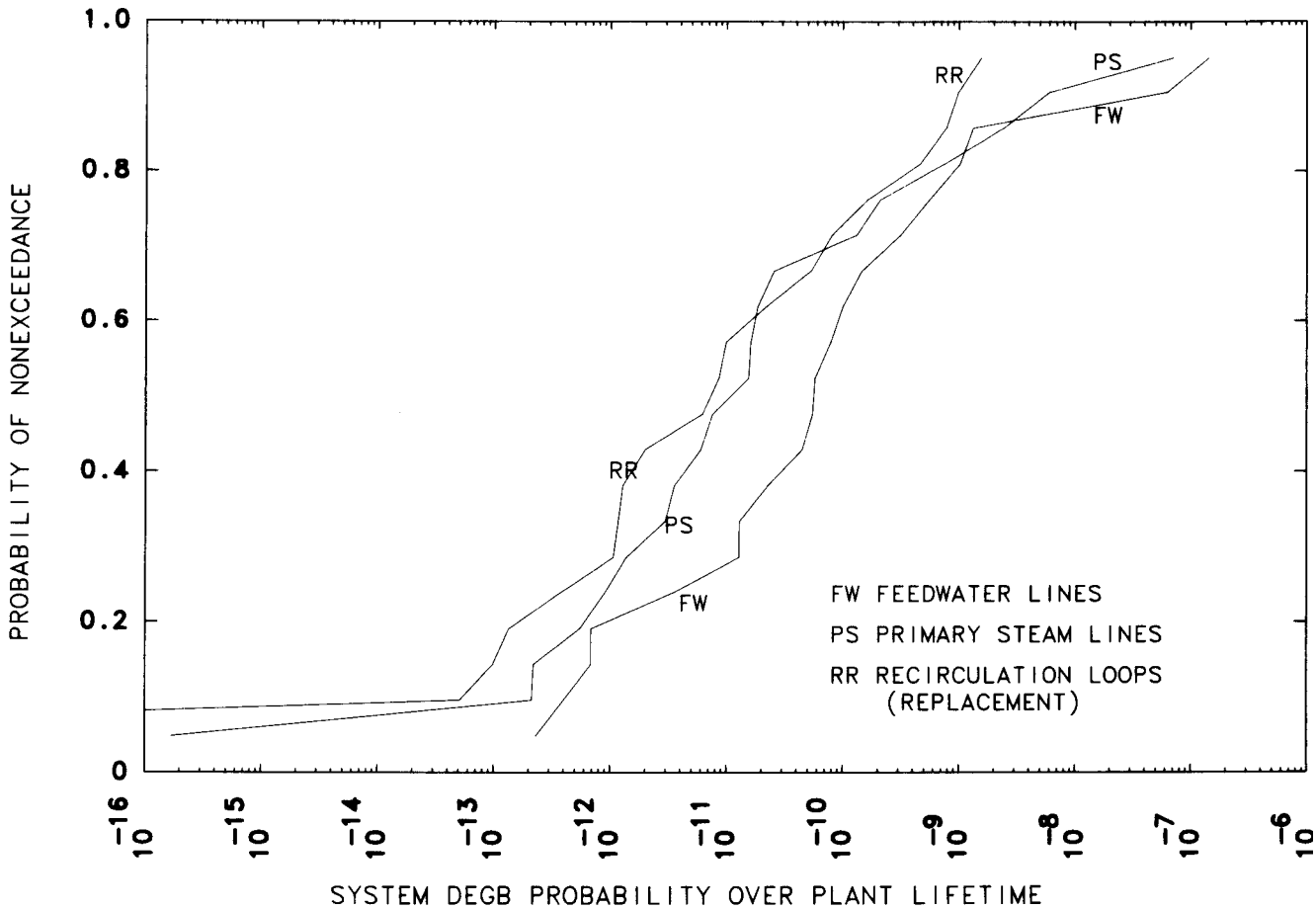

Figure 6.3. Empirical cumulative distribution function for the DEGB probability of the Brunswick major coolant systems.

7. SEISMICALLY-INDUCED FAILURE OF INTERMEDIATE SUPPORTS

7.1 General Discussion

In our earlier work on PWR reactor coolant loop piping, the effects of earthquakes on pipe failure probability were addressed in two separate studies: the direct and the indirect pipe failure analyses. Direct pipe failure is defined as pipe failure caused by crack growth and instability in the piping. Indirect pipe failure is failure due to causes other than crack growth and instability. In the direct pipe failure analysis (Section 3.2), the probability of seismically-induced pipe failure is represented by Event 1. Indirect pipe failure starts with the failure of other structures or components, which in turn cause the pipe to fail. One major source of indirect pipe failure is support failure during an earthquake. That is, the earthquake causes the supports (either the pipe or the component supports) to fail first and this failure in turn breaks the pipe.

In our earlier work on the reactor coolant loops of PWR plants, the probability of indirect pipe failure was assumed to be zero during normal operation. We found that support failure during an earthquake dominated all other possible sources in the indirect pipe failure analyses. In the RCL systems, the pipes are rather short and are supported by the loop components. There are no intermediate pipe supports. The loop components are generally very heavy and have supports comprising skirts, columns, beams, snubbers, and tie rods.

In this BWR plant pilot study using the Brunswick Plant, the piping systems of interest are all inside the drywell containment, which is much smaller and contains less equipment and fewer structures than the PWR plant containments. It is unlikely that sources other than support failure (SF) would play a significant role in the indirect part of the pipe failure analysis. Therefore, we again address only the pipe failure indirectly induced by support failure and neglect all other indirect sources.

As mentioned above, the earlier pipe failure assessment was divided into direct and indirect pipe failure studies. This separation was possible due to the following simplifications:

1. It was assumed that the supports do not fail during an earthquake in the direct DEGB analysis, and

2. the effect of existing cracks and the growth and possible instability of these cracks in the weld joints were neglected in the indirect DEGB analysis.

A comprehensive probabilistic analysis of the pipe failure induced by earthquake should address these two simplifications in a combined analysis including both the direct and the indirect parts in the following formulation:

$$P[PF] = P[PF|\text{no SF}] * P[\text{no SF}] + P[PF|SF] * P[SF] \quad (7\text{-}1)$$

In this equation, P[PF|SF] and P[PF|no SF] are the conditional pipe failure (PF) probabilities with and without support failure, respectively. Each of these probabilities includes failure due to both direct and indirect sources. P[SF] is the probability of failure in at least one of the supports in the system and P[no SF] is the probability of no support failure at all.

As stated earlier, in the work on the PWR plants, the probability of pipe failure due to indirect source was found to be small and was neglected if no support failure was involved. In this situation, the first term on the right-hand side of Eq. (7-1) represents only the direct pipe failure. Corresponding to P[PF|no SF] of the first term, P[PF|SF] of the second term included only the indirect pipe failure in the PWR plant analysis because the pipe was assumed to have no existing cracks. That is, P[PF|SF] did not include failure due to direct source.

As a matter of fact, Eq. (7-1) was simplified even further in the analysis of PWR plants by assuming that the value of P[no SF] and P[PF|SF] were equal to 1.0. The system failure probability became the sum of P[PF|no SF], which represents failure due to direct source, and P[SF], which represents failure due to indirect source. For the PWR reactor coolant loops these were sound assumptions for the following reasons:

1. The components of the RCLs are very heavy, and the pipes are short and stiff. Once the support of a component fails, the integrity of the piping to which these components are attached would not necessarily be assured. Consequently, if we conservatively assume that failure of a "heavy component" support would always result in an "indirect" pipe break, the conditional probability of pipe break

   $$P[PF|SF] = 1.0$$

   is a reasonable estimate.

2. The component supports are generally very strong, and the probability of failure of these supports is very small. In this situation, the value of P[no SF] is close to 1.0 even for a high intensity earthquake.

In a comprehensive analysis, all four parameters on the right-hand side of Eq. (7-1) should be estimated. In addition, P[PF|no SF] and P[PF|SF] should also consider both the without-crack case and the with-crack (or, at least one crack) case in the following formulations:

$$P[PF|\text{no SF}] = P[PF|\text{no SF,cracks}] * P[\text{cracks}] + P[PF|\text{no SF,no crack}] * P[\text{no crack}] \quad (7\text{-}2)$$

and,

$$P[PF|SF] = P[PF|SF,\text{cracks}] * P[\text{cracks}] + P[PF|SF,\text{no crack}] * P[\text{no crack}] \quad (7\text{-}3)$$

In practice, it is not always possible to consider all four parameters on the right-hand side of Eq. (7-1) and to include both the cases of with-crack and without-crack due to the constraints of time and resources. Not following this comprehensive approach is justified when the margin of improvement in results is not worth the amount of additional effort. This was the case when the RCL systems of the PWR plants were analyzed.

In this study, the above stated assumptions are not necessarily true since the pipes are longer and less stiff, and there are no major components that are connected to the piping systems of interest except the reactor pressure vessel. The recirculation pumps are light compared to the coolant components of the PWR plants. Unlike the reactor coolant loops, the BWR pipes of interest have intermediate supports. The impact of the failure of these intermediate supports is expected to be much less than the failure of RCL supports. It might be grossly conservative if the conditional pipe failure probabilities (given that one or more than one support has failed), i.e., P[PF|SF], were assumed to be 1.0. This will be explained further in Section 7.3.

Due to the complexity of the support failure effects, a large amount of the effort (Section 6) still follows the earlier approach of separating direct and indirect pipe failure analyses. However, a comprehensive demonstration analysis using the replacement recirculation system to study the effect of support failure was performed to gain some valuable insight as to whether a simple approach can be found.

There are two essentially identical recirculation loops, Loop A and Loop B. In this demonstration analysis, we chose to study Loop B, which will be the focus in the remainder of this chapter (Chapter 7).

7.2 Methodology

Incorporating the effect of support failure on pipe failure probability is clearly a complicated problem demanding an accordingly complex analytic approach. Many questions can be asked:

1. What is the failure probability of a support for a given earthquake?

2. When does this support failure occur?

3. What is the response of the piping once a support fails?

4. What is the effect of this new response on the pipe failure probability?

5. If there is more than one support, how many supports will fail during an earthquake?

6. What is the failure sequence of these supports?

7. What is the piping response in such a scenario of multiple support failure? How is that going to affect the pipe failure probability?

It is difficult to answer these questions. The problem is further complicated by the fact that these questions are interrelated. For example, the support failure probability (Question 1) is affected by the piping and support responses (Question 3), which is in turn affected by the failure sequence of the supports (Question 6). Obviously, it is beyond our capability to address all of these questions. In this study, we will make the following assumptions to simplify the problem to a manageable level.

1. All support failures occur at the same time and at the beginning of an earthquake. In other words, the piping system experiences the full duration of the earthquake for any given combination of support failures. This assumption is conservative. Thus, timing and the sequence of support failures in an earthquake are not considered. This assumption greatly reduced the complexity of the problem to a manageable size.

2. The supports experience the same stress distribution as if no support failure occurred during an earthquake. This allows the regular fragility development method to be applied to develop one fragility curve for each support for all levels of earthquake intensity. This assumption also allows one single set of in-structure response spectra or one single set of floor time-histories to be used in all seismic analyses.

3. The failure events of the supports are statistically independent of each other. The probability that certain supports will fail together in an earthquake is the product of their individual failure probabilities.

With these three assumptions, we are ready to perform the complicated, even though much simplified, assessment of pipe failure probability with the effects of seismically-induced support failure. The second

term on the right-hand side of Eq. (7-1) can be expressed as the combination of all support failure scenarios. Thus,

$$P[PF] = P[PF|\text{no SF}] * P[\text{no SF}] + \sum_{i=1}^{N} \{P[PF|SFi] * P[SFi]\} \quad (7\text{-}4)$$

where N represents the total number of support failure combinations, and SFi represents the "i"th combination of support failure. For example, a piping system with four supports will have a total of 15 support failure combinations; that is, four cases of one-support failure scenarios, six cases of two-support failure, four cases of three-support failure, and one case of four-support failure.

To describe the general methodology as represented by Eq. (7-4), a flow chart is shown in Fig. 7.1. The analysis can be summarized in four major tasks.

1. Estimate support fragilities.

2. Calculate structural responses for all support failure combinations.

3. Estimate the conditional pipe failure probabilities at weld joints for all support conditions.

4. Perform system failure analyses for all support failure combinations.

In the first task, fragilities of the supports are estimated. The values of P[no SF|a] and P[SFi|a] for a given earthquake peak ground acceleration level, a, can be calculated from the fragility curves of the supports. For each earthquake intensity, P[SFi|a] is simply the product of individual support failure probabilities of the combination scenario number i as stated in assumption number 3. P[no SF] is equal to 1.0 minus the sum of all cases of support failure probabilities. A detailed discussion of the first task is presented in Section 7.3.

In cases of support failure, the seismic responses of a piping system are different from that of the system without support failure. The structural responses for each case should be estimated separately depending upon the specific support failure combination. This estimation is the second task in assessing the effects of support failure. The regular seismic analysis process can be used starting with preparing the seismic analysis model, followed by either response spectrum or time history analysis, and ending with the calculated seismic stresses

at each weld joint. The seismic analysis of the Brunswick replacement recirculation system is discussed in Section 7.4.

Once the seismic stresses are calculated, a probabilistic fracture mechanics analysis is then followed for each case of support failure combination. This analysis is the third task. This analysis yields the conditional failure probabilities at weld joints conditioned on the occurrence of an earthquake of specific intensity and the occurrence of a specific support failure scenario.

The probabilistic fracture mechanics methodology described in Section 3 is a rather complicated procedure and the study of support failure effects does not warrant this level of sophistication. A simplified procedure was developed in this study to estimate the values of P[PF|no SF] and P[PF|SFi] and is described in Section 7.4.

A system failure analysis (Section 3.2), the last task in Fig. 7.1, can be performed to fold in the various results, such as the P[PF|SFi,a], P[SFi|a], and the seismic hazard curves to calculate the probability of failure of a piping system for each support failure scenario. The probability of overall system failure, including all support failure scenarios, can therefore be obtained as simply the sum of the system failure probabilities of the cases according to Eq. (7-4).

7.3 Support Fragility

Three kinds of pipe supports were used in the the recirculation loops of the Brunswick Plant as is characteristic of most vital piping in nuclear power plants except the RCIs. These pipe supports are the rigid supports (or anchors), the spring hangers, and the hydraulic snubbers. The hangers and the snubbers are by themselves supported by structural members. These structural members are, by the requirements of manufacturers' design specification, much stronger than the hangers and the snubbers. Therefore, there is no need to examine the failure mode of the supports due to failure of these structural members in estimating overall support fragility.

The reactor pressure vessel provides a rigid support for the recirculation loops since the reactor vessel is massive and the recirculation loop comes out and returns back to the reactor vessel to form a loop. Failure of reactor vessel supports would most likely induce the recirculation loop to fail. The conditional failure probability of the piping (given that the reactor vessel supports have failed) can be assumed to be 1.0 in this case. This scenario is the same as for the PWR reactor coolant loops. Therefore, the falling down of the reactor pressure vessel is addressed in the same fashion as the earlier indirect pipe failure and is documented in the final report on our earlier evaluations of PWR reactor coolant loop piping (see Ref. 7.1, for example). In this study, we will focus our attention only on the cases where the conditional failure probability is not necessarily equal to 1.0.

Spring hangers are used to support the dead weight of the piping system; the snubbers are used to resist the seismic loads during an earthquake event. Two kinds of spring hangers were used. Constant spring hangers support the recirculation pumps, and variable spring hangers support the the coolant pipes. Hanger failure is not considered in this support failure analysis as discussed in the following paragraph.

The stiffness of the spring hangers is much less than the stiffness of the piping and the active snubbers. During an earthquake, movement of the piping system is mainly restricted by the snubbers and the rigid supports of the piping system. The increase in load in the hangers is expected to be insignificant compared to the snubbers. This expectation implies that there will be no significant difference in the hanger failure probabilities during operation or during an earthquake. On the other hand, the load in snubbers is zero at all times except during a seismic event, during which the load can be very high depending on the earthquake intensity. If a spring hanger did not fail before the earthquake, it is unlikely to fail before the snubbers fail during an earthquake. Therefore, it is reasonable to neglect hanger failure during an earthquake in this study.

Figure 7.2 shows the support arrangement of the existing recirculation loops. The support system of the replacement recirculation loops is essentially the same as the existing system. Note that the Loop B of the replacement system corresponds to the Loop A of the existing system. There are nine snubbers in four natural groups for the Loop B of the replacement system. One snubber supports the suction line. Two are in the discharge line at the same location except in different orientations. There are three snubbers each for the pump motor at the top and the casing at the bottom of the recirculation pump. Each group as a unit provides support for a specific part of the piping system. It is natural to assume that if one in the group fails, the other snubbers in the same group would also lose their function. This conservative assumption simplifies the problem and makes it easier to handle than considering all nine snubbers as individual supports.

In this study the fragilities of all nine snubber supports were estimated first; then, the fragilities of the four support groups were calculated based on the assumption that the support (or the snubber) failure events are statistically independent. If any one of the snubbers in a specific group fails, the whole group is assumed to have lost its function. The following paragraphs summarize the fragility estimations. The detailed description is presented in Ref. 7.2.

The nine snubbers in the recirculation loop B are designated as SB1 to SB6, SB10, SB12 and BB12. The manufacturer is Bergen-Paterson (B-P) Pipe Support Corp. of Boston, Mass. These nine snubbers include three different cylinder sizes represented by their bore diameters: 3.25-inch for SB1 and SB10; 5-inch for SB4, SB5, SB6, SB12 and BB12; and 6-inch for SB2 and SB3. Table 7.1 summarizes all important characteristics of these snubbers. The associated material properties are presented in

Table 7.2. The average effective stiffness of the snubber was established from dynamic tests.

Figure 7.3 shows a typical B-P hydraulic snubber. The B-P snubbers offer an optional relief valve which, if installed, will protect the snubber from being damaged if the dynamic load exceeds the load limit set for the relief valve. The relief valve opens when the load reaches the preset limit so the hydraulic pressure will not continue to build up inside the cylinder. When the load reduces, the valve closes and the snubber is ready to take more load. Thus, a snubber functions like an elastic-plastic axial load member. The snubbers in the recirculation loops are equipped with such a relief valve and are set to open at 133% of the rated load. However, the test results indicated that the minimum valve opening load is actually 160% of the rated load. Under a very high earthquake load, it is possible that the load on the snubbers may exceed this valve opening load. In this situation, the snubbers behave like a non-linear structural member with a large energy absorption capability due to its plasticity effect.

Many failure modes of B-P snubbers were identified by Tsai and Wong (Ref. 7.2). Based on dynamic test results, the governing failure mode is the tensile failure of the threads at the piston rod end nut inside the cylinder. All of these failure modes (including the thread failure) showed higher capacity than the valve opening load. The minimum capacity of these failure modes is still about a factor of 1.8 or more than the relief valve opening load as indicated in Table 7.3. This result is consistent with the relief valve design concept of protecting the snubber assembly from being overstressed. The snubber with relief valve does not simply fail when the relief valve capacity is reached; the snubber just goes into "plastic" deformation. It would be grossly conservative to consider the relief valve opening load as the fragility level of the snubber. Therefore, the nut thread failure will be considered in this study as the best-estimate failure mode. However, fragility estimates based on a relief valve opening load is also listed in Table 7.3 for the purpose of a sensitivity study.

Table 7.3 also lists the loads under SSE conditions. We obtained the SSE loads from the stress report (Ref. 7.3) of the original design calculation. According to the first assumption that the supports fail at the same time, the use of seismic stresses for the no-support-failure case is appropriate. The fragility factors (C/P_{SSE}) documented in Table 7.3 need to be modified in accordance with Section 5.2.3 to obtain the median capacity values. The final fragility information of these snubbers is presented in Table 7.4. These fragility data can also be presented as the probability of failure versus earthquake intensity and are plotted in Fig. 7.4a. These fragilities for the nine snubbers are further combined as shown in Fig. 7.4b to four fragilities representing the four support groups of the replacement recirculation loop B. The method of calculating the fragility information for the four support groups was described earlier in this section.

With the fragilities of the four support groups developed, the next step is to calculate the failure probabilities at different earthquake intensity levels for the various support failure scenarios or combinations. As stated earlier, there are 15 cases of support failure scenarios for a system with four individual supports. These combinations are presented in Table 7.5. Table 7.6 shows the failure probabilities at different earthquake levels for various support failure combinations. To more realistically assess how support failure would affect the likelihood of pipe failure, we evaluated seismic responses for each failure case and then performed a series of probabilistic fracture mechanics analyses.

If we were to follow the indirect DEGB approach adopted in our evaluation of RCLs by assuming P[PF|SF]=1.0, summing the probabilities of the 15 cases of support failure (Cases 2 through 16 in Table 7.6) would yield the probability of the recirculation loop DEGB indirectly caused by failure of intermediate supports, i.e. lifetime indirect DEGB probabilities of 2.4E-10, 3.2E-5, 4.3E-3, 5.9E-2 and 3.0E-1 for seismic hazard cutoffs of 1, 2, 3, 4, and 5 times the SSE, respectively. Some of these indirect DEGB probabilities are very high and may not be realistic judging from the current state (i.e. no DEGB having occurred) of the recirculation loops in the United States. To more realistically assess how support failure would actually affect the likelihood of pipe failure, we evaluated seismic responses for each failure case and then performed a series of probabilistic fracture mechanics analyses.

7.4 Seismic Responses Given Support Failure

To study the pipe failure induced by earthquake, we started with the calculation of the seismic stresses due to one earthquake level. Fifteen cases of seismic analysis of the recirculation loop B were performed and the corresponding pipe stresses were obtained using the response spectrum approach. Each case corresponds to one case of failure scenario of the support groups. Cases 2 to 16 of Table 7.5 show these combinations. Also included in Table 7.5 is Case 1, a support failure case in which no support failure occurs. All sixteen cases of seismic analysis were based on the OBE and a subsystem damping of 0.005. The seismic stresses due to other earthquake levels were estimated following the approach described in Section 5.2.3 using the results of the seismic analyses and a series of response factors.

The input horizontal response spectrum used in these seismic analyses is the broadened horizontal floor response spectrum at the bottom of the sacrificial shield wall used in the original design calculation. The vertical response spectrum is obtained by scaling the horizontal free-field ground spectrum by a 2/3 factor. The reason that the scaled free-field spectrum was used is that the existing design analysis used a constant g-value across the whole frequency range as the vertical floor response spectrum. This constant g-value is equal to 0.106g, which is 2/3 of the peak ground acceleration (PGA). It is more

realistic to use the vertical floor spectrum stated earlier. The horizontal and vertical floor spectra used are shown in Fig. 7.5.

Figure 7.6 shows the maximum normal stresses on the pipe cross-section at all 30 weld joints for the no-support-failure case (Case 1). These stresses are presented as the normalized values with respect to the maximum stress at Weld 23, which has the highest normal stress in the replacement recirculation system. In general, the suction line has the lowest average stress, and the risers have the highest. The discharge line has slightly higher average stress than the suction line. The discharge line is stiffer than the suction line because it has slightly thicker wall thickness and is shorter in length even though both lines have the same outside diameter.

Note that, in the Brunswick coolant systems, the highest normal stress due to earthquake always occurs in the weld joints of the smallest pipe section. In the existing recirculation system, the maximum seismic stress occurs at Weld 42 in the 4-inch bypass line, and at Weld 16 of the feedwater system.

To get a general idea about the stress situation in the pipe if several supports failed during an earthquake, the ratios of the normal stresses for various support failure to the normal stress for no-support-failure case were calculated at individual weld joints. These stress ratios are presented in Figs. 7.7a through 7.7e where the ordinate represents the stress ratio, the abscissa the support-failure combination case number as defined in Table 7.5. Note that the stress ratios, like the support-failure case numbers, are discrete numbers; the points for each weld joint are connected solely for purposes of visualization.

The relative magnitude of the stress at these weld joints is maintained for all levels of earthquake intensities when using the response factor approach of estimating seismic responses. This situation is true for all sixteen support-failure combination scenarios. Thus, Fig. 7.7 can be used together with Fig. 7.6 to obtain the stress situation in the piping system during an earthquake of any specific intensity.

According to Fig. 7.7, the seismic stress increases significantly if the supports fail during an earthquake. However, many more supports failing in an earthquake does not necessarily generate much higher stresses in the piping system. The implication is that the support-failure cases with large number of support failures will most likely contribute little to the overall system failure probability because the probability of so many supports failing in a seismic event is very low.

Also observe that the stress increase in the risers is in general less dramatic than that in the suction line and discharge line. This increase is especially true for the suction line but can not be explained easily. The increase could be due to the different pipe

sizes and lengths or due to the fact that the stress in suction line was low in the base case (Case 1).

7.5 Simplified Analysis Method

In principle, accounting for stress redistribution caused by the failure of intermediate supports would require a separate PRAISE (or equivalent) calculation for each support failure scenario ("case"), dramatically increasing the computational effort associated with a probabilistic fracture mechanics assessment. For the four support groups identified in our study, sixteen separate PRAISE runs would have been required to cover all possible combinations and permutations of support failure (including the case of no failure). As part of our study, we performed sensitivity calculations to determine the relative contribution of each support failure case to the overall system probability of DEGB. In order to minimize computational effort, we developed a simplified analysis method based on modified versions of the standard pre- and post-processing routines used by PRAISE. These routines, normally used, respectively, to develop the stratified sampling space used by PRAISE and to perform the "systems analysis" described in Section 3.2, execute much faster than PRAISE itself. Improved computational efficiency comes at the expense of accuracy in the probabilistic results; however, because we were addressing only relative effects in these sensitivity calculations, we concluded that the simplified analyses were sufficient for our purposes.

The most time-consuming part of the probabilistic fracture mechanics analysis is the Monte Carlo simulation, in which thousands of crack samples are analyzed. Each crack sample is monitored for its growth and instability for all transients during the lifetime of the plant. One approximate approach for dramatically increasing the computational efficiency eliminates the sampling scheme and replaces it by a deterministic estimate of the transition zone on the sampling space (see Ref. 4.16, Appendix A).

The sampling space includes two variables: the initial crack depth, a, and the initial crack aspect ratio. The transition zone is shown schematically on Figure 7.8a. On one side of the transition zone, the cracks have no chance of causing pipe failure. On the other side, the reverse is true. As the name implies, some of the crack samples within the transition zone may and some others may not lead to pipe failure. If crack growth is not a major contributing factor to the pipe failure probability, the transition zone will be quite narrow. In limiting situation, the transition zone can be represented by a line. Rather accurate pipe failure probability can be estimated by calculating the probability of a crack being on the failure side of the transition line.

The only remaining problem is to find the transition line. The transition line can be found by using only one or two hundred selected crack size samples and following the existing probabilistic fracture mechanics approach. The search follows the route as depicted by the

alphabetical order as shown in Fig. 7.8b. If a crack is found to result in failure, a point on the transition line is found, and another crack with the same depth but slightly smaller aspect ratio, or larger b/a ratio, can be tested. If this newly selected crack does not result in failure, a slightly deeper crack is tried next until the selected crack depth results in failure. This process is continued until the other end of the transition line is reached.

A typical transition line is shown in Fig. 7.8c. The shaded region represents the failure zone. Any initial crack size which falls within this region will result in a pipe failure. The total pipe failure probability is the sum of the probabilities within each long and slender rectangular region shown in Fig. 7.8b. The probability of each failure region is the product of the marginal distributions of the crack depth and the marginal crack aspect ratio, which are assumed to be statistically independent.

Following this simplified approach, the conditional failure probability for each weld joint was calculated for all 15 cases of the support failure scenario. The conditional failure probabilities of the weld joint for the no-support-failure case were not obtained in this fashion even though the same method applies, because they are already available from a rigorous analysis done in Section 6.

7.6 Discussion of Results

The conditional pipe break probabilities of individual weld joints for each case of the failure scenario were calculated following the simplified methodology as described in Section 7.5, using the pipe stresses obtained from the seismic analyses described in Section 7.4 along with other operating stresses due to dead weight, pressure, and thermal expansion. These other stresses were described in Section 5.

System failure probability analyses were performed for each of these fifteen cases. These system failure probabilities were then combined with that of Case 1 following Eq. (7-4) to obtain the overall probability of seismically induced system failure.

The seismic hazard curve used in the system analysis was the generic curve described in Section 4.8.1. Because no seismicity data is available at very high levels of earthquake intensity (above one SSE), there remains the question about how far the seismic curve should be extrapolated or truncated. That is, there exists a large modeling uncertainty in seismic hazard curves in the high earthquake intensity level.

To study the effect of different levels of extrapolation or truncation of the seismic hazard curve, several system failure analyses for various levels of truncation were performed. Five truncation levels were considered: 1, 2, 3, 4, and 5 times the SSE. The truncated seismic hazard curves are shown by the dashed lines in Fig. 4.11. The system failure probabilities are shown in Table 7.7 for the case when

the effect of the relief valve is neglected. Table 7.8 presents the same results for the case in which the relief valve opening load is considered as the failure level of the snubbers.

In these tables, the probability of system failure for each of the fifteen support-failure scenarios (Cases 2 through 16) are presented for various seismic hazard truncations along with the probability of system failure for the no-support-failure scenario (Case 1). Note in Tables 7.7 and 7.8 that the total probability of system failure is a straight sum of the individual failure probabilities because each of the 15 support failure scenarios, as well as the no-support-failure case, are statistically independent of one another.

Tables 7.7 and 7.8 show that the overall ("total") probability of system failure generally decreases as the seismic hazard curve is truncated at lower levels. The maximum probabilities of overall system failure are 2.0E-4 and 3.0E-6 per plant lifetime, respectively, for the cases with and without the relief valve at the seismic hazard curve truncation level of five times the SSE. Note, however, that for very large earthquakes (i.e. three or more times the SSE), some calculated probabilities of system failure for Case 1 decrease (albeit by one percent or less) with increasing earthquake level. This clearly unrealistic result reflects numerical round-off in the estimation of the failure transition line (see Figs. 7.8a through 7.8c), rather than any physical phenomenon. The round-off effect is typically seven (or more) orders of magnitude less than the total system break probabilities at these earthquake levels and has no significant effect on the final results.

At first glance, these results appear to contradict the purpose of the snubber relief valve, i.e. to protect the snubbers against extreme seismic loads and thereby reduce the likelihood of overall pipe system failure. It is important to consider, however, that with the relief valve, snubber "failure" -- defined as opening of the relief valve -- would only be momentary, i.e. snubber function would be recovered as soon as the seismic load dropped below the snubber load limit. Without the relief valve, snubber "failure" would be just that -- permanent loss of function -- and therefore the corresponding fragility, based on structural capacity rather than a pre-set load limit, is accordingly higher than for a snubber with the relief valve. The issue of momentary vs permanent loss of function was <u>not</u> accounted for in estimating the respective probabilities of system failure; instead, for computational convenience, we treated relief valve "failure" as if it led to permanent loss of snubber function. How (or even <u>if</u>) momentary loss of snubber function would actually manifest itself as a pipe stress begins to address the time-dependent character of the seismic loads; evaluating this effect was beyond the scope of the current study. It seems reasonable, however, to expect that such pipe stresses would not act long enough to cause the pipe to fail, and that the actual probability of system failure would not only be significantly lower than that

estimated above, but would also be lower than that for the same system equipped with snubbers having no relief valves.

Both Table 7.7 and Table 7.8 clearly show that the truncation of the seismic hazard curve does not have a significant effect on the system failure probability for the no-support case (Case 1). In this case the difference in system failure probability between truncations of 5SSE and 1SSE is less than a factor of 2 for the cases considering and not considering the relief valve opening load in the fragility estimation. This low factor is the reason that the effect of seismic hazard curve truncation was not studied in Section 6.

Note in Table 7.8 that the probability of failure for the no-support case (Case 1) actually decreases -- albeit very slightly -- as the maximum earthquake level increases from 3SSE to 5SSE. This can also be seen in Table 7.9 as the maximum earthquake increases from 4SSE to 5SSE. This effect appears to be a numerical artifact round-off in the analysis, and not a reflection of any actual physical phenomena.

In the cases of various support failures (Cases 2 to 16), the effect of truncation is very significant. For comparison purposes, the no-failure case along with the three dominate support failure cases (Cases 3, 5, and 9) of Table 7.7 were plotted in Fig. 7.9. Curve 6 is the overall system failure probability and is the sum of probabilities of all 16 cases. Figure 7.10 shows the associated support failure probabilities.

As shown in Fig. 7.9, support failure Case 5 is the one most significant among the fifteen support failure scenarios. This case is associated with the failure of supports in the discharge line (Support Group 4, Table 7.5). These supports are the nearest in the recirculation system to the risers. The failure of the discharge line support group induces very high seismic stresses in the risers especially at Weld 23 (Figure 2.2). Note that the failure probability of the discharge line support group is lower than that of the upper and lower pump support groups as indicated in Table 7.6.

As stated in Section 7.4, the stress increase in large-size suction and discharge piping due to support failure is more dramatic than the stress increase in the small-diameter risers. However, the higher rate of increase is still not enough to overcome the initial low stress of the no-support failure case. As a result, the welds in the risers are again the critical locations which contribute most to overall system failure.

Observe in Fig. 7.9 that the overall system failure probability is dominated by the no-support-failure case (Case 1) if the seismic hazard curve is truncated at a ground acceleration level of two SSE or lower. Above two SSE, the support failure cases dominate the overall system failure. Therefore, the relative importance of system failures due to support failure or due to no support failure depends strongly on the

extent of extrapolation of the seismic hazard curve, which has large modeling uncertainty as described earlier in this section.

To better understand the above phenomenon, the detailed calculations of the conditional failure probabilities of Case 1 (no-support-failure) and Case 5 (failure of discharge line supports) for dominate weld joints are presented in Fig. 7.11 and 7.12, respectively. These probabilities are conditional on the occurrence of an earthquake, and the seismic hazard curve is not yet taken into account. The calculation of these conditional failure probabilities of weld joints follows Eqs. (7-2), (7-3), and (7-4). Only the dominant weld joints are considered: Welds 23 and 24 for Case 1 and Weld 23 for Case 5.

In the case of no-support failure (Fig. 7.11), the failure probability is mainly dominated by the instability of existing cracks at Welds 23 and 24 in the piping system as indicated by Curve 2. The contribution of the no-crack case (Curve 4) is negligible. Curve 2 rises only gradually as the earthquake intensity increases. However, Fig. 7.12 tells a different story. The failure probability due to existing cracks in Weld 23 rises much faster than that of Case 1. In addition, the contribution to failure due to the no-crack case (Curve 4) is very significant. The overall failure probability at Weld 23 is dominated by the with-crack case at a low earthquake level. The no-crack case starts to dominate at 1.75SSE. The shapes of Curves 1 and 5 in Fig. 7.9 follow directly from Curves 6 for Cases 1 and 5 in Figs. 7.11 and 7.12.

The analysis presented in this section is complicated and not practical for use for studying every piping system. However, the results of the Brunswick replacement recirculation loop B shows a potential way to reduce significantly the computational effort.

The following paragraphs briefly summarize the findings of this study, which can be used to reduce the amount of work needed to assess accurately the effects of seismically induced support failures.

1. The maximum probabilities of overall system failure are 2.0E-4 and 3.0E-6 per plant lifetime, respectively, for the cases with and without the relief valve at the seismic hazard curve truncation level of five times the SSE (or about 5.0E-6 and 7.5E-8 per reactor-year, respectively, if a 40-year plant lifetime is assumed). These probability levels can be considered as the upper bound values. They are not very high probability values considering the fact that the case associated with the relief valve very conservatively assumes the valve opening load limit to be the "failure" (or fragility) level of the supports.

   If we only consider earthquakes up to twice the SSE, the lifetime probabilities of failure with and without the relief valve drop to 7.7E-8 and 1.7E-11, respectively (or about 1.9E-9 and 4.3E-13 per reactor-year, respectively).

2. The seismic stresses of cases when many supports fail during an earthquake are not significantly higher than those cases in which only one or two supports fail. It is unlikely that these cases will have any significant contribution to the overall system failure because the probability of so many supports failing in an earthquake is very small.

3. The welds which have high seismic stress in a no-support-failure case are most likely the dominate welds for the overall system failure probability. The welds with low seismic stress in Case 1 may have higher rates of stress increase for the with-support-failure cases from Case 1. However, the higher rate may still not make them major contributors to overall system failure.

4. The shape of the seismic hazard curve has a major effect on the overall system failure probability. Seismic hazard curves which do not extend far beyond the one SSE level indicate that evaluation of the no-support-failure case might be sufficient. Otherwise, the with-support-failure cases dominate. Following these observations, the effects of support failure may be assessed with the evaluation of a few carefully selected welds and support failure combinations using the methodology presented in this section.

Besides the extrapolation or truncation of seismic hazard curves, a large modeling uncertainty also exists in the support fragilities. To study the effect of this uncertainty in support failure fragility, we considered two levels of uncertainties (90% and 10%) on the modeling uncertainty distribution of the support fragility. The logarithmic standard deviation of the modeling uncertainty distribution of the support fragility is equal to 0.35 according to Table 7.4. Tables 7.9 and 7.10 show the results for the 90% and 10% on the uncertainty distribution in the same format as Tables 7.7 and 7.8, which represent the median of the support fragility; as in Tables 7.7 and 7.8, the individual "SF" system failure probabilities will not necessarily sum to the total "SF" probability given. Not surprisingly, the overall system failure probability is again heavily dependent on the truncation level of the seismic hazard curve. At 90% on the modeling uncertainty distribution, the maximum overall system failure probability reaches 7.3E-4 per plant lifetime at the seismic hazard truncation level of 5SSE. It is close to the maximum probability of 3.0E-4 calculated for the case when the relief valve opening load was considered as the fragility level (see Table 7.8). This probability level is still not high.

REFERENCES

7.1 **Probability of Pipe Failure in the Reactor Coolant Loops of Westinghouse PWR Plants**, Lawrence Livermore National Laboratory, Report UCID-19988, NUREG/CR-3660, Vol. 1-4 (1984).

7.2 N. C. Tsai and W. L. Wong, **Snubber Capacity and Seismic Response Factors for the Recirculation Loops at Brunswick Unit 2**, NCT Engineering, Lafayette, CA, Prepared for the Lawrence Livermore National Laboratory (September 1985).

7.3 General Electric Company, **Brunswick Steam Electric Plant, Unit 2, Recirculation System Piping Stress Report**, Report 23A1949 (December 1983).

Table 7.1. Properties of snubbers in the Brunswick recirculation system.

Snubber	Bore Diameter (in)	Pin Diameter (in)	Snubber Length (in)	Extension Pipe Diam. (in)	Effective Stiffness (k/in)
SB1	3.25	1.00	41.2	3	348
SB2	6	1.75	61.4	6	800
SB3	6	1.75	60.7	6	800
SB4	5	1.50	66.4	5	452
SB5	5	1.50	65.9	5	452
SB6	5	1.50	46.6	5	452
SB10	3.25	1.00	53.5	3	348
SB12	5	1.50	36.1	5	452
BB12	5	1.50	36.1	5	452

Table 7.2. Material properties of B-P snubbers.

(1) Piston Rod: ASTM A193, Grade B7

Bore Size (in)	Yield Stress (ksi)	Ultimate Strength (ksi)
1-1/2	105	125
1-1/2 to 4	95	115
4 to 7	75	100

(2) Attachment Pin: SA 564, Type 630

Yield Stress: 75 ksi

Ultimate Strength: 100 ksi

Table 7.3. Snubber capacities with and without relief valve.

Snubber	SSE Load, P_{SSE} (kip)	Catalog Rated Load (kip)	Ultimate Capacity, $\breve{C}$ (kip)		Fragility ($\breve{C}/P_{SSE}$)		Variability	
			Without Valve	With* Valve	Without Valve	With* Valve	$\beta_{c,u}$	$\beta_{c,r}$
SB1	20.7	20	66.5	32.0	3.21	1.55	0.14	0.15
SB2	67.5	70	254.0	102.0	3.76	1.51	0.14	0.15
SB3	92.0	70	254.0	102.0	2.76	1.11	0.14	0.15
SB4	41.2	50	147.0	80.0	3.57	1.94	0.14	0.15
SB5	34.2	50	147.0	80.0	4.30	2.24	0.14	0.15
SB6	57.5	50	147.0	80.0	2.56	1.39	0.14	0.15
SB10	12.3	20	66.5	32.0	5.41	2.60	0.14	0.15
SB12	49.6	50	147.0	80.0	2.96	1.61	0.14	0.15
BB12	40.9	50	147.0	80.0	3.59	1.96	0.14	0.15

* The specification value of the load limit is 133% of the rated load. Tests showed a mean valve-opening load at about 160% of the rated load, which is adopted here as the capacity of the snubbers with the relief valve.

Table 7.4. Snubber fragilities.

Structural response factor:

Median = 1.77
Logarithmic std. dev. (Modeling uncertainty) = .26
Logarithmic std. dev. (Random uncertainty) = .20

Subsystem response factor:

Median = 1.34
Logarithmic std. dev. (Modeling uncertainty) = .18
Logarithmic std. dev. (Random uncertainty) = .20

Snubber fragility factors normalized to 1.0*SSE (SSE = 0.16g)

Median :	Without relief valve		With relief valve	
	SB1	3.21	SB1	1.55
	SB2	3.76	SB2	1.51
	SB3	2.76	SB3	1.11
	SB4	3.57	SB4	1.94
	SB5	4.30	SB5	2.24
	SB6	2.56	SB6	1.39
	SB10	5.41	SB10	2.60
	SB12	2.96	SB12	1.61
	BB12	3.59	BB12	1.96

Logarithmic std. dev. (Modeling uncertainty) = .14
Logarithmic std. dev. (Random uncertainty) = .15

Final snubber fragility values

Median :	Without relief valve		With relief valve	
	SB1	1.22g	SB1	.588g
	SB2	1.43g	SB2	.573g
	SB3	1.05g	SB3	.421g
	SB4	1.35g	SB4	.736g
	SB5	1.63g	SB5	.850g
	SB6	.972g	SB6	.528g
	SB10	2.05g	SB10	.987g
	SB12	1.12g	SB12	.611g
	BB12	1.36g	BB12	.744g

Logarithmic std. dev. (Modeling uncertainty) = .35
Logarithmic std. dev. (Random uncertainty) = .32

Table 7.5. Support failure combinations of the Brunswick replacement recirculation loop B.

Case No.	No. of failed supports	Group 1 SB4,SB5,SB6 Pump Motor	Group 2 SB1,SB2,SB3 Pump Casing	Group 3 SB10 Suction	Group 4 SB12,BB12 Discharge
1	0 SF				
2	1 SF	x			
3	1 SF		x		
4	1 SF			x	
5	1 SF				x
6	2 SF	x	x		
7	2 SF	x		x	
8	2 SF		x	x	
9	2 SF	x			x
10	2 SF		x		x
11	2 SF			x	x
12	3 SF	x	x	x	
13	3 SF	x	x		x
14	3 SF	x		x	x
15	3 SF		x	x	x
16	4 SF	x	x	x	x

Table 7.6. Probability of support failure at various levels of earthquake intensity.

Case	SF*	Maximum Earthquake Level					
		0.5 SSE	1 SSE	2 SSE	3 SSE	4 SSE	5 SSE
1	0	.1000E+01	.1000E+01	.1000E+01	.9957E+00	.9417E+00	.7264E+00
2	1	.1729E-16	.1879E-09	.2100E-04	.2381E-02	.2833E-01	.1207E+00
3	1	.2289E-17	.4206E-10	.8191E-05	.1315E-02	.2007E-01	.1018E+00
4	1	.2432E-26	.3912E-17	.6131E-10	.1177E-06	.9775E-05	.1767E-03
5	1	.3247E-18	.9362E-11	.2791E-05	.5616E-03	.9920E-02	.5618E-01
6	2	.3958E-34	.7902E-20	.1720E-09	.3130E-05	.5686E-03	.1229E-01
7	2	.4204E-43	.7351E-27	.1288E-14	.2802E-09	.2769E-06	.2132E-04
8	2	.5566E-44	.1645E-27	.5022E-15	.1547E-09	.1962E-06	.1799E-04
9	2	.5613E-35	.1759E-20	.5860E-10	.1337E-05	.2810E-03	.6779E-02
10	2	.7432E-36	.3937E-21	.2286E-10	.7383E-06	.1991E-03	.5720E-02
11	2	.7894E-45	.3663E-28	.1711E-15	.6610E-10	.9697E-07	.9926E-05
12	3	.9624E-61	.3092E-37	.1055E-19	.3683E-12	.5558E-08	.2171E-05
13	3	.1285E-52	.7398E-31	.4800E-15	.1758E-08	.5640E-05	.6903E-03
14	3	.1365E-61	.6882E-38	.3593E-20	.1574E-12	.2747E-08	.1198E-05
15	3	.1807E-62	.1540E-38	.1401E-20	.8689E-13	.1946E-08	.1011E-05
16	4	.3125E-79	.2894E-48	.2943E-25	.2069E-15	.5514E-10	.1220E-06
Total P[SF]		.199E-16	.239E-09	.320E-04	.426E-02	.594E-01	.304E+00

* number of support failures for case indicated. Case 1 represents the probability that no supports fail.

Table 7.7. Best-estimate seismically induced pipe failure probability (without considering relief valve) and the effects of seismic hazard curve extrapolation.

Case	Failed Supports	Maximum Earthquake Level				
		1 SSE	2 SSE	3 SSE	4 SSE	5 SSE
1	0	.5971E-11	.7837E-11	.8882E-11	.9403E-11	.9754E-11
2	1	.2289E-20	.1184E-14	.5064E-12	.1303E-10	.6170E-09
3	1	.2139E-20	.6142E-14	.1273E-10	.9298E-08	.8913E-06
4	1	.1153E-28	.3215E-21	.7304E-18	.8469E-16	.3060E-14
5	1	.1957E-19	.9124E-11	.1521E-06	.7618E-06	.1684E-05
6	2	.1070E-29	.4974E-18	.4923E-12	.4169E-08	.2147E-06
7	2	.1162E-37	.1282E-24	.1222E-18	.3140E-15	.1211E-11
8	2	.5697E-37	.6615E-23	.8322E-10	.1063E-10	.3116E-09
9	2	.9460E-29	.128E-14	.3445E-09	.1659E-07	.1343E-06
10	2	.4688E-29	.3737E-14	.1909E-09	.1162E-07	.1106E-06
11	2	.1556E-37	.5982E-23	.1217E-13	.5388E-11	.1708E-09
12	3	.5456E-48	.1082E-29	.2183E-21	.6912E-17	.1299E-13
13	3	.5578E-40	.3524E-22	.3993E-12	.3107E-09	.1180E-07
14	3	.2756E-46	.3475E-25	.3991E-16	.1491E-12	.1942E-10
15	3	.5060E-47	.6237E-26	.2204E-16	.1054E-12	.1631E-10
16	4	.1137E-58	.1034E-34	.4881E-24	.1413E-17	.1919E-12
Total P[DEGB]		.597E-11	.170E-10	.153E-06	.804E-06	.305E-05

Table 7.8. Best-estimate seismically induced pipe failure probability (considering relief valve) and the effects of seismic hazard curve extrapolation.

Case	Failed Supports	Maximum Earthquake Level				
		1 SSE	2 SSE	3 SSE	4 SSE	5 SSE
1	0	.5971E-11	.7661E-12	.7807E-11	.7725E-11	.7723E-11
2	1	.8537E-16	.8601E-13	.4645E-10	.3140E-09	.4685E-08
3	1	.7044E-14	.6165E-11	.5519E-08	.4314E-06	.9499E-05
4	1	.4109E-21	.8925E-17	.1309E-13	.2275E-12	.1967E-11
5	1	.1617E-14	.1501E-08	.3136E-04	.5385E-04	.6106E-04
6	2	.1210E-18	.3489E-12	.1723E-07	.4012E-05	.2111E-04
7	2	.1453E-25	.2518E-17	.1787E-12	.1656E-10	.4999E-08
8	2	.6532E-23	.1793E-14	.5753E-07	.1378E-05	.2970E-05
9	2	.2755E-19	.1500E-09	.5972E-05	.2096E-04	.2959E-04
10	2	.1217E-17	.6045E-08	.1732E-04	.3994E-04	.4789E-04
11	2	.4474E-25	.2712E-15	.3845E-07	.6351E-06	.1881E-05
12	3	.2157E-29	.2089E-18	.1293E-12	.1652E-10	.5534E-09
13	3	.5135E-24	.4062E-13	.2594E-05	.1642E-04	.2542E-04
14	3	.2814E-29	.1123E-14	.1085E-07	.3476E-06	.1457E-05
15	3	.4604E-28	.2782E-14	.2888E-07	.5587E-06	.1805E-05
16	4	.3676E-35	.3285E-20	.5362E-13	.1328E-09	.1005E-06
Total P[DEGB]		.597E-11	.770E-07	.574E-04	.139E-03	.203E-03

Table 7.9. The effects of uncertainty in estimating support fragility on the seismically induced pipe failure probability (90% on the uncertainty distribution of the support fragility).*

Case	Failed Supports	Maximum Earthquake Level				
		1 SSE	2 SSE	3 SSE	4 SSE	5 SSE
1	0	.5971E-11	.7826E-11	.8667E-11	.8692E-11	.8630E-11
2	1	.7160E-17	.2048E-12	.1863E-10	.1769E-09	.3576E-08
3	1	.9488E-17	.1550E-11	.6646E-09	.1566E-06	.6281E-05
4	1	.8799E-24	.1249E-17	.5221E-15	.1862E-13	.2755E-12
5	1	.1140E-15	.2939E-08	.1042E-04	.2275E-04	.2909E-04
6	2	.1442E-22	.2137E-13	.8870E-09	.8669E-06	.9661E-05
7	2	.2709E-29	.8499E-19	.3005E-14	.8291E-12	.5764E-09
8	2	.1891E-28	.6442E-17	.2969E-09	.3929E-07	.2181E-06
9	2	.1684E-21	.7053E-10	.8141E-06	.5345E-05	.1083E-04
10	2	.1189E-21	.3024E-09	.6652E-06	.4997E-05	.1063E-04
11	2	.6826E-29	.7472E-17	.5436E-09	.2570E-07	.1562E-06
12	3	.5561E-36	.1801E-21	.2738E-15	.3024E-12	.4243E-10
13	3	.4344E-29	.4878E-15	.4605E-07	.1496E-05	.5574E-05
14	3	.3715E-34	.7422E-17	.6277E-10	.8530E-08	.9609E-07
15	3	.9720E-35	.1957E-17	.5059E-10	.8147E-08	.9687E-07
16	4	.6712E-43	.5549E-24	.3917E-16	.1286E-11	.5471E-08
Total P[DEGB]		.597E-11	.332E-08	.120E-04	.357E-04	.726E-04

* no snubber relief valve

Table 7.10. The effects of uncertainty in estimating support fragility on the seismically induced pipe failure probability (10% on the uncertainty distribution of the support fragility).*

Case	Failed Supports	Maximum Earthquake Level				
		1 SSE	2 SSE	3 SSE	4 SSE	5 SSE
1	0	.5971E-11	.7837E-11	.8886E-11	.9448E-11	.9973E-11
2	1	.1091E-24	.1085E-17	.2438E-14	.1913E-12	.2177E-10
3	1	.7266E-25	.3918E-17	.4237E-13	.9705E-10	.2157E-07
4	1	.2197E-34	.1221E-25	.1556E-21	.6053E-19	.5512E-17
5	1	.4997E-24	.4442E-14	.3840E-09	.5318E-08	.2467E-07
6	2	.1762E-38	.2921E-24	.8152E-17	.6743E-12	.1777E-09
7	2	.1069E-47	.4480E-32	.1298E-24	.3534E-20	.8140E-16
8	2	.3729E-47	.1607E-30	.6035E-20	.8023E-16	.1348E-13
9	2	.1166E-37	.5733E-21	.4384E-14	.2003E-11	.8252E-10
10	2	.4110E-38	.1162E-20	.1652E-14	.9591E-12	.4767E-10
11	2	.7624E-48	.1108E-30	.6835E-20	.3204E-16	.5939E-14
12	3	.1719E-62	.2415E-40	.7807E-30	.8201E-24	.2165E-19
13	3	.2355E-53	.1008E-31	.1730E-19	.4115E-15	.1948E-12
14	3	.6504E-61	.5916E-36	.1109E-24	.1393E-19	.2503E-16
15	3	.8490E-62	.7381E-37	.4179E-25	.6689E-20	.1457E-16
16	4	.9188E-78	.1124E-48	.4563E-35	.1400E-26	.6420E-20
Total P[DEGB]		.597E-11	.784E-11	.393E-09	.543E-08	.466E-07

* no snubber relief valve

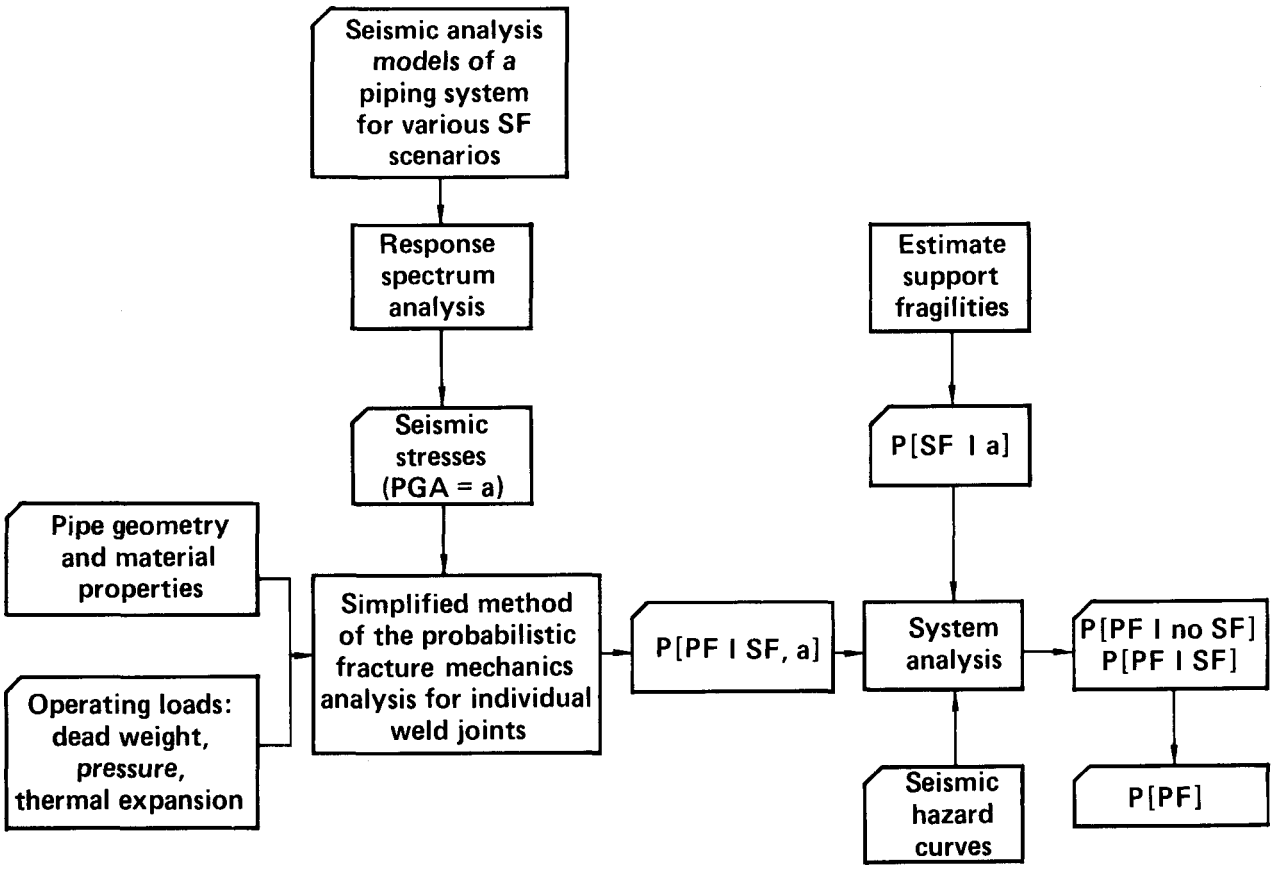

Figure 7.1. Study of seismically induced system failure considering the effects of support failure.

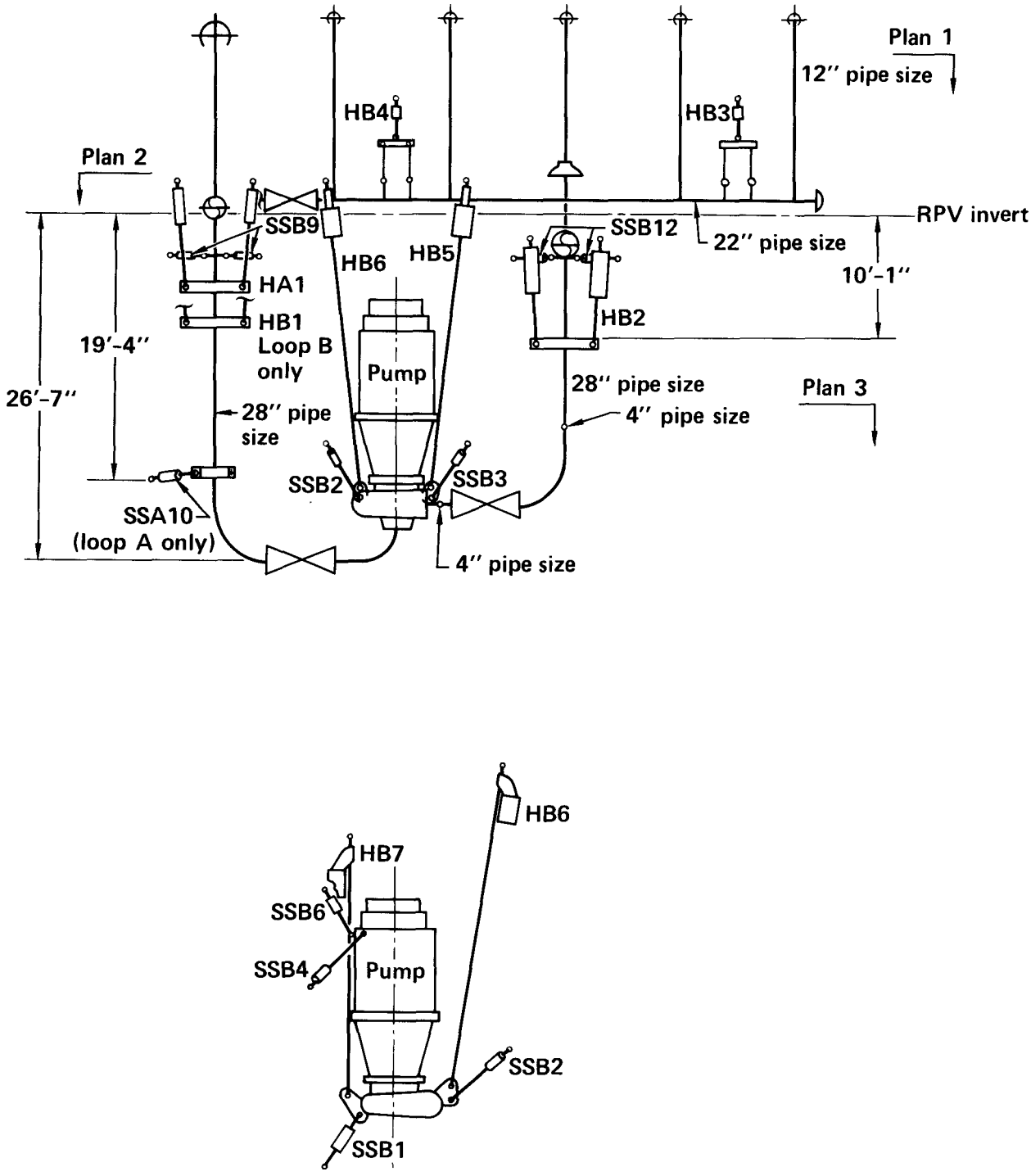

Figure 7.2. Supports of the Brunswick recirculation system.

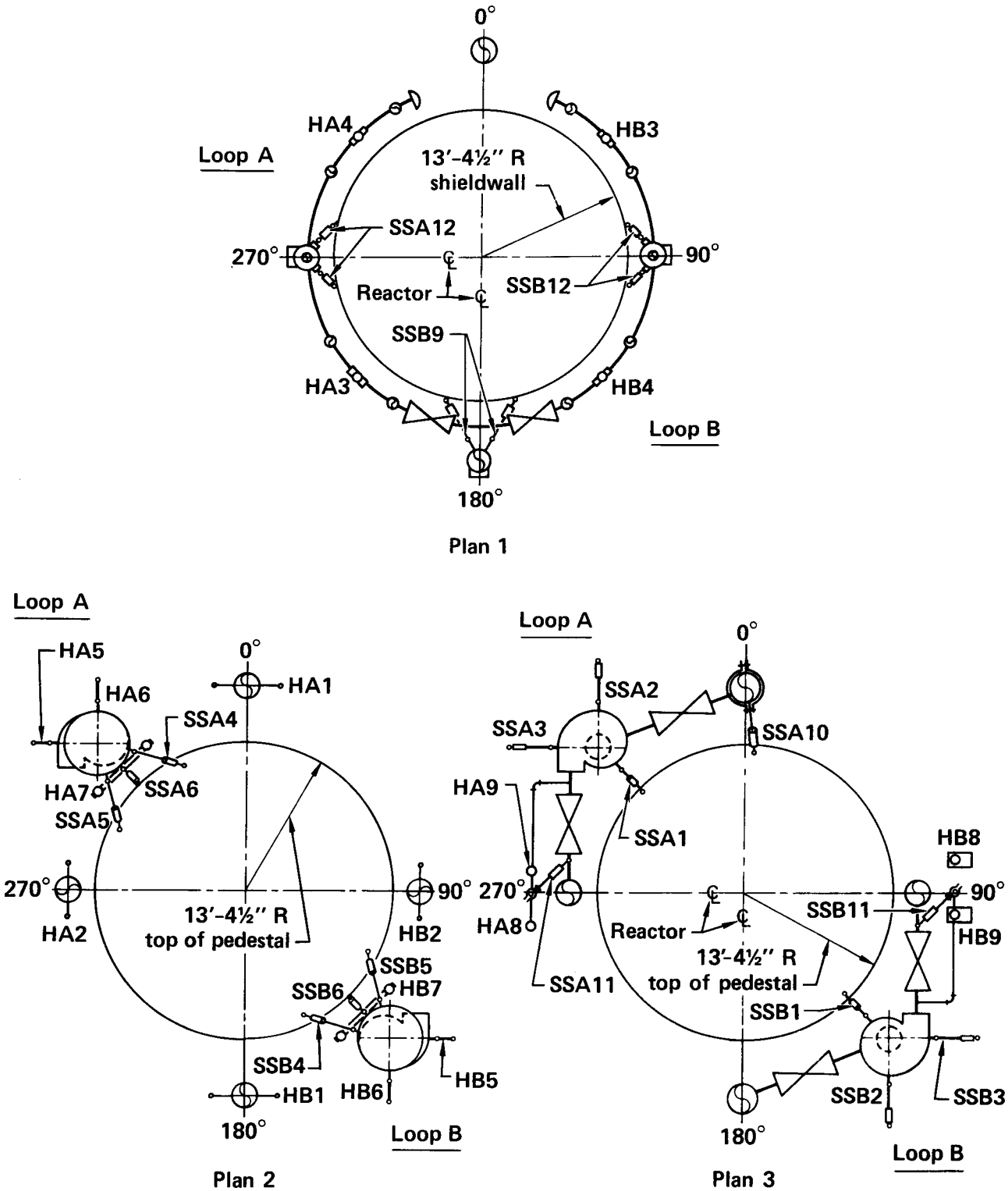

Figure 7.2 (cont.). Supports of the Brunswick recirculation system.

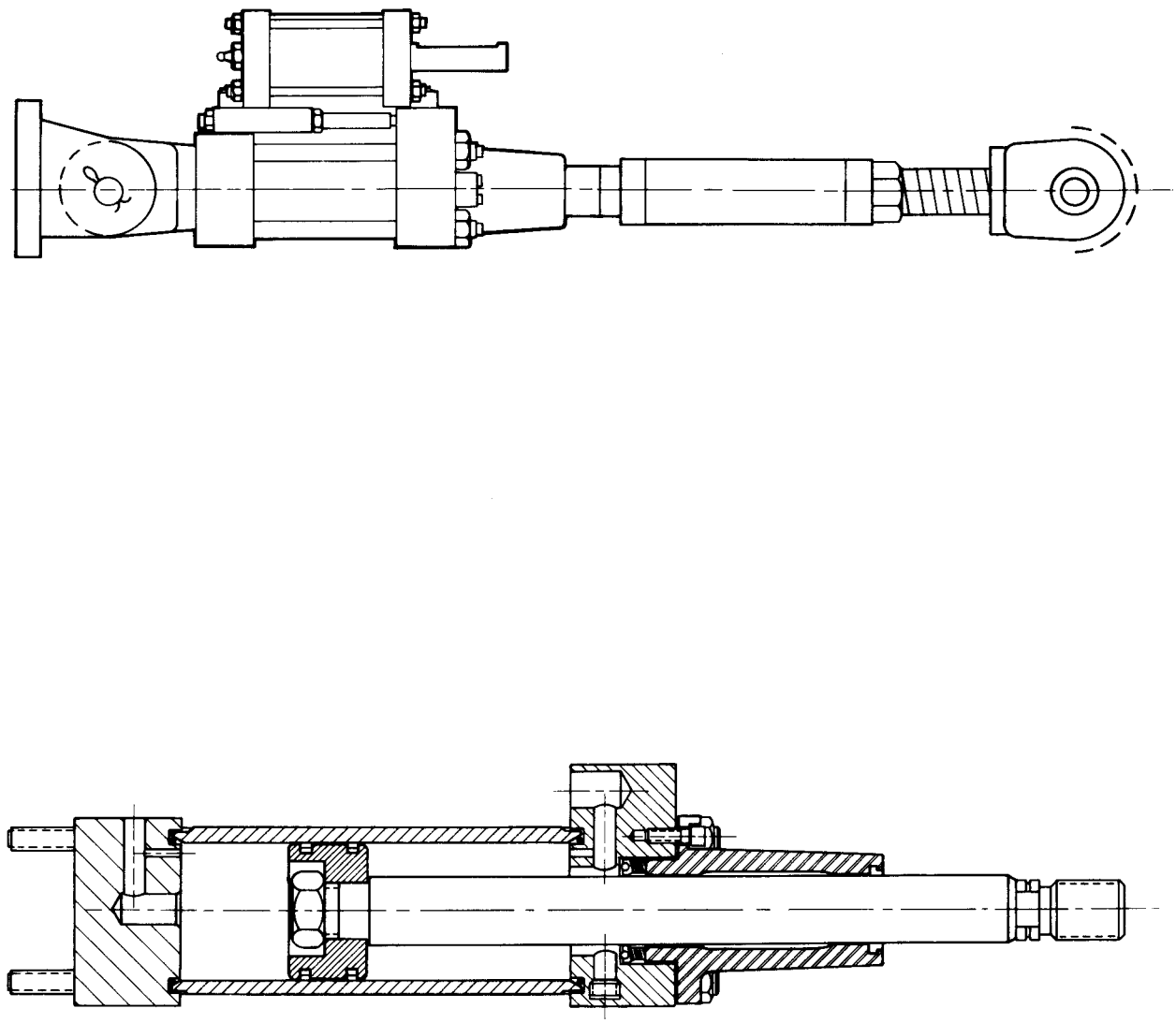

Figure 7.3. Sketch of a typical B-P hydraulic snubber.

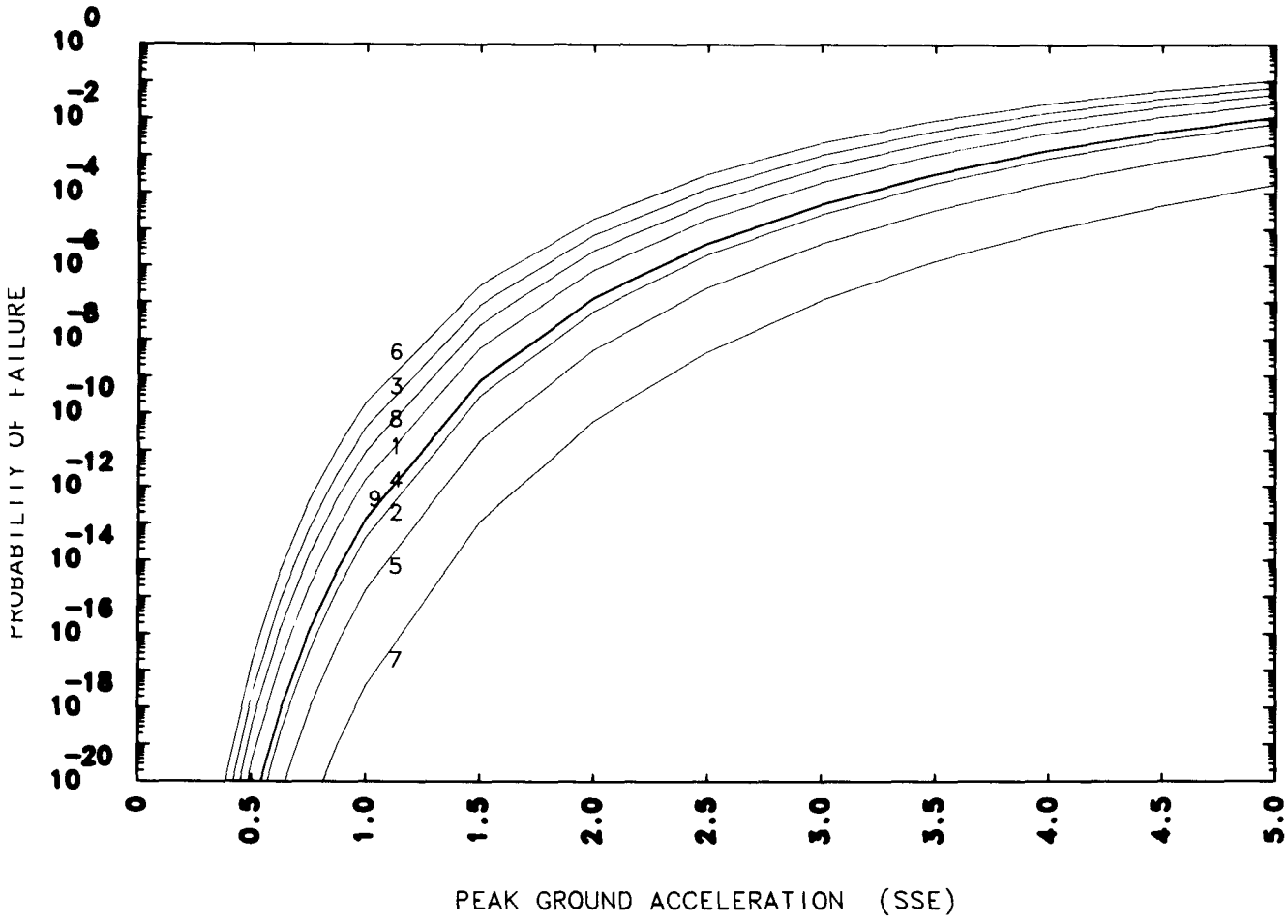

Curve	Snubber
1	SB1
2	SB2
3	SB3
4	SB4
5	SB5
6	SB6
7	SB10
8	SB12
9	BB12

Figure 7.4a. Failure probabilities of nine individual pipe snubbers (without relief valve).

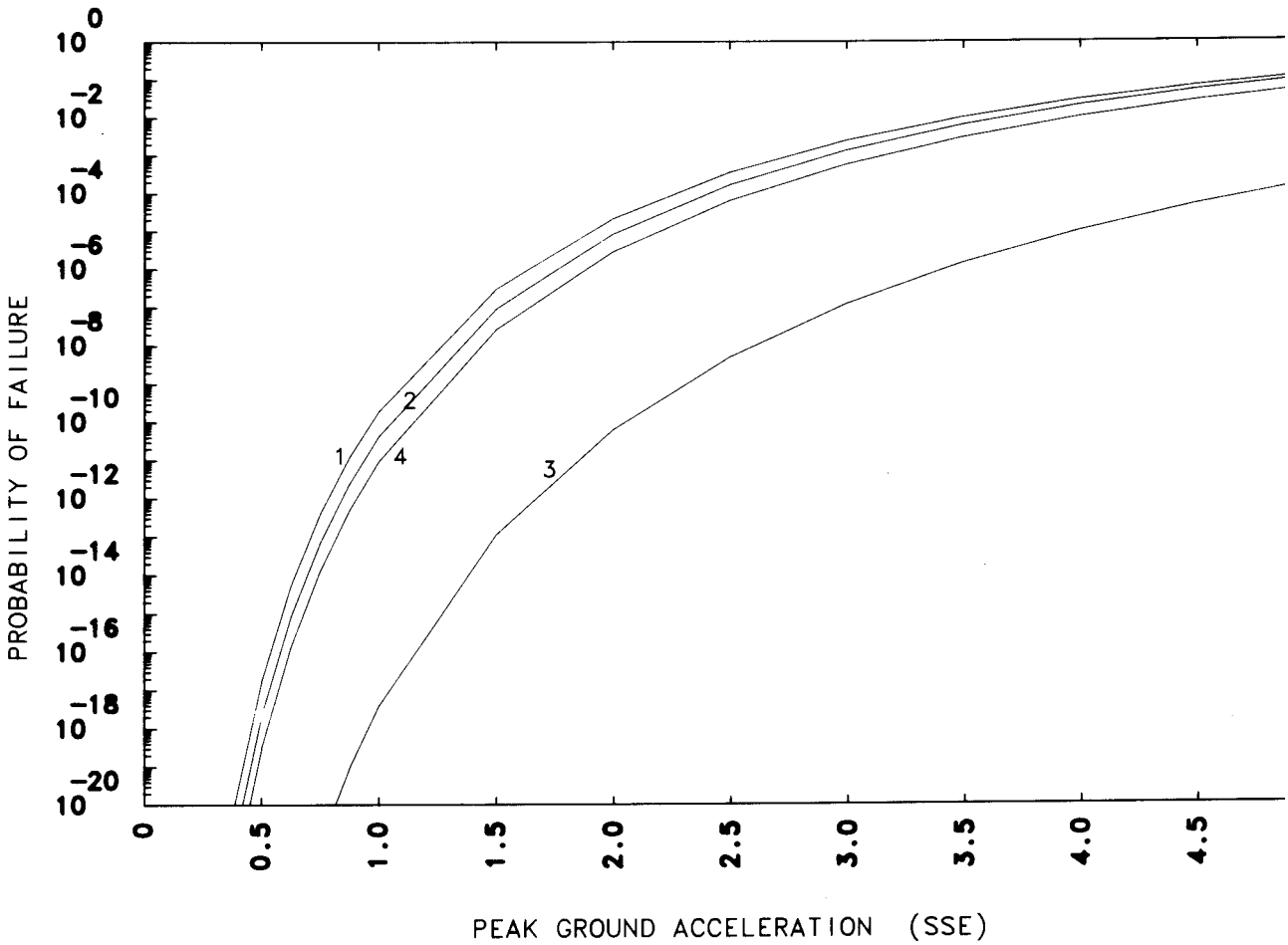

Figure 7.4b. Failure probabilities of four pipe support groups.

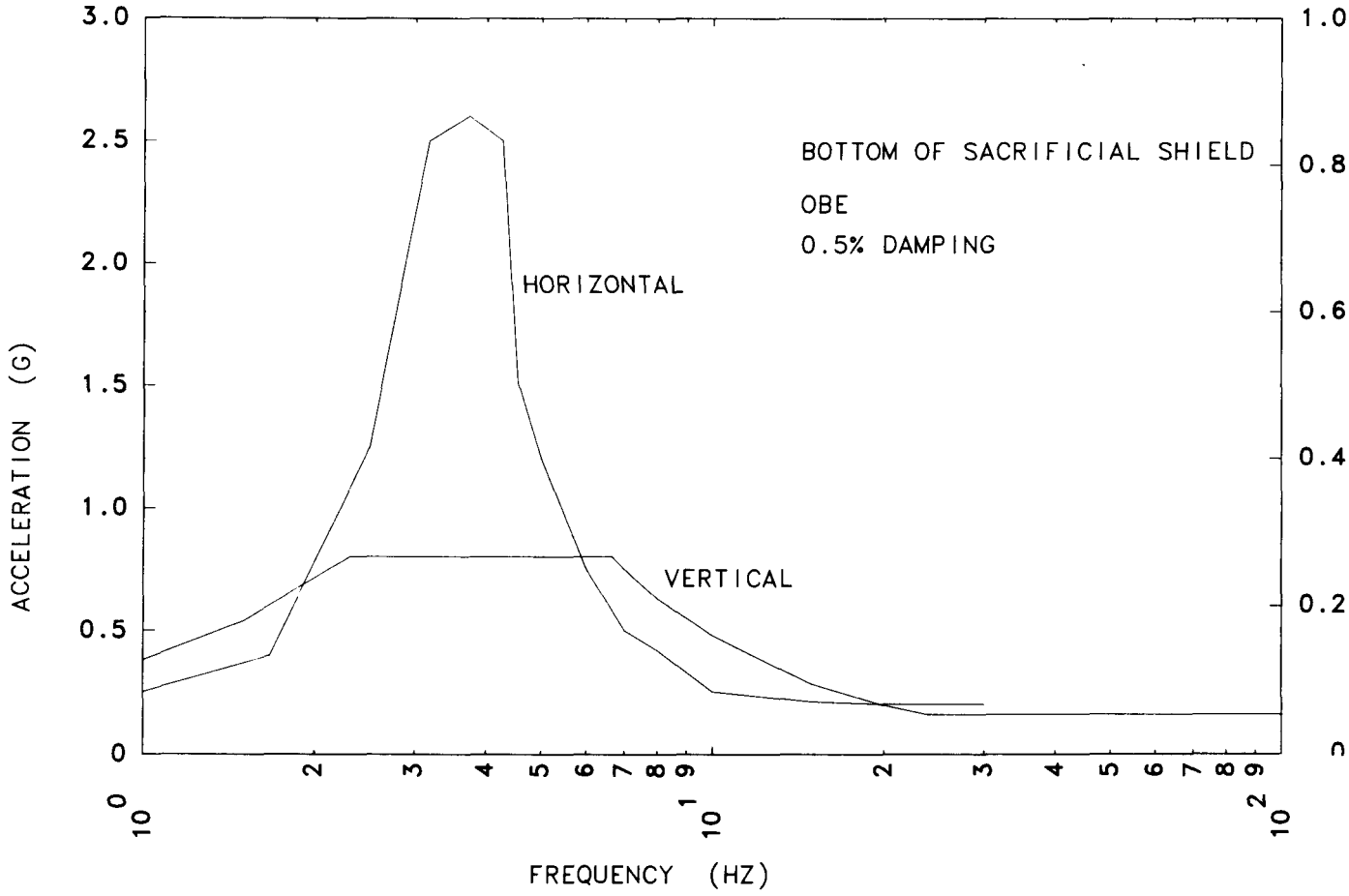

Figure 7.5. Horizontal and vertical in-structure response spectra at the bottom of the sacrificial shield.

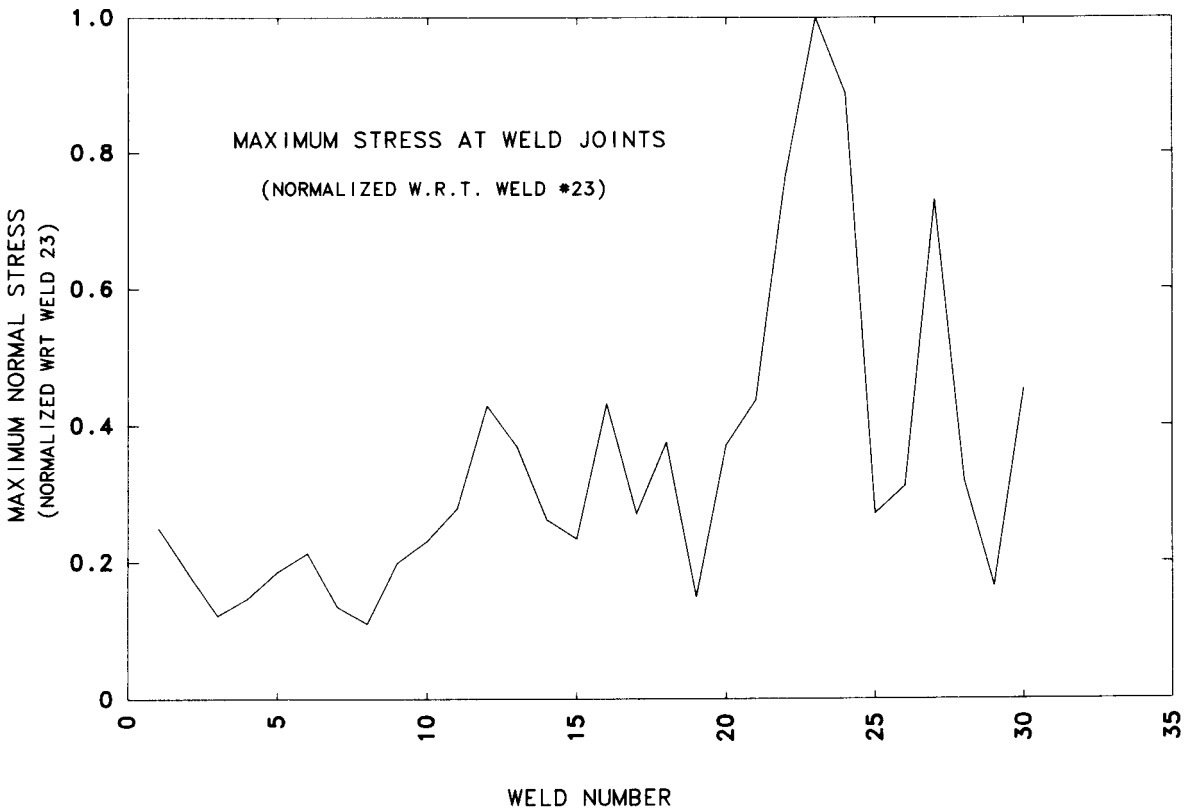

Figure 7.6. Maximum normal stress at weld joints of Brunswick replacement recirculation loops (no-support-failure case). Note that stresses are normalized with respect to those at Weld 23.

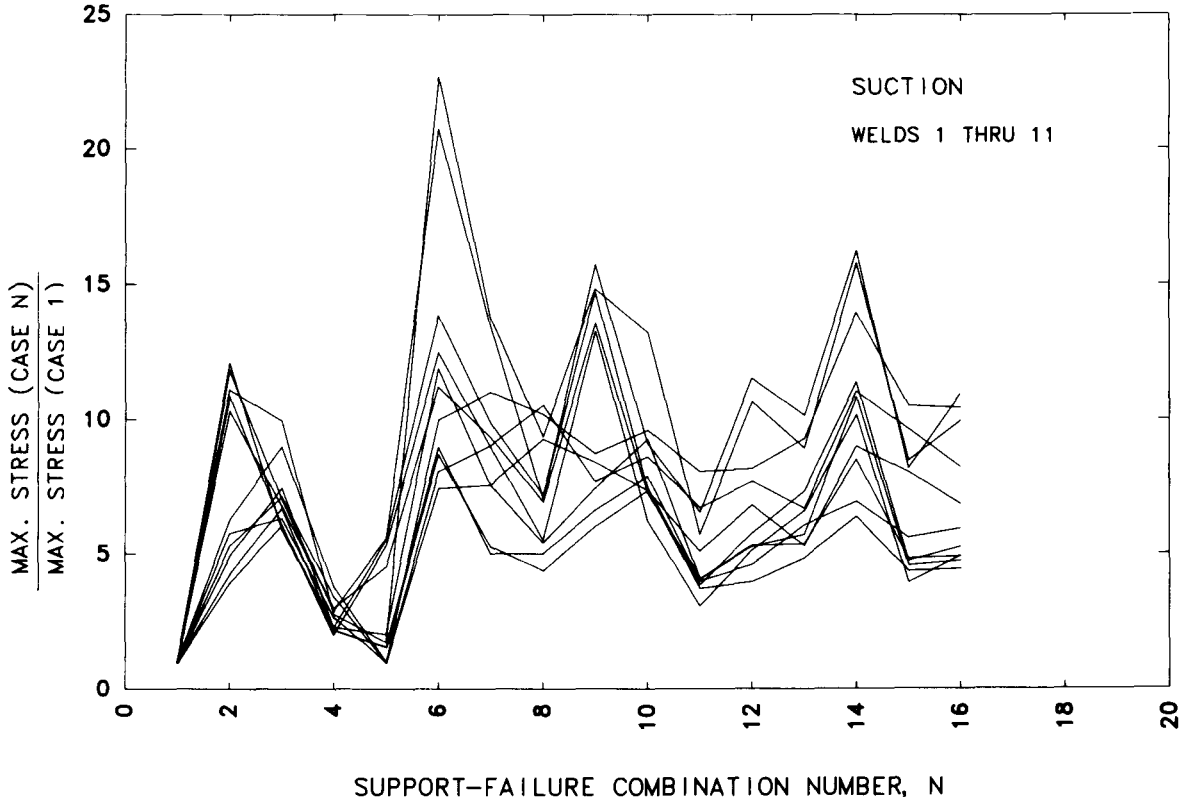

Figure 7.7a. Increase in seismic stresses at weld joints of the suction line due to support failure.

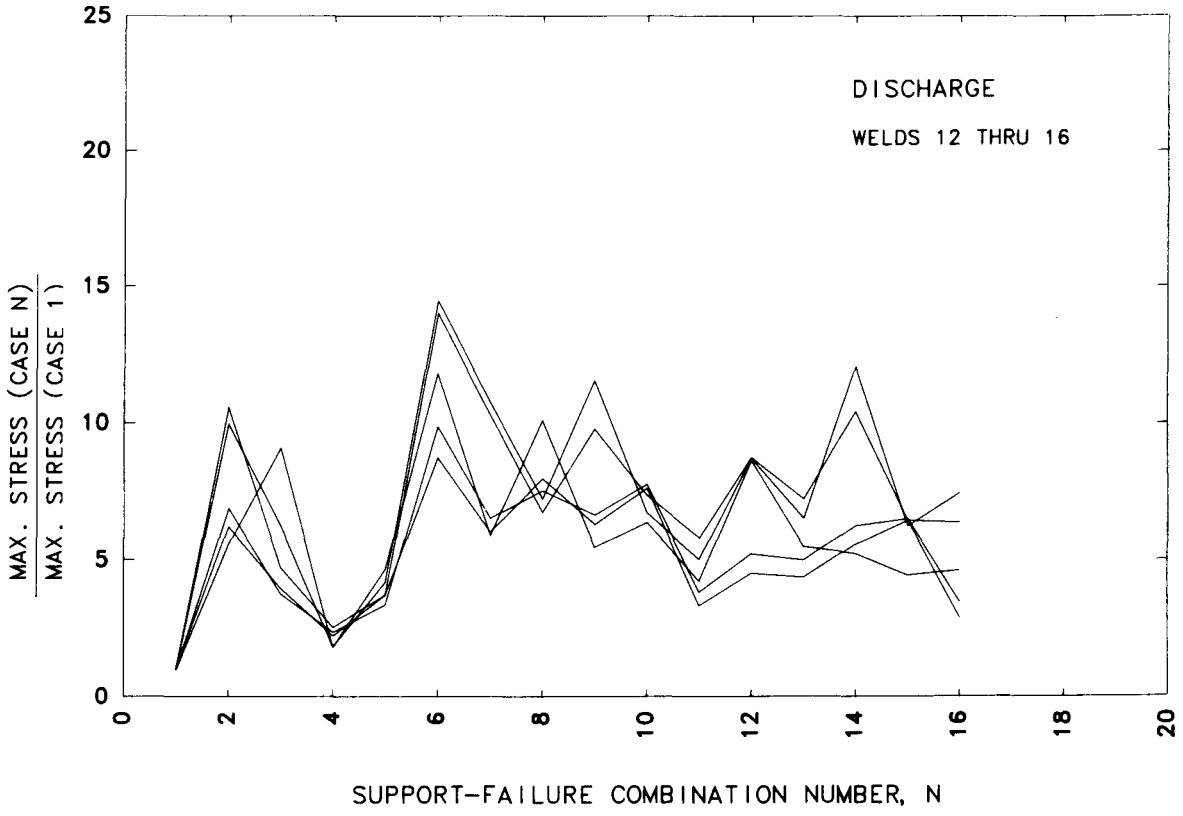

Figure 7.7b. Increase in seismic stresses at weld joints of the discharge line due to support failure.

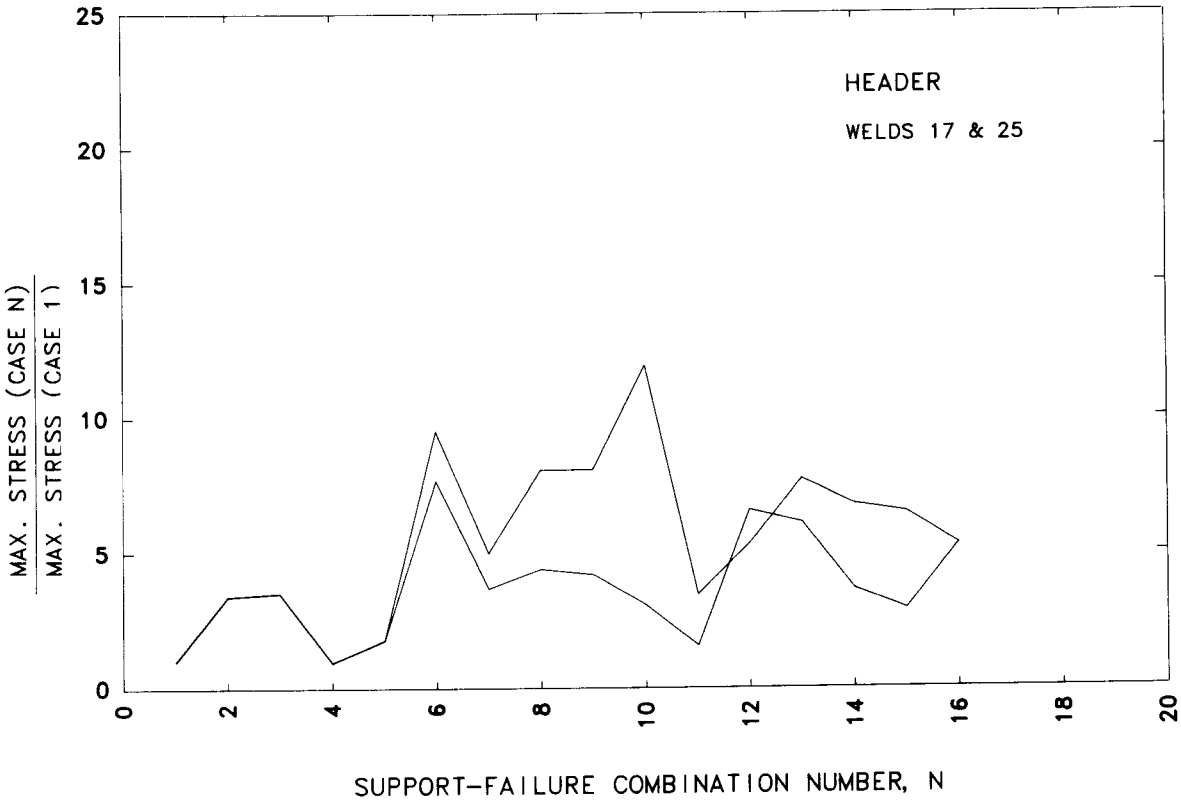

Figure 7.7c. Increase in seismic stresses at weld joints of the header due to support failure.

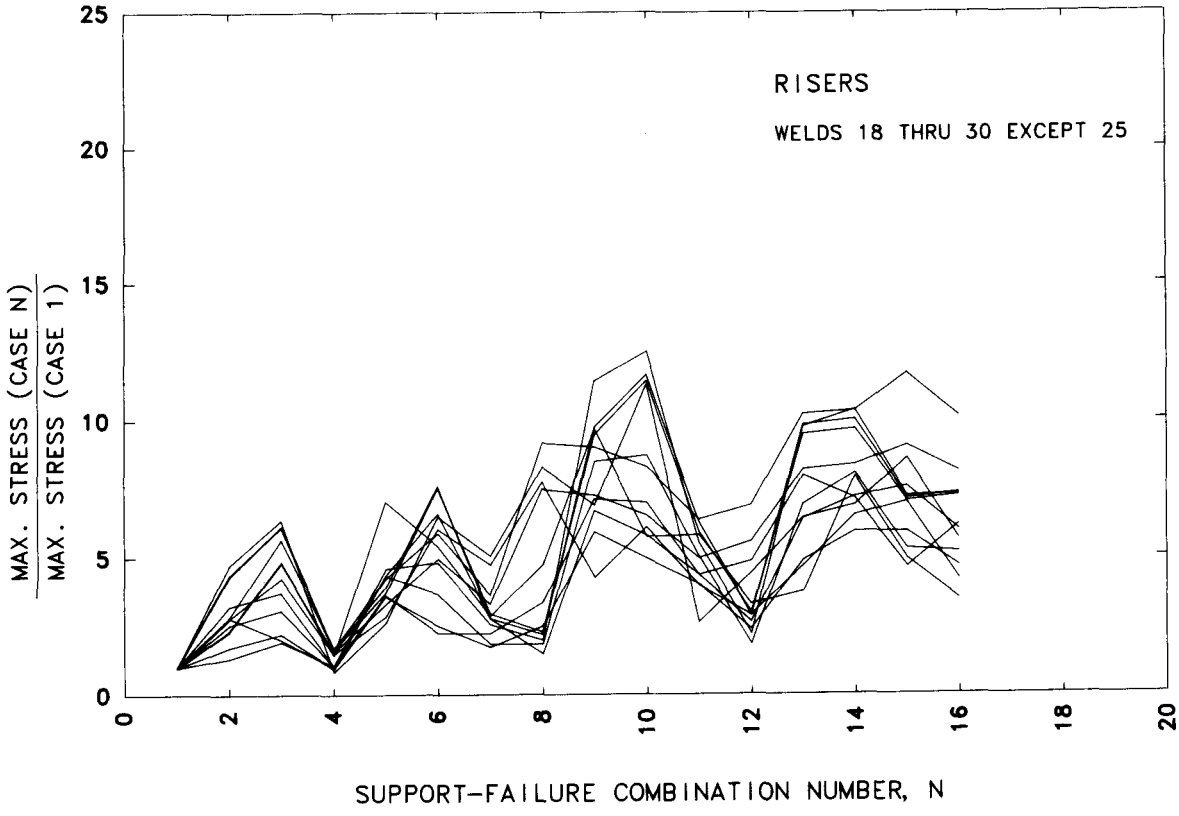

Figure 7.7d. Increase in seismic stresses at weld joints of the risers due to support failure.

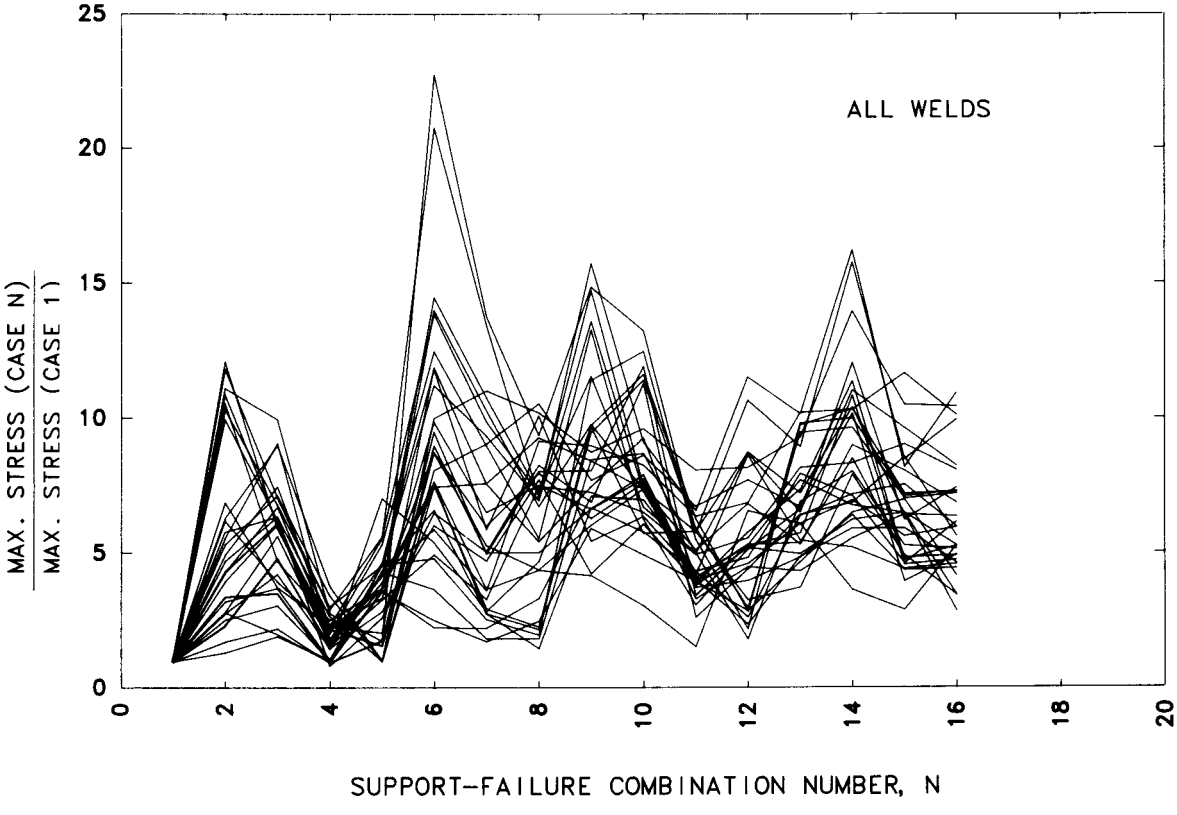

Figure 7.7e. Increase in seismic stresses at all recirculation loop weld joints due to support failure.

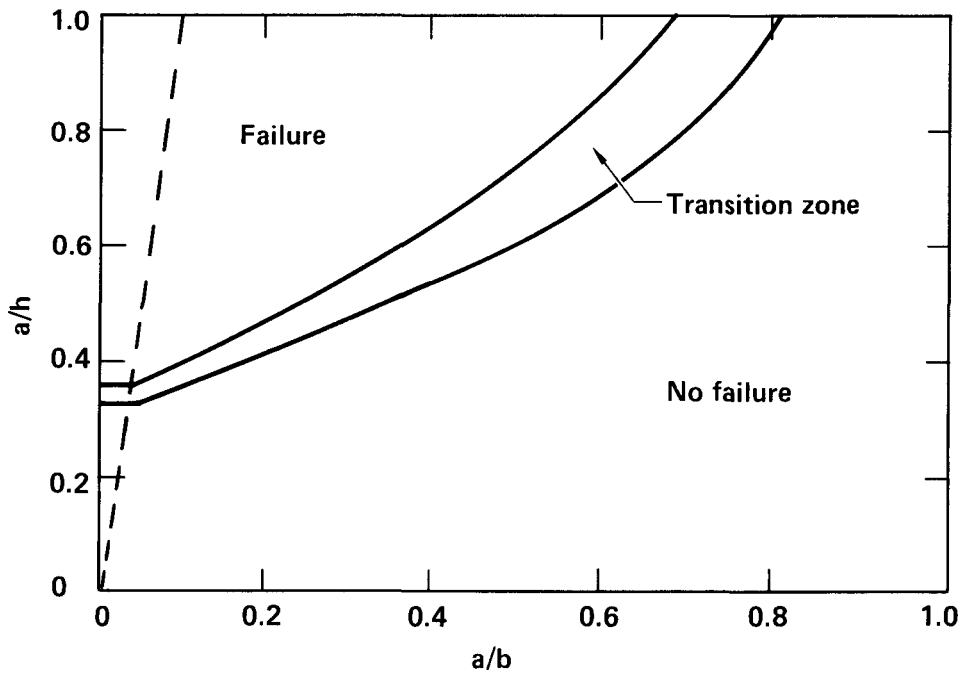

Figure 7.8a. Sampling space and zones of failure.

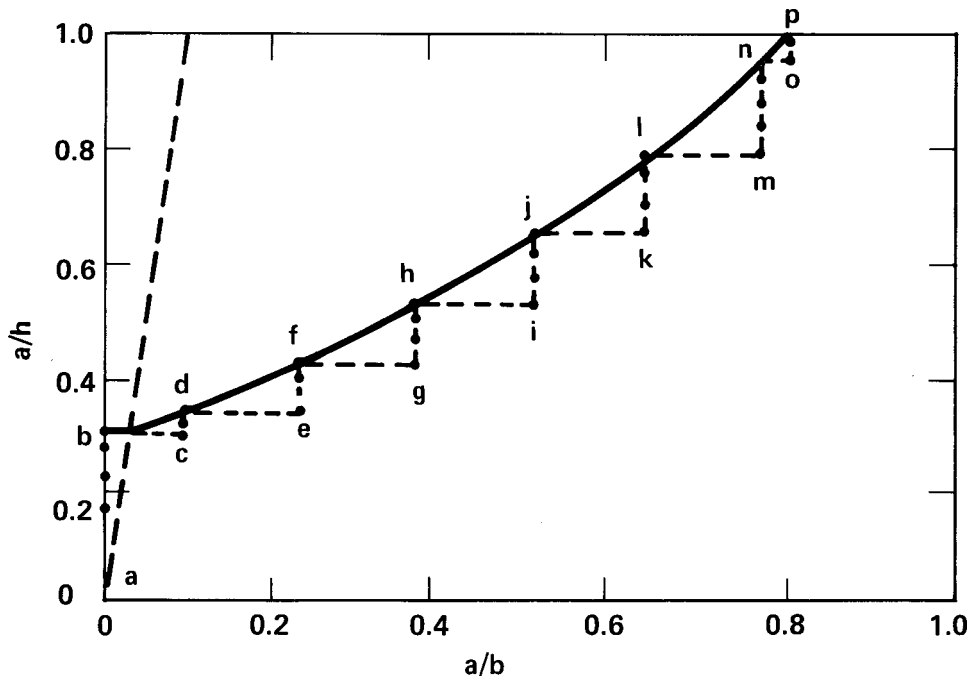

Figure 7.8b. Finding the boundary between failure and no-failure zones.

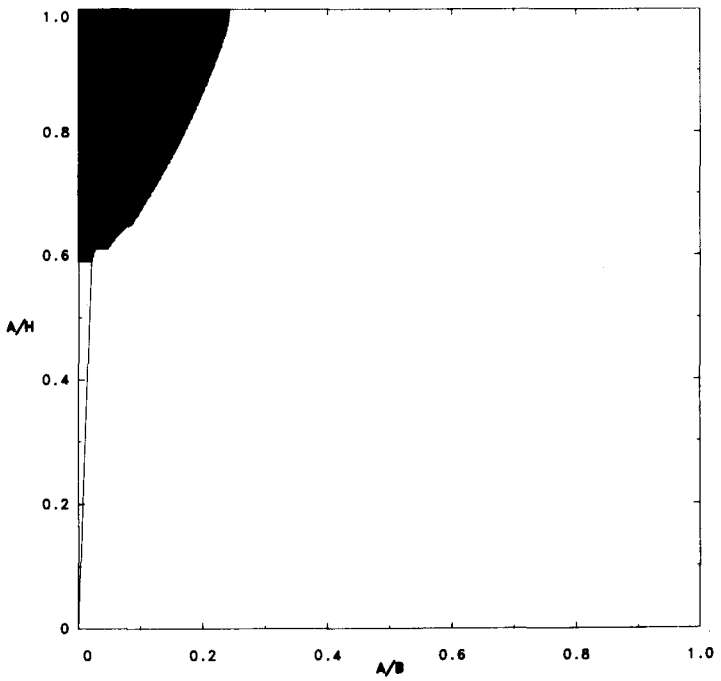

Figure 7.8c. A typical failure zone calculated from the simplified probabilistic fracture mechanics approach.

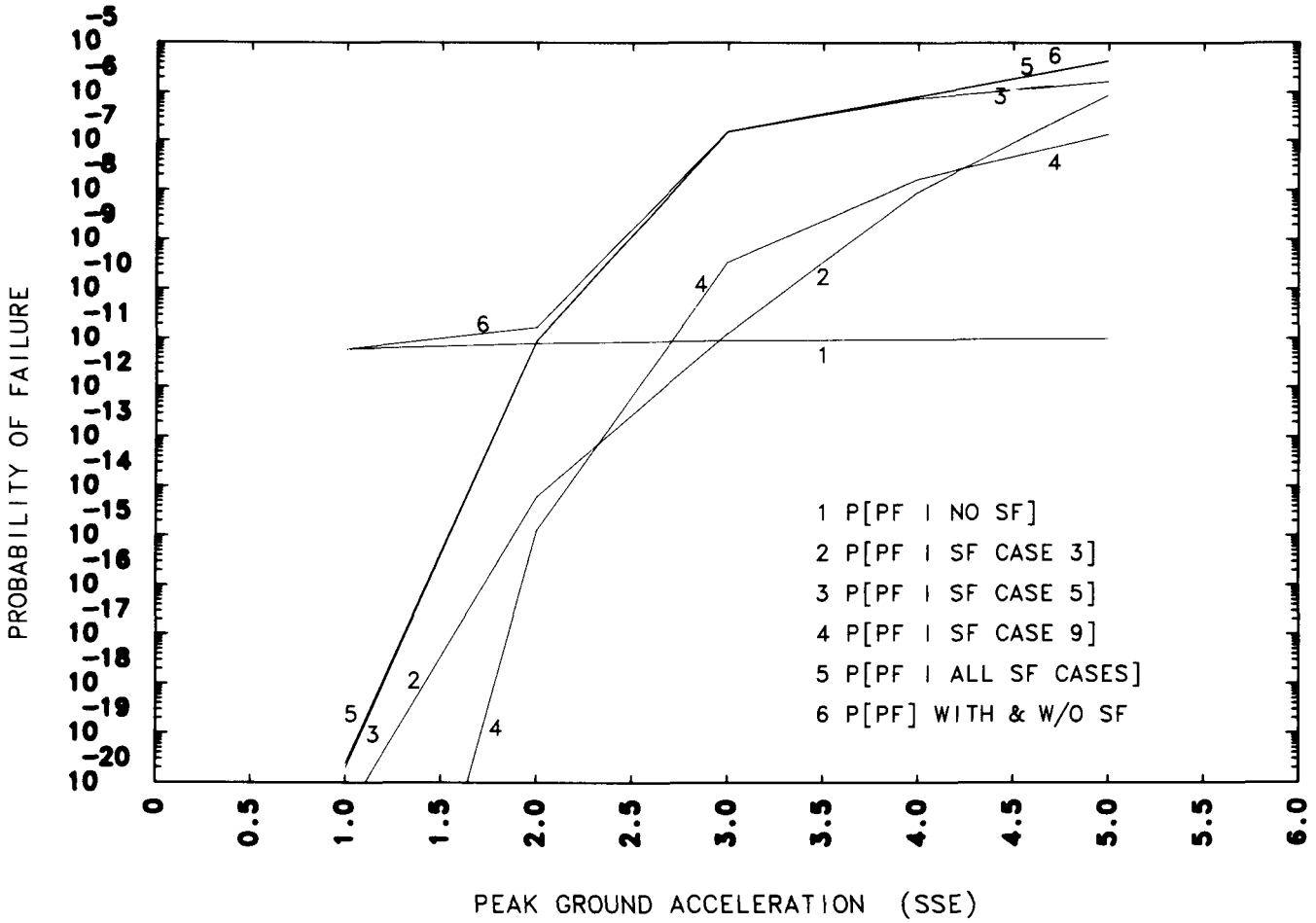

Figure 7.9. The effects of various support failure combinations and seismic hazard curve truncation.

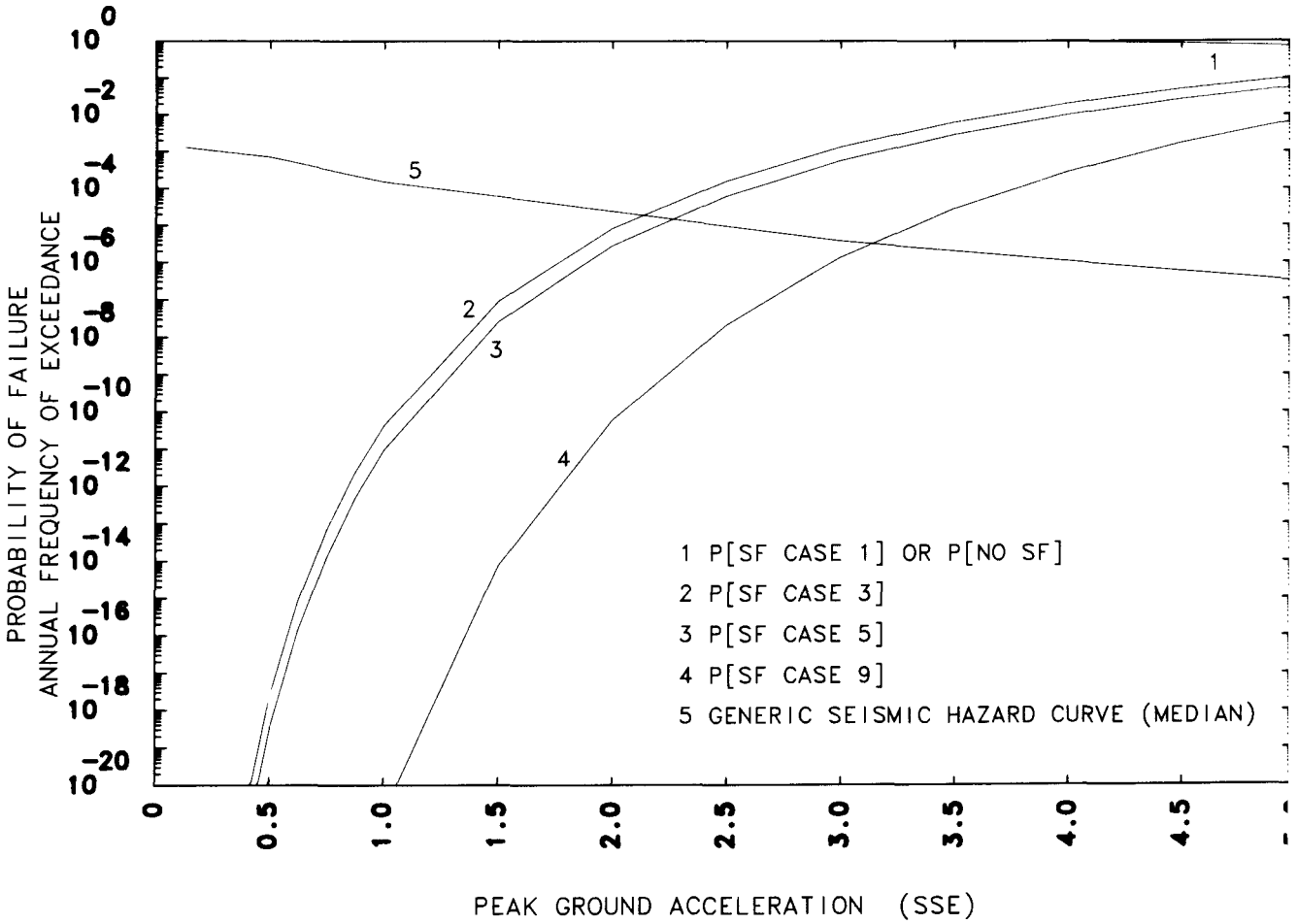

Figure 7.10. Support failure probabilities for several major support failure scenarios.

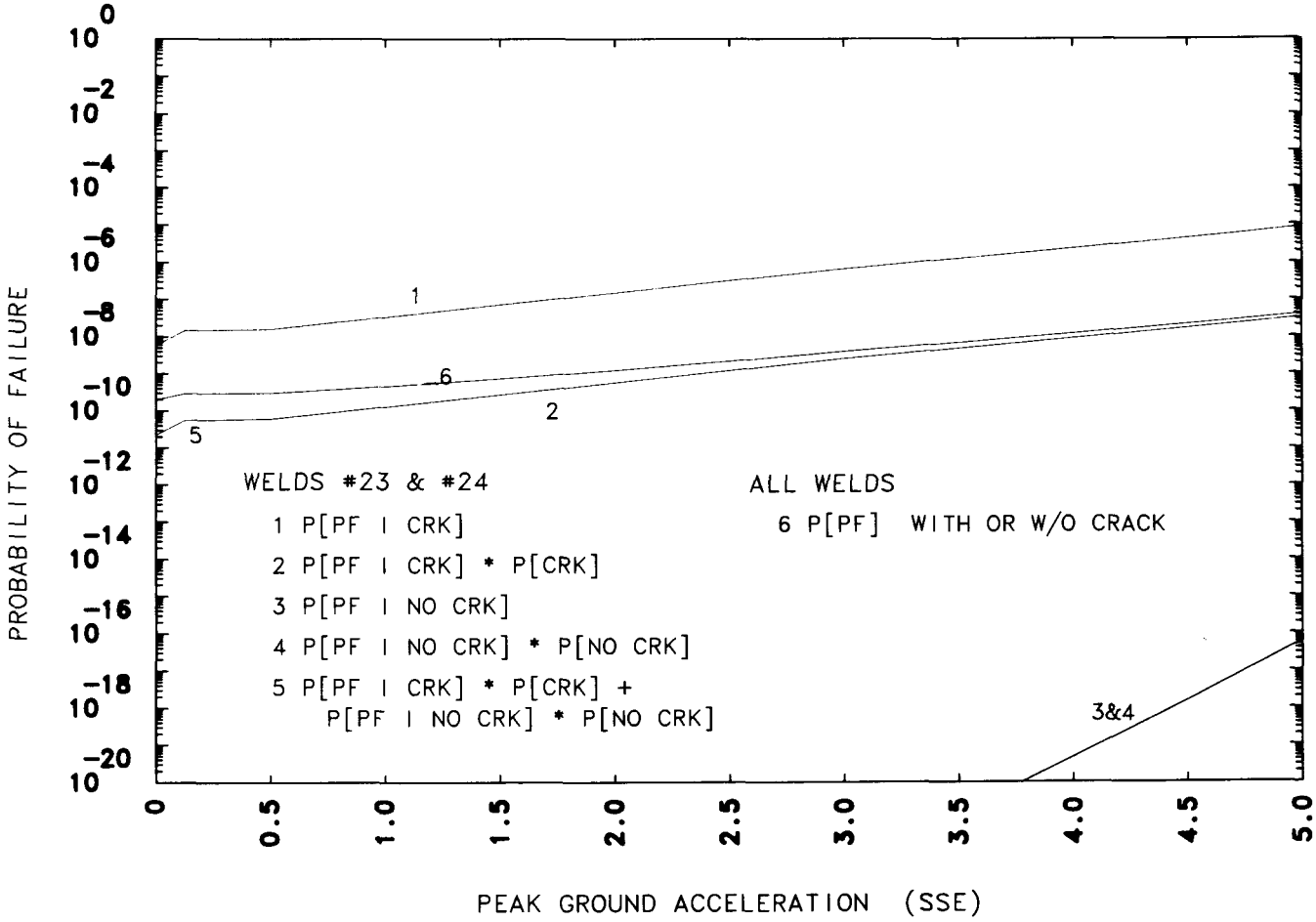

Figure 7.11. Contributing elements of the no-support-failure case.

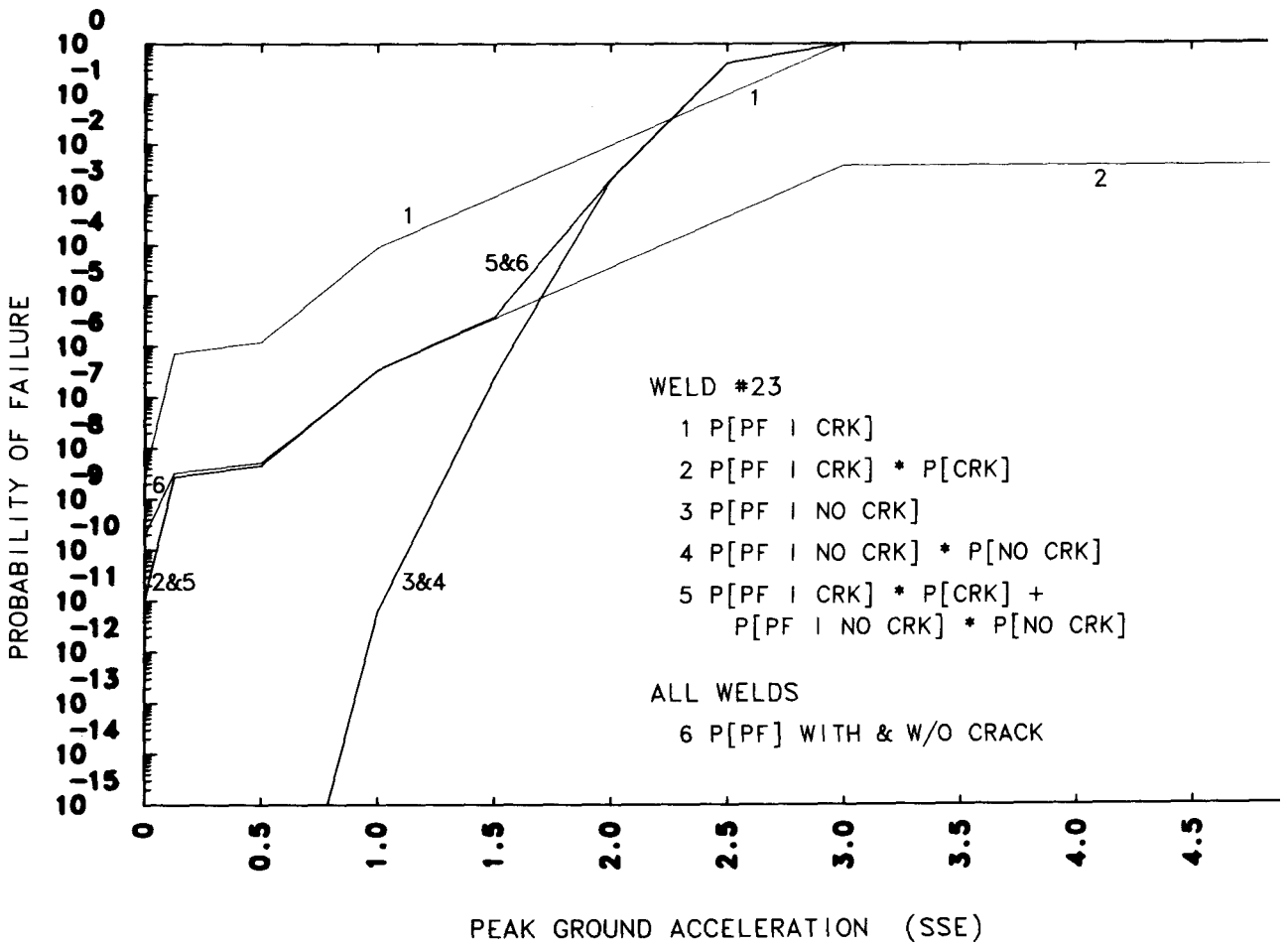

Figure 7.12. Contributing elements of the dominate support failure scenario (Case 5).

8. SUMMARY AND CONCLUSIONS

In nuclear power plants, the postulation of DEGB in many safety-related piping systems has resulted in severe design loading conditions. These loading conditions have created difficulties in design, construction, and maintenance. Many believe that the probability of a DEGB in the nuclear piping systems is small, and the postulation of DEGB in design is not warranted and should be eliminated. Under the sponsorship of the U.S. NRC, we estimated the probability of failure of the reactor coolant loops of PWR plants in the United States. This estimate includes the RCL piping associated with the nuclear steam supply systems manufactured by the three major vendors: Westinghouse (Ref. 8.1), Combustion Engineering (Ref. 8.2), and Babcock & Wilcox (Ref. 8.3).

After the study of PWR plants, we started a pilot study of BWR plants; Unit 2 of the Brunswick Steam Electric Plant was selected as the pilot plant. We studied several major piping systems of the Brunswick Plant including the recirculation loops, the primary steam lines, and the feedwater lines. Due to the symmetry or the similarity of the loops or the lines within each system, only one loop or one line per system was studied. In the case of the recirculation loops, we studied both the Intergranular Stress Corrosion Cracking (IGSCC) susceptible existing system and the proposed IGSCC-resistant replacement system. The effects of the IGSCC were not studied here. It is the topic of another volume of this report (Ref. 8.4).

The BWR study documented in this volume of the report includes two parts. The first part considers the probability of pipe failure due to seismically-induced inertial loads in the piping itself. The second part considers pipe break caused by the seismically-induced failure of "intermediate" pipe supports, such as hangers and snubbers.

The first part follows essentially the same approach taken in our previous study of PWR plants except for some modifications. In this part of the study, the pipe supports were assumed to maintain their intended function during an earthquake. We performed two kinds of analysis, a "best-estimate" analysis and an uncertainty analysis. The best-estimate analysis considered the best-estimate models of all the relevant parameters and their associated randomness. The results of the best-estimate analysis indicated that the lifetime system leak and DEGB probabilities for the Brunswick major coolant piping systems are low and fall within narrow ranges. The lifetime leak probabilities vary from 2.4E-6 to 5.4E-5. The best-estimate DEGB probabilities are at least four orders of magnitude lower than the leak probabilities, varying from 1.0E-11 to 7.0E-11 over the lifetime of the plant.

One observation differs from our previous experience with the PWR plants: The seismically induced DEGB probabilities for the existing and the replacement recirculation loops are higher than the probabilities due to other causes during normal operation of the plant. This difference is probably due to the importance of seismic stress compared with

other operating stresses in the small pipes in a system consisting of both large and small pipes.

Seven parameters which have large modeling uncertainty are considered in the uncertainty analysis. These parameters are crack depth, crack aspect ratio, crack existence probability, non-detection probability, thermal expansion stresses, seismic stresses, and shape of seismic hazard curves. We used the Latin Hypercube sampling technique in the uncertainty analysis and obtained results in the form of empirical cumulative distributions of the system failure probability. The modeling uncertainty distribution of the leak and DEGB probabilities are very wide for all piping systems considered. The probability range for leak between the 10th and 90th percentiles for the replacement recirculation loops, the primary steam lines, and the feedwater lines are 6.2E+2, 1.7E+3, and 1.7E+3, respectively, on the logarithmic scale. The ranges for DEGB are 1.7E+4, 2.7E+4, and 1.1E+5. These wide distributions are consistent with our previous studies of the PWR plants.

As noted earlier, the second part of this study addressed how the failure of intermediate pipe supports affects the DEGB probability. No leak probability was assessed. The intermediate support of a piping system consists of hangers and snubbers. Pipe failure due to the failure of rigid pipe supports and other indirect causes is addressed in another volume of this report (Ref. 8.5). The failure in both of these types of supports has different implications on the pipe failure probability. In general, the integrity of the piping system cannot be maintained if a rigid support fails; i.e., the failure probability of the piping system is close to 1.0. On the other hand, the failure of intermediate supports may not cause the pipe to fail and the conditional pipe failure probability may be much less than 1.0 because the intermediate pipe supports are usually less massive than the rigid supports and may fail at lower earthquake intensity level. The problem of intermediate supports does not exist in the RCLs of the PWR plants because the RCLs are supported by heavy loop components, and there are no intermediate supports. The failure of the supports of a heavy loop component has the same effect as the rigid support failure. In other words, the pipes are assumed to have a high probability of rupture once the heavy component is no longer adequately supported.

Because of the complexity of the problem involving the failure of intermediate supports, we performed a demonstrative assessment of the replacement recirculation loops. The goal was to gain insight in the hope that a simple approach could be found. In this demonstration study, a few simplifying assumptions were made. The simplified study uses the system DEGB probability of the no-support failure case described in the previous paragraph and calculates the failure probabilities for fifteen with-support-failure cases in which one or more supports fail. The overall system failure probability is the sum of all the cases including both the cases with and without support failure.

The results of this demonstrative study indicate that extrapolation or truncation of the seismic hazard curve has significant effects on the overall system failure probability. These effects are mainly due to the rapid rise in seismic stresses as the earthquake intensity increases in the with-support failure cases. The system failure probability is not very sensitive to the seismic hazard curve truncation if the supports maintain their function during an earthquake. The overall system failure probability is dominated by the no-support-failure case if the truncation is around two times the SSE or less. The with-support failure cases start to dominate after the truncation level of two SSE.

The seismic hazard curves are believed to have large modeling uncertainty not only because there is a lack of seismicity data at earthquake levels above the SSE but also because there is a limit to the acceleration level the soil medium can transmit. Therefore, the relative contribution to failure between the no-support-failure case and the cases involving support failure is highly uncertain.

The maximum overall system failure probability is 4.3E-6 per plant lifetime at the seismic hazard truncation level of 5SSE. This probability value becomes 4.8E-4 if the relief valve opening load of the snubbers is assumed to be the failure level of the supports. However, as discussed earlier, this assumption is overly conservative because the snubber does not fail permanently when the relief valve opening load is reached. The relief valve simply behaves "plastically." Note that the support fragilities used are the medians on the uncertainty distribution.

The most important result of this demonstration study is that guidelines are now available to reduce greatly the amount of work in studying the effects of the failure of intermediate supports. In general, for a piping system, only a couple of with-support failure cases and a few weld joints for each case need be considered.

Another modeling uncertainty studied in the second part of the study is that associated with the estimation of support fragilities. We calculated overall system failure probabilities associated with fragilities at the 10% and 90% on the uncertainty distribution. The effects of the extrapolation or truncation of the seismic hazard curve are similar to the best-estimate case described in the foregoing paragraph, which uses the median fragility data of the supports. The upper bound of the overall system failure probability of the 90% case is 1.7E-4 per lifetime of the plant at the seismic hazard truncation level of 5SSE.

REFERENCES

8.1 **Probability of Pipe Failure in the Reactor Coolant Loops of Westinghouse PWR Plants**, Lawrence Livermore National Laboratory, Report UCID-19988, NUREG/CR-3660, Vol. 1-4 (1984).

8.2 **Probability of Pipe Failure in the Reactor Coolant Loops of Combustion Engineering PWR Plants**, Lawrence Livermore National Laboratory, Report UCRL-53500, NUREG/CR-3663, Vol. 1-3 (1984).

8.3 **Probability of Pipe Failure in the Reactor Coolant Loops of Babcock and Wilcox PWR Plants**, Lawrence Livermore National Laboratory, Report UCRL-53644, NUREG/CR-4290, Vol. 1-2 (1985).

8.4 D.O. Harris, D.D. Dedhia, E.D. Eason, and S.D. Patterson, **Probability of Failure in BWR Reactor Coolant Piping, Vol. 3: Probabilistic Treatment of Stress Corrosion Cracking in 304 and 316NG BWR Piping Weldments**, Lawrence Livermore National Laboratory, Report UCID-20914, NUREG/CR-4792, Vol. 3 (December 1986).

8.5 G.S. Hardy, R.D. Campbell, and M.K. Ravindra, **Probability of Failure in BWR Reactor Coolant Piping, Vol. 4: Guillotine Break Indirectly Induced by Earthquakes**, Lawrence Livermore National Laboratory, Report UCID-20914, NUREG/CR-4792, Vol. 4 (December 1986).

APPENDIX A

CRITICAL NET-SECTION STRESS FAILURE CRITERION

A.1 Net-Section Failure Involving Axial Force Only

The initial approximations that were used to calculate net-section failure were conservative and easy to calculate. The section was assumed to be under a uniform axial stress that could be calculated from the simple formula

$$\sigma_{net} = F_{axial}/A_{net} \qquad \text{(A-1)}$$

where

σ_{net} = the stress in the remaining net ligament,

F_{axial} = the total equivalent axial force due to the dead weight, thermal, pressure, etc., loads, and

A_{net} = the net area of the remaining ligament in the pipe.

The section was then considered to fail when the calculated stress σ_{net} equalled or exceeded the given flow stress σ_{flo}.

$$\sigma_{net} \geq \sigma_{flo} \qquad \text{(failure inequality)} \qquad \text{(A-2)}$$

The original version of PRAISE approximated A_{net} by assuming that the crack area is a sector that totally encloses the assumed elliptical crack. This assumed shape is shown in Fig. A.1. The singly hatched area shows the area of the sector and the doubly hatched area shows the area of the crack. The area of this sector conservatively approximates the area of the crack and is given by

$$A_{crack} = ab\left(2 + \frac{a}{r_i}\right) \qquad \text{(sector approximation)} \qquad \text{(A-3)}$$

where

a = the maximum depth of the crack

b = the half width of the crack, and

r_i = the inside radius of the pipe.

Then the net remaining ligament area is simply given by

$$A_{net} = A_{pipe} - A_{crack} \tag{A-4}$$

where A_{pipe} is the uncracked pipe (outside radius r_o) area. However, the exact area of the assumed elliptical crack can be readily calculated as detailed below. The elliptical crack is described by the following equation for an ellipse in polar coordinates:

$$\left(\frac{\Delta r}{a}\right)^2 + \left(\frac{\theta}{\theta_b}\right)^2 = 1 \tag{A-5}$$

Here θ_b is given by

$$\theta_b = b/r_i. \tag{A-6}$$

The geometry also has

$$\Delta r = r_e - r_i \quad \text{or} \tag{A-7}$$

$$r_e = r_i + \Delta r = r + a\left[1 - \left(\frac{\theta_e}{\alpha}\right)^2\right] \tag{A-8}$$

where $\alpha = b/r_i$ and r_e is the radius to any point on the elliptical crack at an angle θ_e from the crack center as shown in Fig. A.1.

The area of the crack can then be computed from the following integral:

$$A_{crack} = \int_0^{\theta_b} \frac{1}{2}\left(r_e^2 - r_i^2\right) d \tag{A-9}$$

Substituting the above equations into this integral expression we get eventually

$$A_{crack} = ab\left(\frac{\pi}{2} + \frac{2}{3}\frac{a}{r_i}\right) \qquad \text{(A-10)}$$

This equation has been substituted throughout the PRAISE code where pure axial net section failure is being computed. Also, this equation has been substituted in all other places where the crack area is calculated.

A.2 Net-Section Failure Involving Axial Force and Bending Moment

The original version of PRAISE used only an axial stress, or equivalently an axial force, to calculate failure. The basic criterion for failure was that the updated stress on the remaining ligament in the pipe must equal or exceed the flow stress. Symbolically, this relationship is expressed as

$$|\sigma_{net}| \geq \sigma_{flo} \qquad \text{(failure inequality)} \qquad \text{(A-11)}$$

where σ_{net} is the net stress on the remaining ligament and σ_{flo} is the prescribed flow stress.

A relatively straightforward failure criterion can be developed for loadings that include not only an axial force but also a bending moment.

For the more general case of an axial force plus bending moment at the ideal fully plastic flow stress limit, the cross section is assumed to be everywhere at the magnitude of the limiting flow stress and have complete stress reversal. Figure A.2 illustrates this assumed stress loading for a beam of rectangular cross-section. This concept can be used on the cracked pipe cross-section to derive limit expressions for the applied bending moment.

Proceeding, we will first assume that the geometry and loading is as shown in Fig. A.3. Figure A.3 shows that the crack has also been assumed to occur at the most severely strained location, i.e. at the place where the pipe would be exposed to the maximum tensile strain, which would tend to open the crack even more. Figure A.4 also shows that β, the angle to the stress reversal axis, is greater than α, the angle to the tip of the crack. For this loading at impending failure, we must have

$$\begin{aligned} P &= \sigma_{flo}(A_1 - A_2), \text{ or} \\ A_1 - A_2 &= P/\sigma_{flo} \end{aligned} \qquad \text{(A-12)}$$

where A_1 and A_2 are the areas above and below the stress reversal axis,

respectively, and P is the axial load. But we also have the simple relationship concerning the total area of the ligament:

$$A_1 + A_2 = A_{net} = A_{pipe} - A_{crack} \tag{A-13}$$

Subtracting the above two equations yields

$$A_2 = \frac{1}{2}\left(A_{net} - \frac{P}{\sigma_{flo}}\right) \tag{A-14}$$

But from the geometry alone, A_2 is given by the formula

$$A_2 = 2\,(\pi - \beta)\,r_m h \tag{A-15}$$

where r_m is the mean radius of the pipe ($r_m = r_i + h/2$), and h is the thickness of the pipe. Elimination of A_2 from the above two equations yields a result for calculating β which locates the stress reversal axis.

$$\beta = \pi + \frac{\frac{P}{\sigma_{flo}} - A_{net}}{4\, r_m h} \tag{A-16}$$

The moment can then be examined analytically. Simple strength of materials gives

$$M_{bx} = \sigma_{flo}\,(Q_{A_1 x} - Q_{A_2 x}) \tag{A-17}$$

where

M_{bx} = the bending moment about the x-axis,

$Q_{A_1 x}$ = the first moment of area of A_1 about the x-axis, and

$Q_{A_2 x}$ = the first moment of area A_2 about the x-axis.

The first moment of area is given by

$$Q_{A_1 x} = 2\int_0^{\beta} r_m^2 \, h \cos\theta \, d\theta - Q_{crack\alpha x} \tag{A-18}$$

$$= 2 r_m^2 \, h \sin\beta - Q_{crack\alpha x} \tag{A-19}$$

where $Q_{crack\alpha x}$ is the first moment of area of the crack about the x-axis (note that the crack subtends an angle α). Similarly, we have

$$Q_{A_2 x} = -2 r_m^2 \, h \sin\beta \tag{A-20}$$

Thus the equation for the limiting bending moment about the x-axis becomes

$$M_{bx} = \sigma_{flo} (4 r_m^2 \, h \sin\beta - Q_{crack\alpha x}) \tag{A-21}$$

Thus once $Q_{crack\alpha x}$ is found, the limiting moment that the remaining ligament can support can be calculated from the above formula. If the applied moment is equal to or more than this limiting moment, then the section is considered to have failed.

$$M_{applied} \geq M_{bx} \qquad \text{(failure inequality)} \tag{A-22}$$

The foregoing derivations were concerned with the case where β is greater than α. For completeness the case must be addressed where β is less than α. For this case the crack closes on the compressive stress side.

For this case, the area of the pipe is now given by

$$A_1 + A_2 + A_\eta = A_{pipe} \tag{A-23}$$

where A_η is the area of the open crack up to the stress reversal axis. Elimination of A_1 from previous equations gives

$$2 A_2 + A_\eta = A_{pipe} - P/\sigma_{flo} \tag{A-24}$$

Geometry gives

$$A_2 = 2\ (\pi - \beta)\ r_m h \qquad \text{(A-25)}$$

From integration in polar coordinates we get

$$A_\eta = \frac{a r_i}{\alpha}\left[\beta\sqrt{(\alpha^2 - \beta^2)} + \alpha^2\ \text{arcsin}\frac{\beta}{\alpha}\right] + a^2\beta\left[1 - \frac{1}{3}\left(\frac{\beta}{\alpha}\right)^2\right] \qquad \text{(A-26)}$$

Returning to the equation

$$2\,A_2 + A_\eta = A_{pipe} - P/\sigma_{flo}$$

we see that, even though all quantities can be written in terms of , we cannot solve for β explicitly. Therefore, a Newton-Raphson scheme is adopted in iterating to find β.

The initial value β_0 is assumed to be the β that can be calculated when α is less than β, that is, the β given in Eq. (A-16). Experience has shown that one iteration is sufficient for convergence. Also, similar to what was developed previously, it can be stated that when β is less than α

$$M_{bx} = \sigma_{flo}\ (4\ r_m^2\ h \sin\beta - Q_{crack\beta x}) \qquad [\beta < \alpha] \qquad \text{(A-27)}$$

where $Q_{crack\beta x}$ is the first area of moment for that part of the crack up to the angle β.

Until now the first moments of area, $Q_{crack\alpha x}$ and $Q_{crack\beta x}$, for the crack have not been calculated. This calculation was deferred to here because it is essentially the same for both cases. The only difference is that the angle used in the calculation is either corresponding to the full crack ($Q_{crack\alpha x}$) or the converged corresponding to the partially closed crack ($Q_{crack\beta x}$). This derivation starts from the basic integral formulation for first moment of area, that is

$$Q_{crack\alpha x} = 2\int_0^{\theta_\alpha}\int_{r_i}^{r_e} y\ r\ dr\ d\theta \qquad \text{(A-28)}$$

or

$$Q_{crack\,\beta\,x} = 2\int_0^{\theta_\beta}\int_{r_i}^{r_e} y\, r\, dr\, d\theta \qquad \text{(A-29)}$$

depending on the angle used in the calculation.

For $y = r\cos\theta$ and for r_e, substitutions and simplifications yield an equation that cannot be integrated in closed form, but within the PRAISE program it is evaluated numerically using standard two point Gaussian quadrature. With this last evaluation all quantities have then been obtained to make the test concerning net section failure as embodied in Eq. (A-22).

A previous version of PRAISE used a much simplified theory to test for net section failure involving both axial force and bending moment. This theory calculated the dimensions of a symmetric rectangular beam that was equivalent in area. The P vs M interaction equation could then be derived in closed form and compared to the applied axial force and bending moment. The theory that has been derived above cannot be manipulated to give a closed form P vs M equation. However, a graphical presentation of this equation can be found numerically. These graphs were then compared to the same plots as derived from the closed form P vs M equation. These comparisons are shown in Figs. A.5, A.6, and A.7.

Figure A.5 shows the interaction diagrams from the two theories as they are applied to a nominal pipe configuration where the crack is small compared to the dimensions of the pipe. That is, the depth of the crack is one-tenth of the thickness of the pipe and the width of the crack is one-tenth the inside circumference of the pipe. For such a small crack it is reassuring that both theories yield the same interaction diagram, i.e. the one for the essentially uncracked pipe.

Figure A.6 shows the two interaction diagrams for a pipe that has a crack of intermediate dimensions. That is, the depth of the crack is one-half the circumference. Discrepancies in the simpler, symmetric theory start to show up in this figure.

Finally, Fig. A.7 shows two diagrams for a deeply cracked pipe where the crack dimensions are nine-tenths of the pipe dimensions. These diagrams show that the simpler, symmetric theory is not conservative for these critical cracks, which are the ones most likely to cause net section failure. PRAISE results show a factor of 2.5 to possibly 3.0 between the DEGB probabilities that were calculated using the simpler theory as compared to the above theory for net-section failure. This difference can be explained somewhat by the approximate factor of 3 that shows up in the comparison of the moments in Fig. A.7 (for P=0). That is, the ratio between the more critical failure moment M for zero load P from the simpler theory is approximately three times that for the same moment derived from the theory developed here.

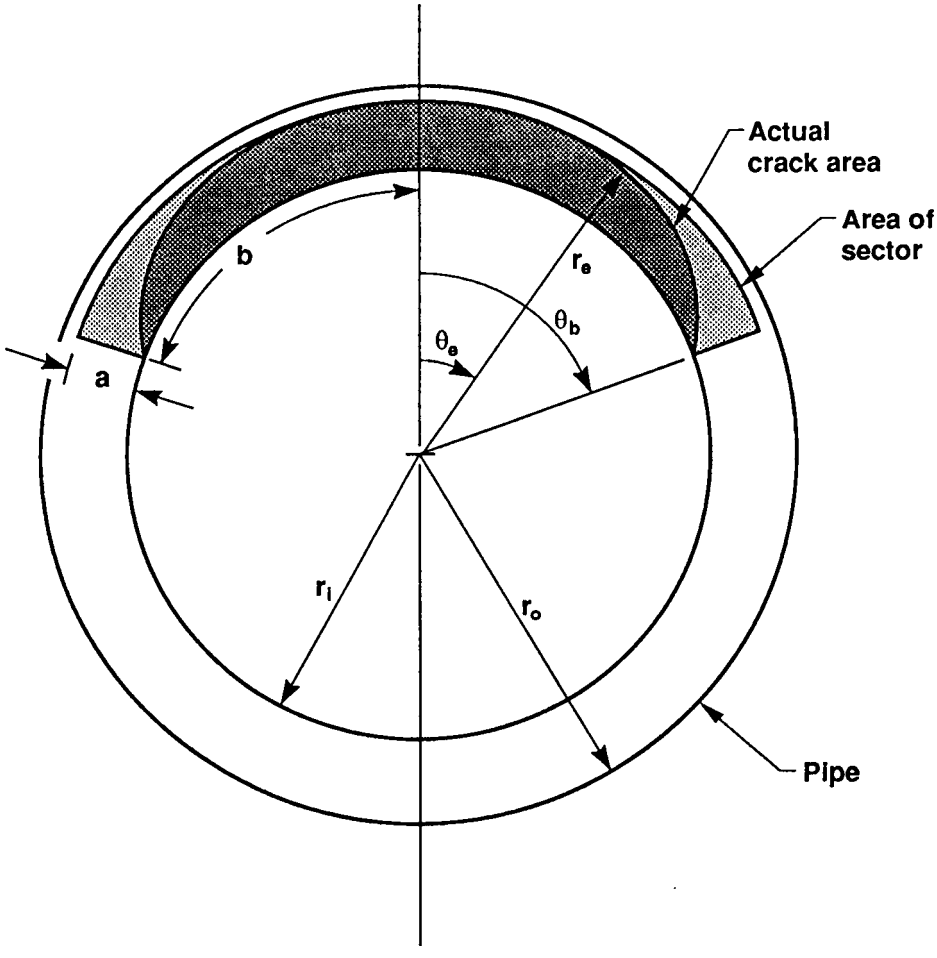

Figure A.1. Assumed area of crack.

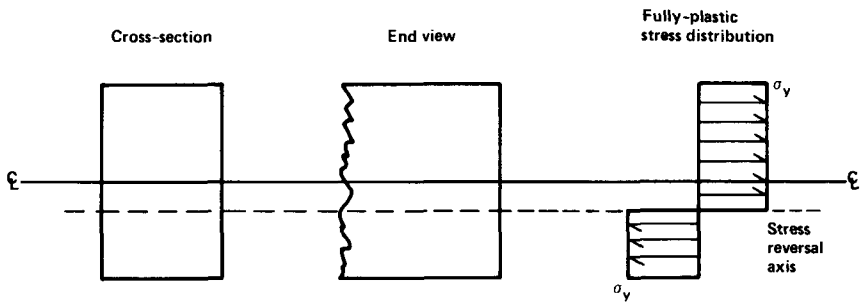

Figure A.2. Assumed fully plastic stress distribution for a rectangular beam.

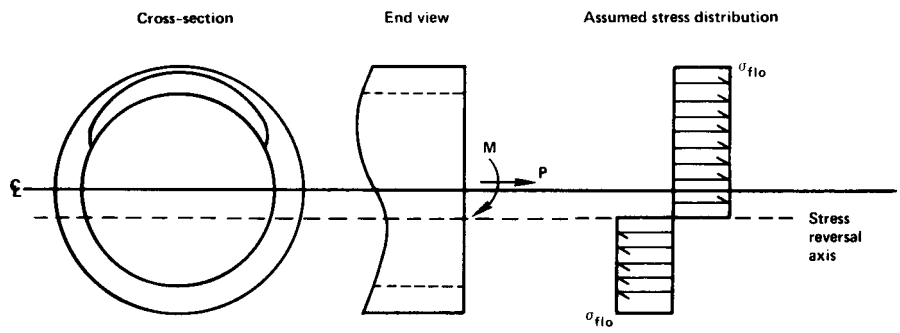

Figure A.3. Loading and assumed stress distribution on cracked pipe

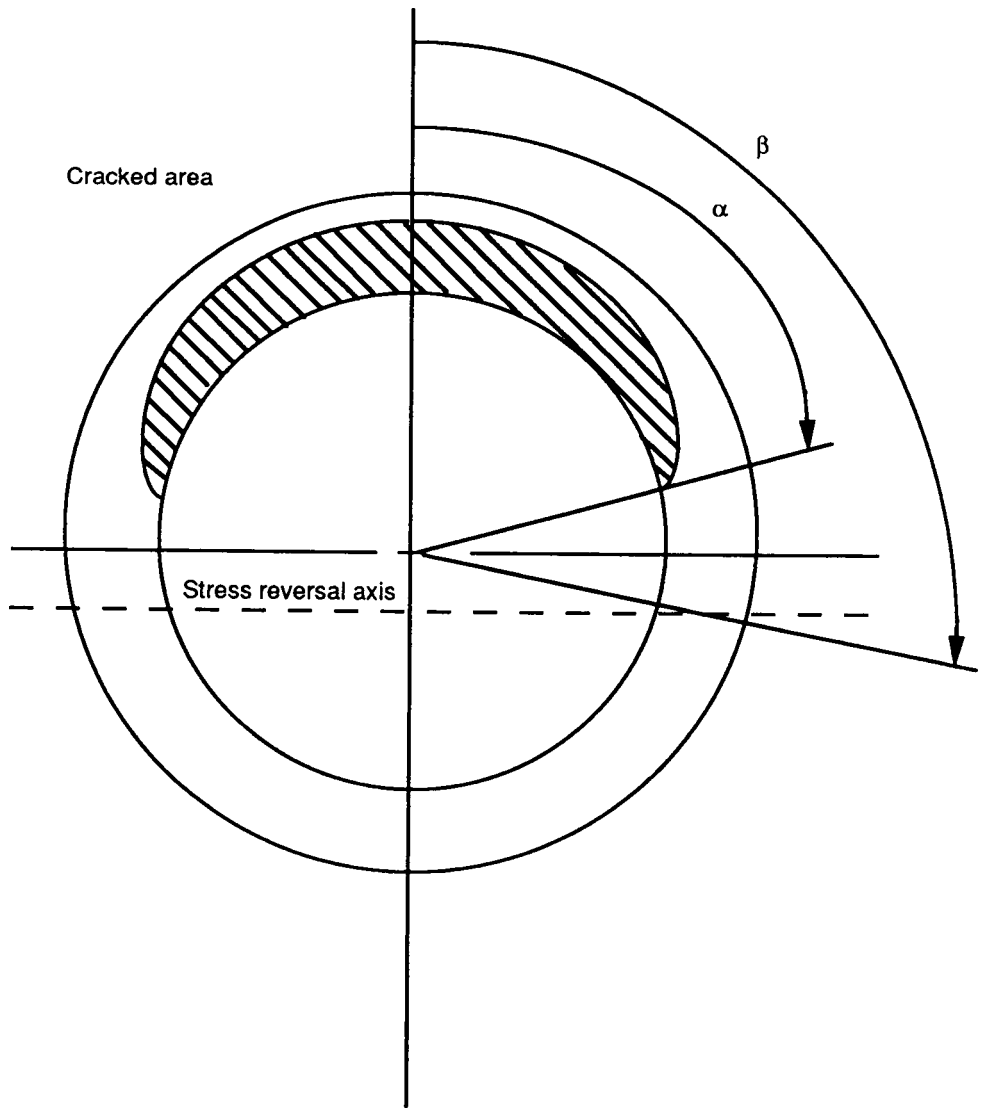

Figure A.4. Distribution of angles, $\beta > \alpha$.

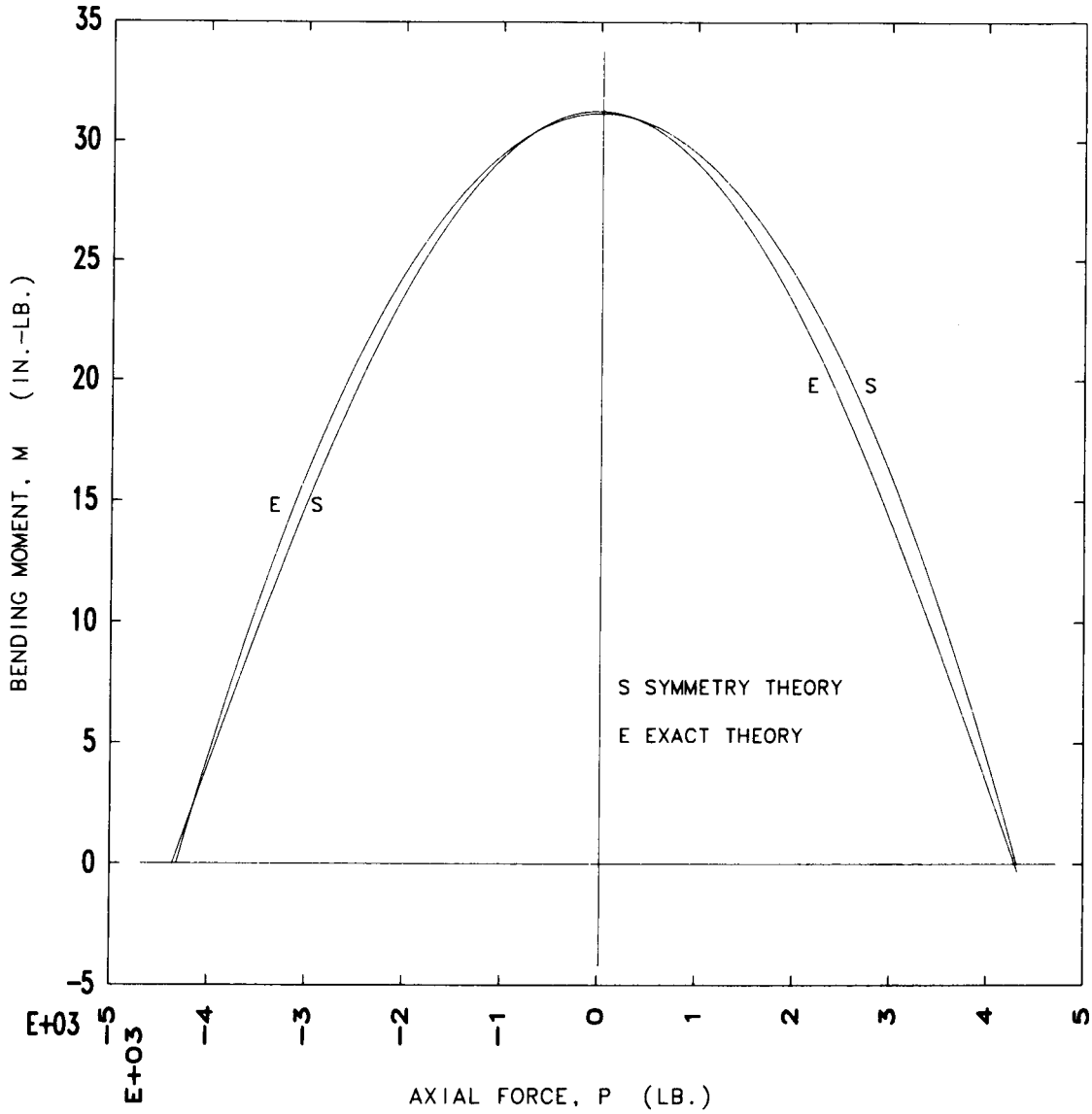

Figure A.5. Interaction diagram for cracked pipe with $a/h = 0.1$ and $b/(\pi r_i) = 0.1$.

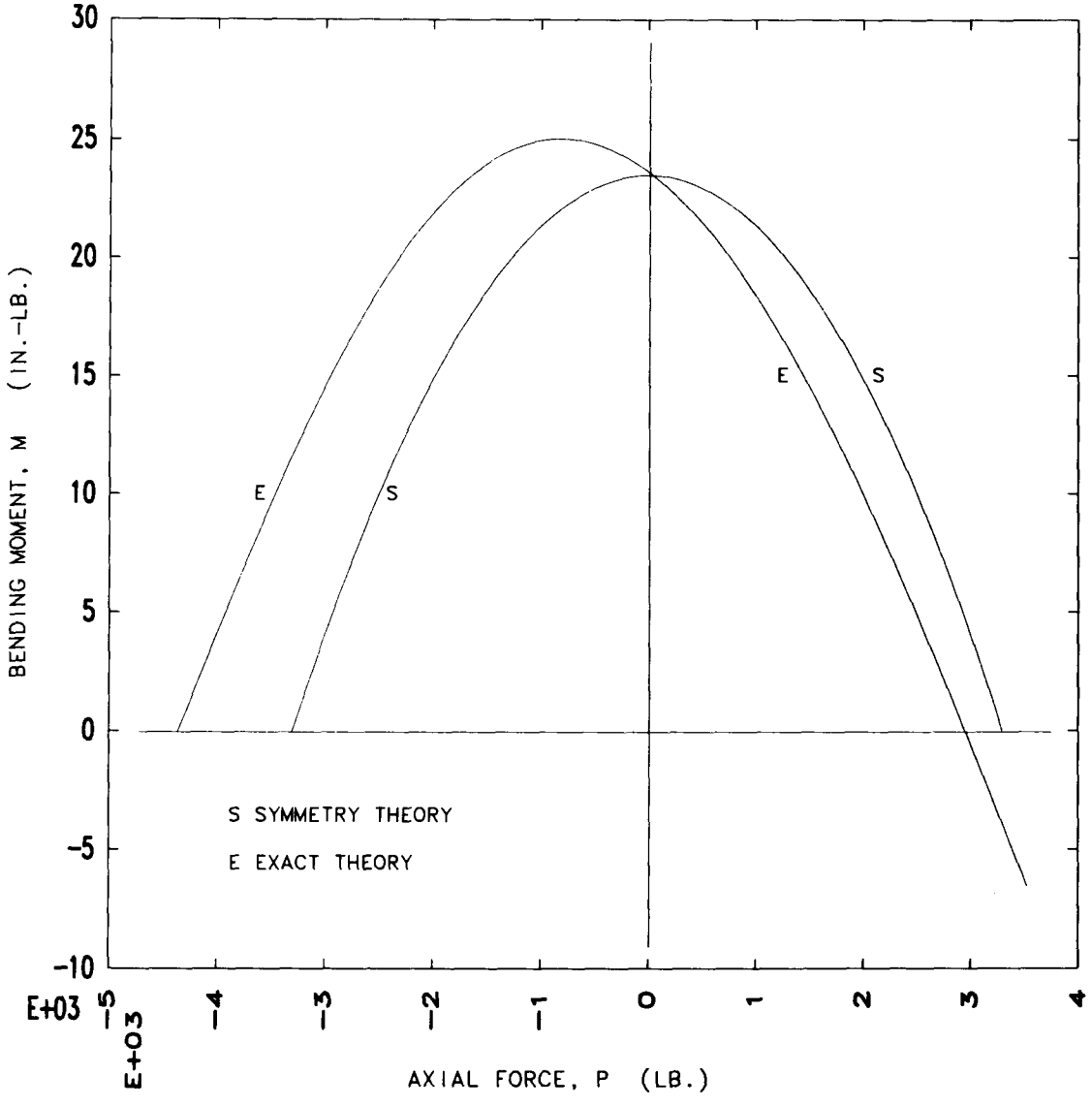

Figure A.6. Interaction diagram for cracked pipe with a/h = 0.5 and $b/(\pi r_i) = 0.5$.

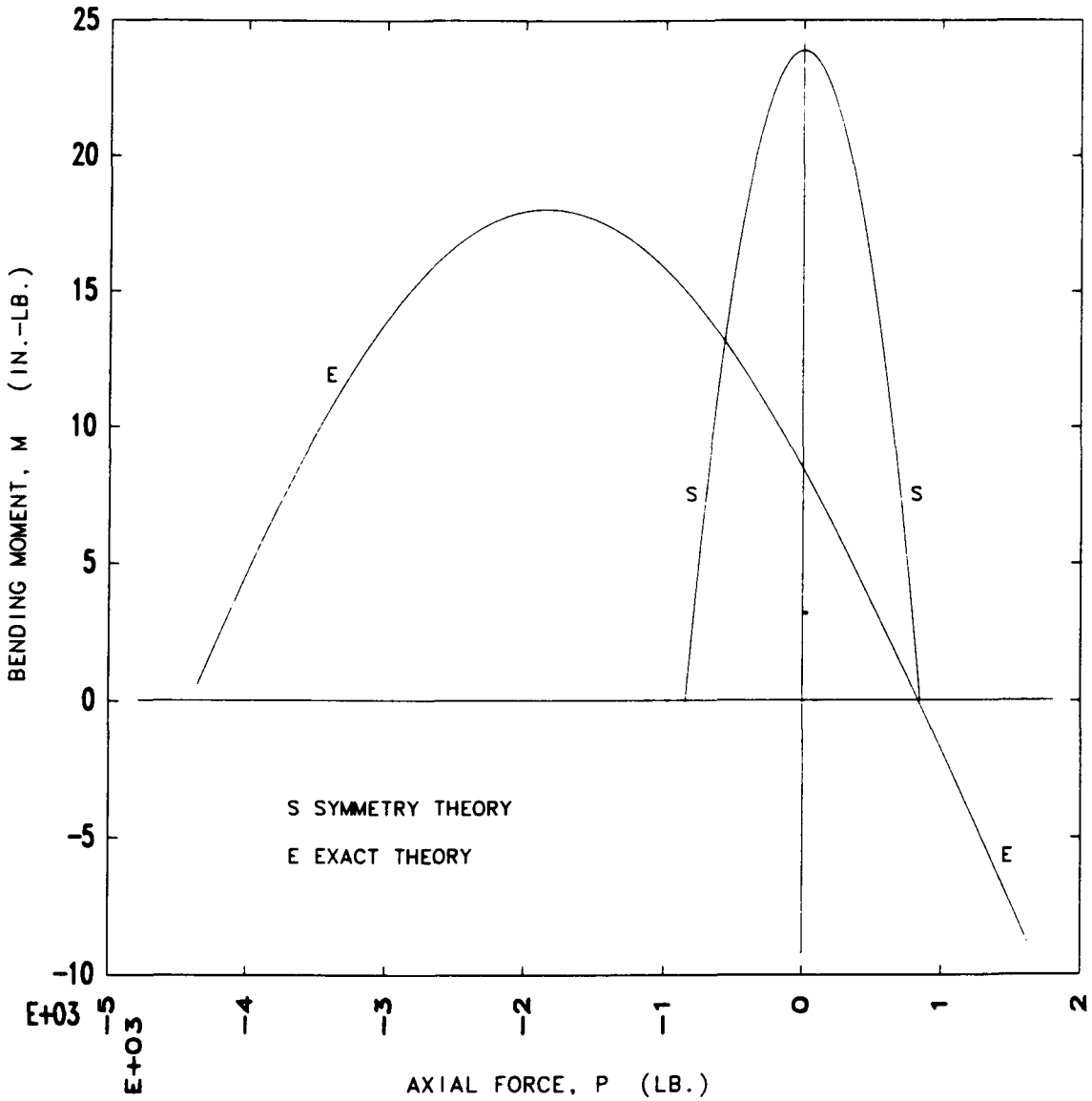

Figure A.7. Interaction diagram for cracked pipe with a/h = 0.9 and $b/(\pi r_i) = 0.9$.